



Gyore, Domokos (2015) *Noble gases as tracers of injected CO₂ in the Cranfield enhanced oil recovery field*. PhD thesis.

<https://theses.gla.ac.uk/7127/>

Copyright and moral rights for this work are retained by the author

A copy can be downloaded for personal non-commercial research or study, without prior permission or charge

This work cannot be reproduced or quoted extensively from without first obtaining permission in writing from the author

The content must not be changed in any way or sold commercially in any format or medium without the formal permission of the author

When referring to this work, full bibliographic details including the author, title, awarding institution and date of the thesis must be given

Enlighten: Theses

<https://theses.gla.ac.uk/>
research-enlighten@glasgow.ac.uk

Noble gases as tracers of injected CO₂ in the Cranfield enhanced oil recovery field

Domokos Györe

Doctor of Philosophy

Scottish Universities Environmental Research Centre (SUERC)

College of Science and Engineering

University of Glasgow

August, 2015

Abstract

Identifying how injected CO₂ is retained underground is a fundamental challenge for carbon capture and storage. Developing tracers that are cheap and widely applicable will increase confidence that stored CO₂ remains in place. This PhD examines the applicability of the isotopic composition of noble gases (He, Ne, Ar, Kr and Xe) that are present as minor natural constituents in CO₂, as tracers of the fate of injected CO₂. The Cranfield oil field (MS, USA), into which natural CO₂ is injected for enhanced oil recovery (EOR), was developed as a site for a parallel study of carbon capture and storage, and is the focus of this research. Samples of gas from the transported CO₂, and the injection and production wells were taken 18 and 45 months after the commencement of injection in July 2008.

Neon isotope data are consistent with simple binary mixing between the injected and *in situ* natural gas. This relationship allows the Ne isotope composition of the pre-injection gas in Cranfield to be determined. Coherent correlations between Ne, He and Ar isotopes allow the natural gas end-member composition to be calculated as well. The noble gas isotopic ratios ($^3\text{He}/^4\text{He} = 0.05 R_A$, where R_A is the atmospheric value of 1.39×10^{-6} , $^{20}\text{Ne}/^{22}\text{Ne} = 9.62$, $^{21}\text{Ne}/^{22}\text{Ne} = 0.0384$, $^{40}\text{Ar}/^{36}\text{Ar} = 836$ and $^{40}\text{Ar}^*/^4\text{He} = 0.09$, where $^{40}\text{Ar}^*$ is the sum of the radiogenic and mantle derived ^{40}Ar) of the natural gas in Cranfield are typical of natural gases derived from the continental crust.

Helium isotope ratios and the $^{40}\text{Ar}^*/^4\text{He}$ ratio notably correlate with CO₂ concentrations, indicating that the noble gas fingerprints of the injected gas are preserved, and may offer utility as a tracer of the CO₂. The He and Ar isotope systematics of the four sampled wells that have the lowest CO₂ concentrations identify the loss of a significant amount of CO₂ from the free gas phase. The amount of loss in each of the four wells can be quantified

from the measured $^3\text{He}/^4\text{He}$ and $^{40}\text{Ar}^*/^4\text{He}$ ratios and changes in the $\text{CO}_2/{}^3\text{He}$ values.

Losses vary between 22% and 96%, with good agreement between the different methods. It is notable however, that these four wells do not have significant gas production, and do not contribute significantly to the total amount of produced and re-injected gas. So, even though there is a significant loss from these wells, the total amount of CO_2 lost is estimated to be only ~0.1% of the total injected gas, equivalent to 10kt gas. Notwithstanding this, the new data indicate that, across the entire field, CO_2 is retained as a free phase and stratigraphic trapping is the most important storage mechanism. The fractionation of $^{40}\text{Ar}^*/^4\text{He}$, $\text{CO}_2/{}^3\text{He}$ and $\delta^{13}\text{C}_{\text{CO}_2}$ in the CO_2 -poor samples is consistent with dissolution in water.

The non-radiogenic noble gases (^{20}Ne , ^{36}Ar , ^{84}Kr , ^{132}Xe) originate from the atmosphere and are present in the gas, water and oil phases in the reservoir to differing degrees. It has been revealed that groundwater degassing, induced by CO_2 injection plays an important role in fractionating $^{20}\text{Ne}/^{36}\text{Ar}$, $^{84}\text{Kr}/^{36}\text{Ar}$ and $^{132}\text{Xe}/^{36}\text{Ar}$ at the early stage of injection, but a large heterogeneity in the degree of degassing has been observed throughout the reservoir. Some wells have shown 100% water degassing, while others are close to 0%. Oil degassing, and therefore the active CO_2 – oil contact, became important during the later phase of injection, which is consistent with the fact that more CO_2 injection was required to degas the oil than water. Temporal variations in the non-radiogenic noble gas ratios and $^3\text{He}/^4\text{He}$ are indicative of the evolution of the oil displacement efficiency. This fully agrees with the injection – production well data recorded in the field during sampling. This suggests that noble gases can also be used as a reservoir engineering tool to better understand the interaction of CO_2 , water and oil in the subsurface not only during CO_2 storage but also to track EOR operations.

Table of contents

Table of contents	4
List of Tables.....	7
List of Figures	8
Acknowledgements	11
Declaration	14
Chapter 1 Tracing CO ₂ injection in carbon sequestration sites	16
1.1 Introduction	16
1.2 Climate change and the need for climate mitigation.....	16
1.3 Carbon Capture and Storage (CCS)	20
1.3.1 Outline.....	20
1.3.2 History of CO ₂ injection and the importance of EOR	24
1.3.3 Near future development of CCS.....	26
1.4 Tracing injected CO ₂	28
1.4.1 Natural CO ₂ fields	28
1.4.2 CO ₂ injection fields	32
1.5 Outline of this thesis	35
Chapter 2 Gas sampling and analytical technique	36
2.1 Introduction	36
2.2 Gas sampling technique	36
2.3 Analytical technique.....	39
2.3.1 The gas inlet and purification line.....	39
2.3.2 Gas analysis procedure.....	44
2.4 Commissioning and testing of the new system	55
Chapter 3 The Cranfield EOR field and tracing CO ₂ by $\delta^{13}\text{C}_{\text{CO}_2}$	57
3.1 Introduction	57
3.2 The Cranfield field	57
3.3 Previous geochemical tracing studies from Cranfield	62
3.3.1 Anthropogenic tracer injection test	62
3.3.2 Stable carbon isotopes.....	63
3.4 Sampling strategy.....	63
3.5 Recent CO ₂ and $\delta^{13}\text{C}_{\text{CO}_2}$ results from Cranfield.....	65
3.6 Tracing CO ₂ by $\delta^{13}\text{C}_{\text{CO}_2(\text{gas})}$	67

3.7	Conclusions	68
Chapter 4	Tracing injected CO ₂ in Cranfield with noble gas isotopes	69
4.1	Introduction	69
4.2	Results	72
4.2.1	Bulkline CO ₂	72
4.2.2	Injected and produced gas	75
4.3	Defining the natural gas end-member composition	79
4.4	Noble gas isotope composition of the in-place natural gas	84
4.5	Tracing injected CO ₂	85
4.6	Conclusions	88
Chapter 5	Storage mechanism of the injected CO ₂ in the Cranfield field	89
5.1	Introduction	89
5.2	Quantifying CO ₂ loss from the gas phase	89
5.2.1	³ He/ ⁴ He and ⁴⁰ Ar*/ ⁴ He vs. CO ₂	89
5.2.2	CO ₂ / ³ He	92
5.2.3	Quantifying the total CO ₂ loss	94
5.3	Mechanism of CO ₂ loss	96
5.3.1	He and Ar isotope constraints	96
5.3.2	Carbon isotopes	99
5.4	Storage of injected CO ₂	102
5.5	Conclusions	105
Chapter 6	Examining the interaction of injected CO ₂ , brine and oil in the Cranfield fluid reservoir using non-radiogenic noble gases	106
6.1	Introduction	106
6.2	The influence of injected Kr and Xe at the DAS site	107
6.2.1	⁸⁴ Kr/ ¹³² Xe in the DAS site in March 2012	108
6.2.2	Assessing the potential leak from the DAS reservoir	113
6.3	Non-radiogenic noble gas data: mixing with air-saturated water	115
6.4	Partial degassing of groundwater	121
6.4.1	The composition of non-radiogenic noble gases prior to injection in the gas phase	121
6.4.2	⁸⁴ Kr/ ³⁶ Ar	122
6.4.3	¹³² Xe/ ³⁶ Ar	125
6.5	Partial degassing of oil	125

6.5.1	The composition of non-radiogenic noble gases prior to injection in the oil phase	125
6.5.2	$^{84}\text{Kr}/^{36}\text{Ar}$	128
6.5.3	$^{132}\text{Xe}/^{36}\text{Ar}$	131
6.6	Future development.....	133
6.7	Conclusions.....	135
Chapter 7	Conclusion and future work.....	137
7.1	Summary.....	137
7.2	Future work.....	139
Appendix I	Raw data.....	141
Appendix II	Publications of this work.....	152
References	154

List of Tables

Table 2.1. Comparison between the theoretical and measured composition of air.....	56
Table 3.1. CO ₂ concentration and $\delta^{13}\text{C}_{\text{CO}_2}$ data from Cranfield.....	66
Table 4.1. The average noble gas composition of the Jackson Dome CO ₂ compared to two independent measurement of the bulkline gas	73
Table 4.2. Major gas and noble gas isotope data from the Cranfield EOR field.	76
Table 4.3. Details of wells from where samples have been taken for this study.....	78
Table 5.1. Measured and theoretical $^{40}\text{Ar}^*/^4\text{He}$ of well gases that have lost CO ₂	91
Table 5.2. The percentages of CO ₂ loss from the 2009 well gas samples based on CO ₂ / ³ He and noble gas ratios.....	91
Table 5.3. The observed and calculated CO ₂ concentration and amount of gas produced where CO ₂ loss has been found.....	95
Table 5.4. The average amount of injected gas around the production wells and the amount of produced oil in 2009 production wells.	104
Table 6.1. Kr and Xe concentrations of the three main components in the Cranfield reservoir.....	112
Table 6.2. The non-radiogenic isotopic composition of CO ₂ well gases from Cranfield.	116
Table 6.3. Degree of oil degassing from well gases from Cranfield.	130
Table I.1. The mass 44/15, measured on the QMS from calibration gases with different CO ₂ contents.....	141
Table I.2. Selected calibration data of mass 44/15 over time from the QMS.....	141
Table I.3. The measured ^{84}Kr of selected samples on both QMS and noble gas mass spectrometer.....	142
Table I.4. Selected $\delta^{13}\text{C}_{\text{CO}_2}$ calibration data over time from the IRMS.....	143
Table I.5. Selected He calibration data from the noble gas mass spectrometer.....	144
Table I.6. Selected Ne calibration data from the noble gas mass spectrometer.....	145

Table I.7. Selected Ar calibration data from the noble gas mass spectrometer.....	146
Table I.8. Selected Kr and Xe calibration data from the noble gas mass spectrometer....	147
Table I.9. The obtained $^{40}\text{Ar}/\text{aliquot}$ from the air calibration bottle from two different standards.....	147
Table I.10. Recorded production well data on the Cranfield field at the time of sampling.....	148
Table I.11. Fractionation of $\text{CO}_2/{}^3\text{He}$ and $^{40}\text{Ar}^*/{}^4\text{He}$ during gas dissolution in the Cranfield reservoir.....	148
Table I.12. Fractionation of $\text{CO}_2/{}^3\text{He}$ and $\delta^{13}\text{C}_{\text{CO}_2}$ in Cranfield during CO_2 precipitation and dissolution.....	149
Table I.13. The isotopic composition of the injected tracer into the DAS site in 2009 and in 2010.....	149
Table I.14. The fractionation of ASW-like noble gases with decreasing G/W ratio in the Cranfield reservoir.....	150
Table I.15. The fractionation of ASW-like noble gases during water-oil contact in the Cranfield field.....	150
Table I.16. The fractionation of noble gases during the degassing of the oil phase in the Cranfield field.....	151

List of Figures

Figure 1.1. The concentration of atmospheric CO_2 and the isotopic composition of hydrogen (δD) from Antarctic ice cores from the last 800,000 years.....	17
Figure 1.2. The global temperature anomaly compared to the average temperature from the last 150 years.....	18

Figure 1.3. The contribution of CO ₂ storage capacity of the four main mechanisms over time.....	23
Figure 1.4. The carbon isotope composition of CO ₂ with respect to its source.....	29
Figure 1.5. Illustrative picture of the distinct sources of the different noble gas isotopes..	30
Figure 2.1. Sampling of high pressure gases by the Cu-tube method.....	38
Figure 2.2. Schematic picture of the noble gas extraction line.	42
Figure 2.3. Diagram of the pre-existing noble gas purification line.	43
Figure 2.4. Calibration of the mass 44/15 (CO ₂ /CH ₄) ratio on the quadrupole mass spectrometer.	45
Figure 2.5. The stability of the QMS with respect to 44/15 over time.....	46
Figure 2.6. The expected amount of ⁸⁴ Kr in the noble gas mass spectrometer and the ⁸⁴ Kr signal/amount of gas in the QMS.....	48
Figure 2.7. The variability of the measured δ ¹³ C _{CO2} of the calibration gas over time.	49
Figure 2.8. He isotopic ratio data of the calibration gas.	50
Figure 2.9. Ne isotope data from the calibration bottle compared to air.....	52
Figure 2.10. Fractionation of Ar isotopes in the calibration gas compared to air.	52
Figure 2.11. The variation of the ratio of ⁸⁴ Kr and ¹³² Xe of the calibration gas.	53
Figure 2.12. The calculated concentration of ⁴⁰ Ar / aliquot from the calibration bottle from two different international standards.....	54
Figure 3.1. The map of the Cranfield EOR field in Mississippi, USA.	58
Figure 3.2. Stratigraphic column of the region of Cranfield, MS, USA.	59
Figure 3.3. Plot of δ ¹³ C _{CO2} (‰) against CO ₂ concentration for Cranfield well gases.	65
Figure 4.1. The relation of mass fractionation of the Jackson Dome gas and the composition of the bulkline.....	74
Figure 4.2. Well gas data from Cranfield plotted on the Ne three-isotope plot.....	80
Figure 4.3. ²⁰ Ne/ ²² Ne of Cranfield well gases plotted against He and Ar isotopic ratios. ...	83

Figure 4.4. The CO ₂ content of Cranfield well gases plotted against He and Ar isotopic ratios.....	87
Figure 5.1. Plot of CO ₂ / ³ He against CO ₂ concentration for Cranfield well gases.	93
Figure 5.2. Plot of CO ₂ / ³ He against ⁴⁰ Ar*/ ⁴ He for Cranfield well gases.....	97
Figure 5.3. The plot of CO ₂ / ³ He versus δ ¹³ C _{CO2} for Cranfield well gases.....	101
Figure 6.1. Schematic picture of the gas cycle in Cranfield.	110
Figure 6.2. The concentration of ¹³² Xe and ⁸⁴ Kr in Cranfield injection and production well gases.	114
Figure 6.3. ⁸⁴ Kr/ ³⁶ Ar and ¹³² Xe/ ³⁶ Ar of gases from injection and production wells from Cranfield.....	117
Figure 6.4. The non-radiogenic noble gas ratios plotted against ²⁰ Ne/ ²² Ne for gases from Cranfield.....	120
Figure 6.5. The plot of ⁸⁴ Kr/ ³⁶ Ar against ²⁰ Ne/ ³⁶ Ar for well gases from 2009.	124
Figure 6.6. The plot of ¹³² Xe/ ³⁶ Ar against ²⁰ Ne/ ³⁶ Ar for well gases from 2009.	127
Figure 6.7. The plot of ⁸⁴ Kr/ ³⁶ Ar against ²⁰ Ne/ ³⁶ Ar for well gases from 2012.	129
Figure 6.8. Combined diagram of ⁸⁴ Kr/ ³⁶ Ar against ²⁰ Ne/ ³⁶ Ar from 2009 and 2012.	130
Figure 6.9. The plot of ¹³² Xe/ ³⁶ Ar against ²⁰ Ne/ ³⁶ Ar for well gases from 2012.	132
Figure 6.10. Combined diagram of ¹³² Xe/ ³⁶ Ar against ²⁰ Ne/ ³⁶ Ar from 2009 and 2012. ..	133

Final word count = 40752

Acknowledgements

Firstly I would like to thank Glasgow University for its financial support and Denbury Resources Incorporated for the permission for taking gas samples and giving assistance in the Cranfield field (MS, USA).

I would like to express how grateful I am to my supervisors: Prof. Fin Stuart, Dr Stuart Gilfillan and Prof. Susan Waldron for choosing me for this Ph.D. adventure despite my broken English.

During my studies in SUERC I have been in the comfortable situation of learning from the bests. Fin Stuart's enthusiasm couldn't really be reduced by the numberless dead ends I have attacked. His office door has always been open for me. He has always managed to devote some time for discussion that helped me to find the final pathway to write this thesis. He has always been managed to find the necessary resource for solving a problem. Fin has been the brain and soul of the mass spectrometer and an invaluable help in editing.

I thank Stuart Gilfillan's advices, helps and recommendations that have also been indispensable. His pace of working is remarkable and has always been in touch to discuss my ideas. I also thank Stuart for organising the sampling trips.

I would like to thank Susan Waldron, whose ability to see the bigger picture of my research is remarkable. Her contribution not only gave a special taste of this work but also contributed a lot to my personal development.

I have had the beauty of using a great selection of equipment and instruments and therefore interacting with many people in SUERC.

Firstly I would like to thank Andrew Tait, who has always been behind me with up to date knowledge regarding anything can possibly happen to any type of mass spectrometer. I

would like to say thank to him for the uncountable times of replacing filaments, multipliers and the likes.

I would like to thank Luigia Di Nicola for taking time out of her very tight schedule to help me in the noble gas laboratory, to tackle a problem in the UHV system and to teach me to set up the diagnose based on symptoms in the mass spectrometer.

Thanks Jim Imlach and Ross Dymock whose technical expertise in ultra-high vacuum technologies has massively reduced the time of fixing a problem.

Thanks to Terry Donnelly, whose knowledge in vacuum line parts and stable isotope analysis is remarkable and without him I would not have been able to get my stable isotope data.

I would like to thank Julie Dougans and Alison McDonald for assisting me in the stable isotope laboratories.

I would like to say thank Leah Morgan and Angel Rodés who has always been a great deal of help anytime in a computational and mathematical problem.

I thank Adrian Boyce, Dan Barfod, Philippa Ascough, Darren Mark, Pauline Gulliver and Gillian MacKinnon for their help and input.

I thank Graham Muir and Elaine Dunbar for their contribution to the stable isotope analysis.

I would like to say thank Callum Murray and Frank Elliot, whose regulator and adaptors, which have never been returned, allowed me to sample cylinder gases.

I would like to thank Robert MacLeod for his glassblowing work and Simon Murphy for his help in electronics and Ian Cameron for general maintenance.

I thank Vincent Gallagher for not switching on his light next door that would have masked my multiplier measurement readings.

I would like to say thank Nicole Doran, Tracey Mark and Maureen Hastings for their warm welcome anytime I walked into the buildings.

I would like to say thank Delia Gheorghiu and Maria Miguens-Rodriguez for helpful conversations.

I would like to say thank the students in SUERC for general background noise in the office. Thanks to Ana Carracedo Plumed, Brett Davidheiser-Kroll, Leisa Douglas, Piotr Jacobson, Jessica Bownes, Kieran Tierney, Kim Woods, Sevasti Modestou and Helen Hastie. As well as Katarzyna Łuszczak, Anna Varga-Vass and Callum Graham from Glasgow University and Rory McKavney from the University of Edinburgh.

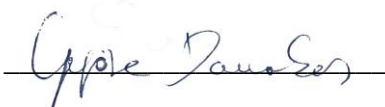
I thank Derek Hamilton, Kerry Sayle and Alex Brasier to help me to find my way at the very early stage of my PhD studentship.

I thank my wife, Lenke Mattyasovszky for pushing me up to 192 summits in Scotland, classified as Munro during my study, giving me the chance to focus on something else, refresh my brain and let an interpretation suddenly hit me.

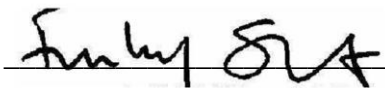
Lastly I would like to thank Róbert, my five month old son who has constantly reminded me, particularly in the writing phase, that sleeping is such a waste of time.

Declaration

No part of the work presented in this thesis has been submitted for any other degree or qualification. The thesis is the result of my independent research, carried out between October 2011 and August 2015 at SUERC, University of Glasgow, under the supervision of Prof. Finlay Stuart, Dr Stuart Gilfillan and Prof. Susan Waldron. Any material, published or unpublished used in this thesis is given full acknowledgement.

Signature 

Printed name Györe Domokos

Signature 

Printed name Finlay Stuart

A geochemist is a person who has the special ability to lose in a fraction of a second in the laboratory a sample that has been created over millions of years.

Chapter 1

Tracing CO₂ injection in carbon sequestration sites

1.1 Introduction

The geologic storage of man-made carbon dioxide (carbon sequestration) is thought to be a way to significantly reduce its emission into the Earth's atmosphere, which is responsible for climate change. In order to deploy the technique safely methods need to be developed for monitoring and verifying secure storage (IPCC, 2005). Enhanced oil recovery by CO₂ injection (CO₂-EOR) has the potential to make CO₂ injection economically sustainable but also gives an excellent opportunity for carrying out research into the transport and sequestration of anthropogenic CO₂ (Moniz and Tinker, 2010).

This study is devoted to identifying tracers of injected CO₂ in an EOR field, investigating the mechanisms by which CO₂ is retained in the reservoir, and determining the history of CO₂ interaction with the reservoir fluids. This chapter is a review of the current status of underground carbon sequestration and the development of techniques that have been developed to trace injected CO₂.

1.2 Climate change and the need for climate mitigation

The global temperature of the Earth is fundamentally influenced by the presence of greenhouse gases (GHG) in the atmosphere because they absorb and emit infrared (thermal) radiation. The most important GHGs are CO₂, CH₄, N₂O and chlorofluorocarbons (CFC) (IPCC, 2007). CO₂ is the most abundant GHG compound in the atmosphere (~0.04 %), and its mean lifetime is estimated to be several decades (EPA, 2015). Consequently it is the most critical terrestrial greenhouse gas. The concentration of atmospheric CO₂ over the last 800,000 years has been determined from Antarctic ice cores

where the ancient air had been trapped as bubbles. It has been found to have an average at around 230 ppmv. The largest changes (± 100 ppmv) are between glacial and interglacial periods (Figure 1.1) (Jouzel et al., 2007; Lüthi et al., 2008).

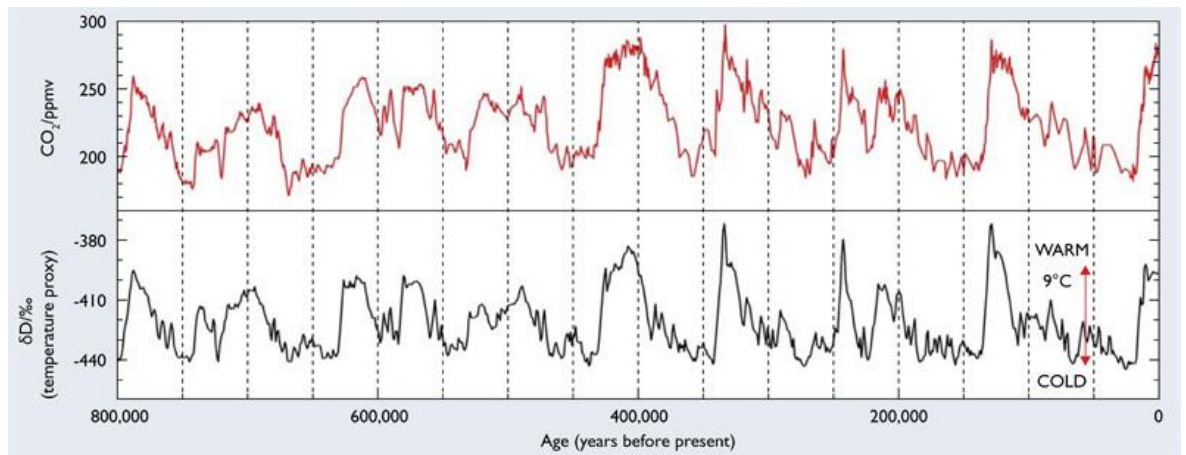


Figure 1.1. The concentration of atmospheric CO₂ and the isotopic composition of hydrogen (δD) from Antarctic ice cores from the last 800,000 years. The average CO₂ concentration is largely stable around 230 ppmv, with largest changes (± 100 ppmv) observed between interglacial and glacial periods. The isotopic composition of hydrogen, which is a proxy for the temperature of the atmosphere, correlates well with the CO₂ concentration. Consequently the Earth's temperature shows stability in the last 800ka. Picture is modified from <https://www.bas.ac.uk>

The most rapid natural increase in atmospheric CO₂ recorded from ice cores was a 20 ppmv increase in 1,000 years from 12,000 year old ice cores (Jouzel et al., 1987). The concentration of CO₂ in the atmosphere has increased since the industrial revolution from ~280 ppmv to near 400 ppmv by 2007, with 20 ppmv increases occurring in less than 10 years (IPCC, 2007).

The isotopic composition of hydrogen (δD) is a proxy for the temperature of the atmosphere (e.g. Jouzel et al., 2007). It correlates well with the concentration of CO₂ from ice core records and therefore the temperature of the Earth in the last 800,000 years (Figure

1.1) (Jouzel et al., 2007; Lüthi et al., 2008). Global temperature has increased by approximately 0.6°C compared to the average temperature of the past ~150 years since 2000s (Brohan et al., 2006) (Figure 1.2). A similar increase has been recorded in 115,000 year old Greenland ice cores by $\delta^{18}\text{O}$ data (Andersen et al., 2004). This is explained by the sudden change in heat transport in the ocean from the tropics, caused by the presence of a massive ice sheet over North America (Andersen et al., 2004).

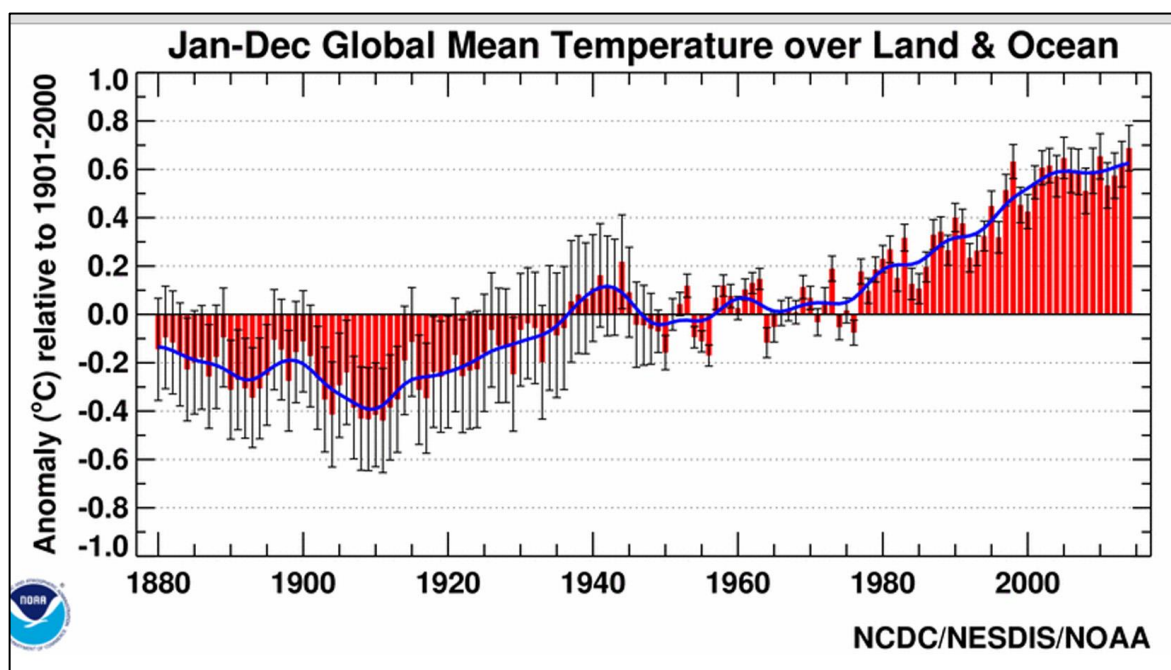


Figure 1.2. The global temperature anomaly compared to the average temperature from the last 150 years. Globally the temperature has increased by about 0.6°C in recent years in comparison to the average value. Picture obtained from <http://www.ncdc.noaa.gov/sotc/global/201113>

The energy industry, in particular the burning of fossil fuels, is the most significant CO_2 emitter (e.g. Mackenzie et al., 2001). The United Nation Framework Convention on Climate Change (UNFCCC) was signed in 1992 with the primary aim of stabilizing greenhouse gases in the atmosphere. The UNFCCC conference in Kyoto, Japan, in 1997 recommended that developed countries should reduce their GHG emission to below 1990

levels by the end of the period of 2008-2012. Although many countries agreed on different reduction targets based on their individual circumstances, not all countries, including the USA and Australia, ratified the so-called Kyoto Protocol (Gale, 2004 and references therein).

Estimations from climate models suggest that the world could warm up by 5.8°C by the end of the 21st century as the result of GHG emissions (IPCC, 2001). Reducing emissions of the GHGs according to the Kyoto Protocol by all countries will still see a rise in the global temperature of ~2°C by that time. This means that actions taken now will generally influence the Earth temperature significantly after 2100 (IPCC, 2001). CO₂ emissions will be reduced rapidly and significantly by switching from burning coal to gas due to the different heat capacities (e.g. IEA, 2014a). This trend has started with the increasing availability of shale gas (unconventional gas) in the US (Heath et al., 2014). However, burning methane will not decarbonise the energy industry in the long-term. There has been a considerable increase in the use of renewable energy sources such as solar and wind turbines globally. Since 2007, the contribution of renewables to the total power generation increased by 4% by 2014 (IEA, 2014b) but the complete fuel ‘switch’ is unlikely to happen in the next few decades and based on the most optimistic modelling, fossils fuels will remain the major source of energy for decades (Cozzi, 2011). Thus in order to achieve GHG emissions targets CO₂ reduction technologies are being widely investigated (Gale, 2004 and references therein).

1.3 Carbon Capture and Storage (CCS)

1.3.1 Outline

The capture of anthropogenic CO₂ from power plants and its consequent storage in a suitable repository is thought to be the only way to reduce CO₂ emissions by the degree required to mitigate climate change (e.g. Herzog, 2011). Carbon capture and storage is the integration of a few different technologies to fulfil this purpose:

Capture: There are three principal approaches by which CO₂ can be captured: (i) post-combustion, where the CO₂ removal is carried out after ‘normal’ combustion; (ii) pre-combustion, where the CO₂ is removed after gasification but before final combustion of the fuel (relevant to oil and coal); and (iii) the oxyfuel combustion technique, which produces highly concentrated waste CO₂ (e.g. Tondeur and Teng, 2008).

Treating, compression and transportation: The different capture techniques and the variety of fuels (coal, oil, gas) means that the composition of CO₂ for sequestration varies. Consequently a treatment that produces gas suitable for injection and storage needs to be applied. CO₂ is typically transported to the storage site via pipelines under supercritical conditions. Currently thousands of miles of onshore pipelines are in operation for CO₂ transport (mostly in the USA, Herzog (2011)). In contrast the offshore pipeline infrastructure is less well established. The complexity of international transport is summarized by Coleman (2009).

Storage: CO₂ storage can be achieved in two basic ways: i) by the enhancement of natural CO₂ sinks or ii) by carbon capture and storage.

The first group of methods includes forestry (Marland and Schlamadinger, 1999) and soil-based (Paustian et al., 1997) sequestration. These are unlikely to make significant impact on CO₂ reduction and have issues with reversibility (Gale, 2004 and references therein). Carbonation, which is the replacement of silicate minerals by carbonates can also be

considered a natural option and interestingly, has been found a means of CO₂ sequestration on Mars (Tomkinson et al., 2013). CO₂ storage options include deep geology (Lewis and Shinn, 2001), deep ocean (Brewer et al., 1999), ocean floor basalt (see also below) (Goldberg et al., 2008) and deep ocean carbonate sediments (House et al., 2006). Deep ocean storage has a significant uncertainty over its environmental impact (Gale, 2004 and references therein).

Deep geologic storage is the most developed method and carries the least uncertainties. There are three major types of target reservoir for CO₂ storage: saline aquifers, depleted hydrocarbon fields and un-minable coal seams. Natural analogues of all types indicate that they provide long term security. For example the Bravo Dome gas field in New Mexico (USA) has held magmatic CO₂ for over 50,000 years (Baines and Worden, 2004).

The global capacity for CO₂ storage in saline aquifers, the largest target reservoir, is estimated to be $\sim 10^4$ Gt (IPCC, 2005), although there is a debate about the approach hence the absolute value (Thibeau and Mucha, 2011). Nevertheless this is much higher than the annual global emission in 2010 (~ 33 Gt), which means the Earth's crust could host the CO₂ equivalent to several decades of emissions.

CO₂ storage by CO₂-EOR is currently the most significant activity in CCS (Global CCS Institute, 2015) and its success is the key to further develop and understand subsurface storage of the injected CO₂. Despite having orders of magnitude less capacity than saline aquifers, depleted hydrocarbon reservoirs are currently extremely important (Moniz and Tinker, 2010).

Un-minable coal seams could adsorb CO₂ by desorbing CH₄. This phenomenon could be utilized during coal bed methane (CBM) extraction (Shi et al., 2008). The terminology of the mechanisms by which injected CO₂ is retained may be confusing (Zhang and Song, 2014), and can vary from place to place (e.g. Saadatpoor et al., 2009). The four widely accepted trapping mechanisms are:

Physical or stratigraphic trapping - where the microscopic pore space is filled with injected gas (or supercritical) phase and it ascends slowly. Typically a physical barrier, such as a low permeability rock (e.g. mudstone, shale or clay) must prevent migration to the surface. This is the most

Residual trapping - where CO₂ bubbles are disconnected from each other and become immobile as a non-wetting phase between grains.

Solubility trapping - injected CO₂ dissolves in water (or in other fluid such as oil). Water migration out of the reservoir may be a limitation if this led to release of stored CO₂ to the atmosphere.

Mineral trapping - occurs when CO₂ precipitates as carbonate mineral and is thought to be the most permanent storage mechanism.

Each storage mechanism operates on a different timescale (Figure 1.3). Structural trapping has the most significant role (80%) and mineral trapping is negligible at the start of the operational phase, which is measured in decades. The contribution in storage capacity then is slowly taken over by residual and solubility trapping mechanisms. The significance in mineral trapping becomes important on timescales of centuries to millennia. The increasing role in residual, solubility and mineral trapping increases the safety of geologic CO₂ storage because the amount of free phase (mobile) CO₂ decreases (Bachu et al., 2007).

CO₂ capture, transportation and storage requires energy. This ultimately means more CO₂ must be captured, transported, and stored in order to fulfil current energy demand.

However at the current state of knowledge there is no alternative (Scott et al., 2013 and references therein).

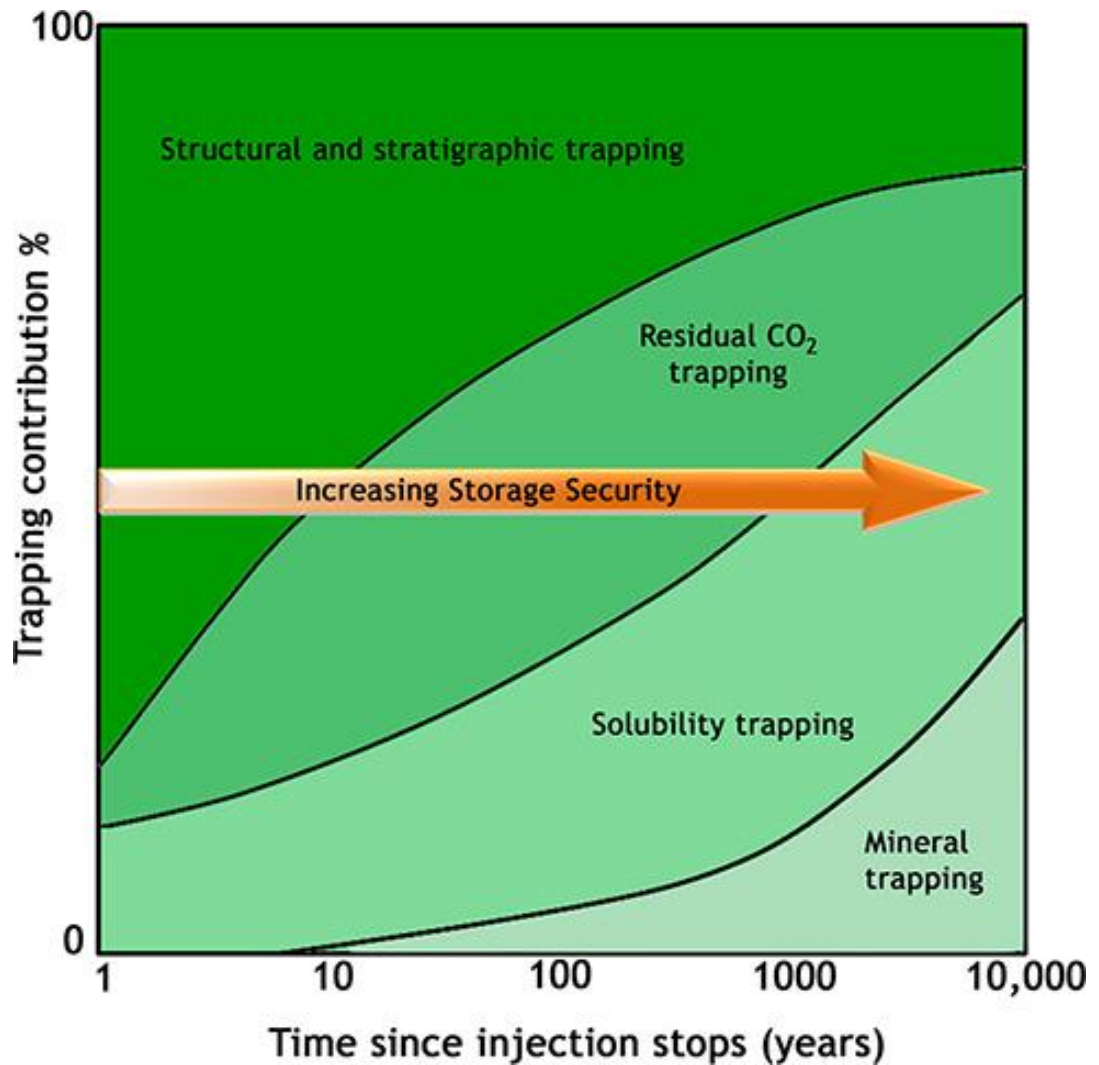


Figure 1.3. The contribution of CO₂ storage capacity of the four main mechanisms over time. At the beginning of injection structural trapping has the most significant role (~80%) and mineral trapping is negligible. Then its contribution to storage capacity is slowly taken over by solubility and residual trapping. They become dominant in a couple of decades, which is the timescale of the operational phase. In the post injection phase (centuries to millennia) the significance of mineral trapping becomes more important, with solubility and residual trapping remaining the major types of sink. The increasing role of mineral, solubility and residual trapping increases the safety of geologic CO₂ storage through reducing the amount of free phase (mobile) CO₂. After IPCC (2005).

1.3.2 History of CO₂ injection and the importance of EOR

The injection of natural gas into depleted oil and gas reservoirs has a long history, while the concept of using it as a climate mitigation tool is relatively recent. The injection of gas is a commercial activity in order to fulfil local seasonal gas demand. The first injection and storage of natural gas into depleted gas reservoirs happened in 1915 in Weland County, Ontario, Canada (NaturalGas, 2015). Since then, the storage of natural gas underground has become widespread, and saline aquifers have been tested as well (Herzog, 2011).

CO₂ injection for enhanced oil recovery (CO₂-EOR) (and enhanced gas recovery (EGR) is a tertiary recovery technique, by which pressurised CO₂ is injected into the reservoir to decrease the viscosity of the oil and to drive it towards production wells. CO₂-EOR was first employed in 1972 (Herzog, 2011). Reményi et al. (1995) have described a CO₂-IOR (Improved Oil Recovery) project carried out on sandstone reservoirs of the Budafa and Lovászi fields, in SW Hungary, commencing in 1972. The project used natural gas from the Nagylengyel gas field and continued until 1992 (Doleschall et al., 1992; Magyari and Udvardi, 1991). There is no clear information regarding the amount of injected gas and its composition.

In the same year the Val Verde project (Texas, USA) started operating (Crameik and Plassey, 1972). It is still in operation and the CO₂ injection rate is 1.3 Mt/a as of May 2015. It is the world's largest anthropogenic CO₂ injection project (Carbon Capture and Storage, 2015). The first countries to implement the technique outside of Hungary and the USA were Canada, Turkey and Trinidad and Tobago. Today the USA, Canada and Brazil are operating large scale CO₂-EOR projects and there is one in the UAE and several in China in the planning phase. The biggest EOR project currently in operation is the Century Plant project in Texas, USA, which is injecting 8.4 Mt gas per year (Global CCS Institute, 2015),

although another source states 5 Mt per year (Carbon Capture & Sequestration Technologies, 2015).

The main limiting factor in CO₂-EOR is the price of the high purity CO₂, hence the low number of countries that are currently using this technology, not least because a significant proportion of the injected CO₂ is retained in the reservoir. For example at the Cranfield EOR field (Mississippi, USA), 4 of the 6.8 Mt CO₂ that have been injected has been stored (Hovorka et al., 2013). However EOR fields offers the ability to verify CO₂ storage for sequestration purposes, and allows other aspects of the technology (e.g. finance, legal, policy) to be tested (e.g. Moniz and Tinker, 2010).

The Sleipner gas field in the Norwegian sector of the North Sea is operated by Statoil and was the first project to inject post-captured CO₂ in order to avoid CO₂ emission in 1996 (Torp and Brown, 2005). This was followed by the In Salah CO₂ Storage Project (Sonatrach, BP and Statoil, Algeria) in 2004 and the Snøhvit Project (Statoil, North Sea, Norway) in 2008, both of which injected post-captured CO₂ (e.g. Eiken et al., 2011). Since then there have been no new large scale CCS projects in operation that are not connected to EOR. The development and future plan is discussed in 1.3.3.

Pilot studies have been carried out in deep sea basalt storage of CO₂. In such a reservoir, the injected CO₂ not only mixes with seawater but also reacts with basalt. Both, brine and basalt are rich in alkaline elements (e.g. Mg, Ca). The release of them from basalt will react with CO₂ and form carbonate minerals (Goldberg et al., 2008). Calculations of basalt-water-supercritical CO₂ have shown the mineralization to be so rapid that it could be validated in pilot studies (see mineralization timescale in Figure 1.3). Basalts with significant storage capacity occur in the US and India (McGrail et al., 2006). The purpose of the CarbFix Pilot Project in Iceland was to optimise methods for CO₂ storage in basalts. (Matter et al., 2009). Geothermal CO₂ from the Hellisheidi Geothermal Power Plant will be

used. Field experiments for sequestering CO₂ in basalt (Columbia River Basalt) have also been carried out in NW United States. (Tollefson, 2013).

1.3.3 Near future development of CCS

The biggest challenge in CCS is the integration of all the techniques in order to make the full CCS chain work. Although this has been achieved at medium scale (Mt) (e.g. Boundary Dam, Saskatchewan, Canada) it has not been demonstrated at the largest (Gt) scale. The recent IPCC report highlighted that if CCS is going to make headway in climate change, 120 Gt of greenhouse gases will need to be stored until 2050. This would require over 3,000 large-scale CCS projects (Global CCS Institute, 2015; IPCC, 2014). Only a handful of large scale projects are currently in operation, of which only the North Sea projects are non-EOR and several (EOR and non-EOR) are in different stages of development.

International organizations provide a high quality overview of the current global status of CCS. The International Energy Agency (IEA) has the most comprehensive platform to gain information about the most recent developments (IEA, 2015). The Global CCS Institute (Global CCS Institute, 2015) and the Zero Emission Research Organization (Zero, 2015) have developed databases on CCS and EOR projects from all over the world. The European CCS Demonstration Project Network shows all the European Projects (European CCS Demonstration Project Network, 2015), while the CO₂CRC covers developments in Australia and in New Zealand (CO₂CRC, 2015).

Six large-scale CCS projects are planned to be in operation by the period of 2019 and 2022 in the UK (Global CCS Institute, 2015). Two of these projects will be in Scotland - the Peterhead CCS Project and Caledonian Clean Energy Project (Grangemouth) - with the remainder in England: C.GEN North Killinghome, Don Valley, Teesside and the White

Rose CCS Projects. Each will have a capture capacity between 1.0 and 3.8 Mt/a.

Additionally there are several small scale project throughout the country at different stages of development (SCCS, 2015).

In the rest of Europe, several countries have made significant developments. Austria, France, Germany and Italy have pilot projects. France, Malta and Norway (including Svalbard) have projects in the planning phase. Other EU countries where CCS projects have been developed but cancelled or finished are: Bulgaria, Denmark, Finland, Poland Romania, Spain, Sweden and The Netherlands (SCCS, 2015).

In the Middle East, the United Arab Emirates and Saud Arabia will employ large scale CO₂-EOR by 2016 and 2015, respectively, both with the injection plan of 0.8 Mt/a. In the Far East, South Korea will have two CCS (non-EOR) projects by 2020, both of them with the plan of injecting 1Mt CO₂/a. China plans to operate 11 projects by 2020, of which 5 will be EOR and the cumulative injection rate will be 15 Mt/a. Australia will operate two projects by 2020 with the combined injection rate of up to 9 Mt/a. Canada will run three more EOR projects by 2019 besides its significant current EOR performance and two CCS by 2020. The United States plans to run two CCS projects and 10 EOR by 2020 (Global CCS Institute, 2015).

Despite the high volume of research in CO₂ monitoring including core analysis, seismic, geophysical and geochemical methods (e.g. Ajo-Franklin et al., 2013; Arts et al., 2004; Boreham et al., 2011) and the high pace of development globally, there are significant uncertainties in the understanding of CO₂ tracing and storage, and consequently its safety (Watson et al., 2014). As a result the In Salah Project was suspended in 2011 (e.g. Verdon et al., 2015) due to concerns about the seal. The issue of safety drives the question of public acceptance (Watson et al., 2014). Public acceptance requires the demonstration of the reliability of the technology, and education. In the absence of that, similar events in the future such as the leak allegation in Weyburn (Saskatchewan, Canada) (Beaubien et al.,

2013) and the Barendrecht project cancellation (The Netherlands) (Feenstra et al., 2010) will continue.

1.4 Tracing injected CO₂

Tracing the movement of the CO₂ in the subsurface started initially with numerical modelling and laboratory experiments. Fluid flow and physical-chemical processes acting on injected CO₂ have been extensively studied (e.g. Ennis-King and Paterson, 2007; Knauss et al., 2005; White et al., 2005; Xu et al., 2005) and trapping mechanisms within engineered fields have been developed (Arts et al., 2004; Emberley et al., 2005). However these models require that the constraining parameters are determined by field techniques (see Jeandel et al., 2010). Studies from CO₂ injection fields have used existing techniques that are routinely employed in natural gas fields, as summarized below.

1.4.1 Natural CO₂ fields

Natural CO₂ accumulations in the crust provide analogues for the long-term storage of man-made CO₂ (e.g. Baines and Worden, 2004; Haszeldine et al., 2005). Therefore all research that has aimed to understand the origin and migration of the CO₂ and reservoir processes in such fields can make a significant contribution to the ongoing development of a global CO₂ monitoring technique for carbon sequestration.

The carbon isotope composition of the CO₂ ($\delta^{13}\text{C}_{\text{CO}_2}$) has been used for several decades for tracking carbon derivatives in geochemical research. The quantification of isotope fractionation under entirely different conditions for different CO₂-fluid-rock systems was carried out in early studies (e.g. Deines et al., 1974; Mook et al., 1974; Vogel et al., 1970). The application of $\delta^{13}\text{C}_{\text{CO}_2}$ is now widespread, and includes tracing of atmospheric CO₂ in oceans (e.g. Bauch et al., 2000), and of the origin of CO₂ in deep reservoirs (e.g. Clayton et

al., 1990; Javoy et al., 1986). Although the carbon isotope composition of CO₂ is diagnostic of the process that formed it (Wycherley et al., 1999), in fields with high CO₂ concentration (> 70%) δ¹³C_{CO2} typically overlaps the range produced by carbonate breakdown and magmatic degassing (δ¹³C_{CO2} = -8 to + 3‰) (Figure 1.4) (Jenden et al., 1993). As a result, the origin of CO₂ in most high concentration fields cannot be reliably constrained by δ¹³C_{CO2} alone, so that additional methods are required (e.g. Matthews et al., 1987; Sherwood Lollar et al., 1997). Additionally, the high reactivity and solubility of CO₂ in water requires a precise knowledge of the degree of interaction in order to, for example, quantify the amount of CO₂ that has dissolved (e.g. Gilfillan et al., 2008).

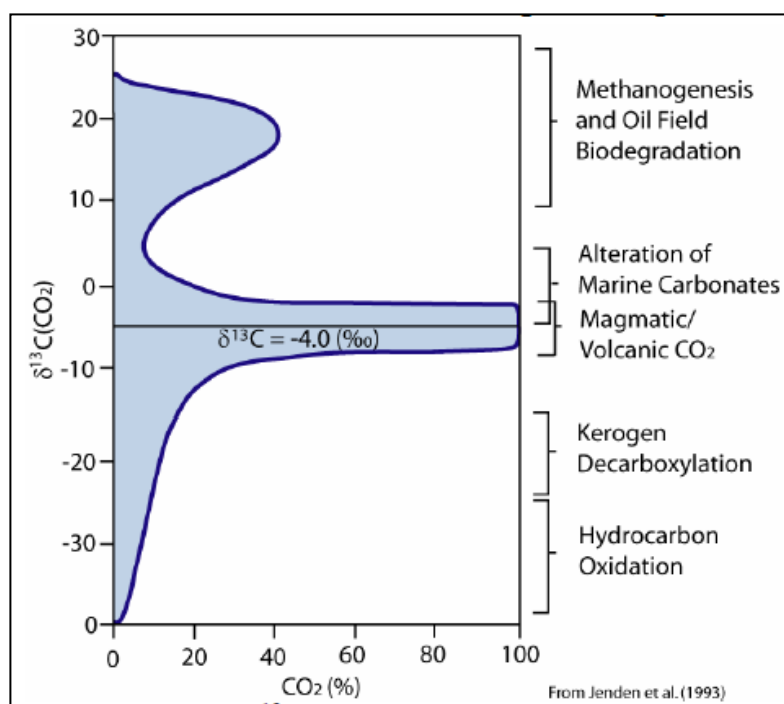


Figure 1.4. The carbon isotope composition of CO₂ with respect to its source. The majority of CO₂-rich crustal fluids have δ¹³C(CO₂) that are confined to a narrow range (between -8 and +3‰). The average value covers the typical value of both CO₂ formed by alteration of marine carbonates and magmatic CO₂. Hence, if there is a need for distinguishing between these two sources in crustal fluids, δ¹³C alone does not provide an unambiguous identification. From Jenden et al. (1993).

Noble gases (He, Ne, Ar, Kr and Xe) are present in crustal fluids in minor quantities and they have several isotopes with distinct sources (Figure 1.5). They are chemically inert and can be used to trace the physical processes that have affected the fluid that hosts them (e.g. Ballentine et al., 2002 and references therein). The study of the noble gases as tracers dates back to the 1960s (Zartman et al., 1961) and the technique has been used since then to study gas origin in a wide selection of reservoirs worldwide.

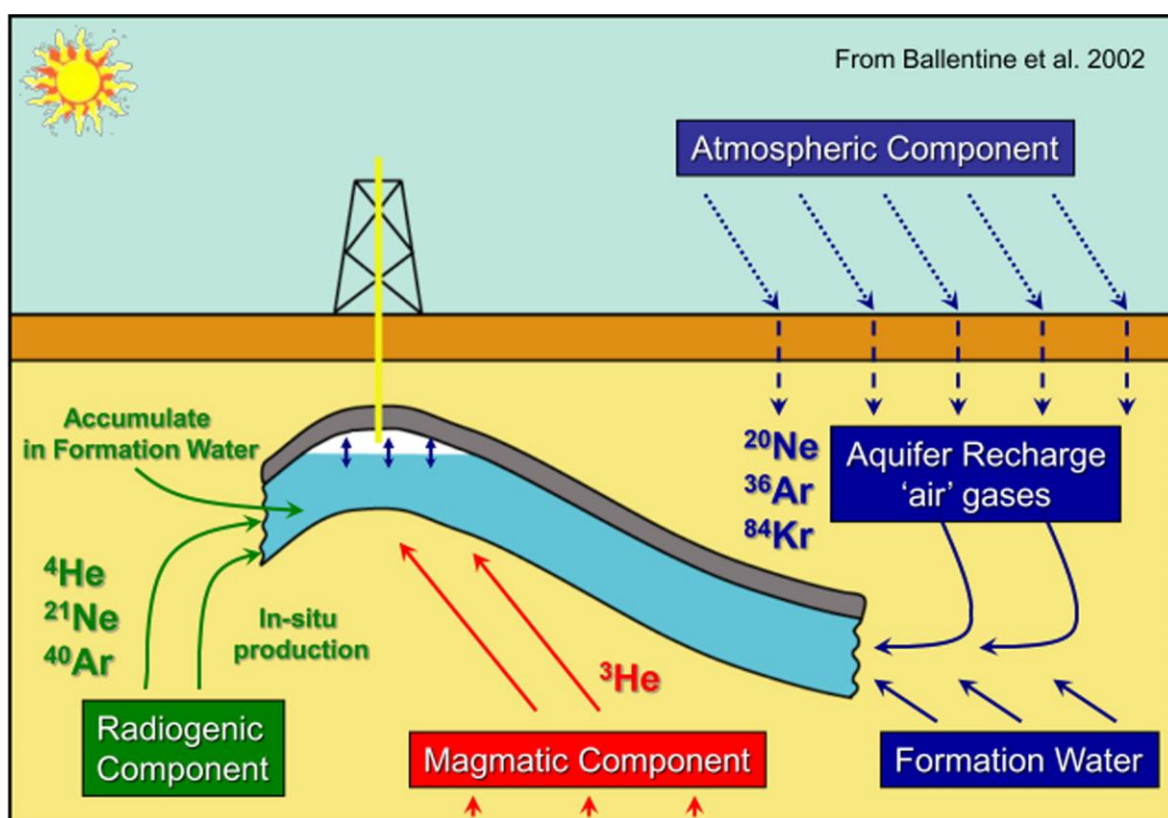


Figure 1.5. Illustrative picture of the distinct sources of the different noble gas isotopes. Noble gases (He, Ne, Ar, Kr, Xe) are typically minor components in crustal fluids. These can originate from the crust, the mantle and the atmosphere. The contribution of each reservoir can be estimated via distinct isotope composition. Redrawn from Ballentine et al. (2002).

Early studies demonstrated an enrichment in heavier noble gases relative to air from well gases in Mexico (Hennecke and Manuel, 1975) and in Japan (Nagao et al., 1981). The origin of deep (mantle) sourced gases has been identified in the Yellowstone geothermal area (USA) (Kennedy et al., 1985, 1988) and in Iceland (Marty et al., 1991) by He isotopes. Helium also has shown mantle origin in the Western USA in connection to arc volcanism (Jenden et al., 1988; Poreda et al., 1986; Welhan et al., 1988), in the Rhine Graben, where also recent volcanism occurred (Griesshaber et al., 1992) and in the Songliao Basin (China) (Xu et al., 1995). Regions of recent crustal thinning also show mantle-sourced gas, for example the North Sea gas fields (Hooker et al., 1985) and the Carpathian Basin (Cornides et al., 1986; Martel et al., 1989).

The interaction between CO₂ and reservoir fluids and solubility-controlled fractionation of noble gas isotopes has been intensively studied in crustal fluids from France (Pinti and Marty, 1995) where a qualitative assessment on the duration of water-oil contact has been shown. From some SE Mediterranean oil accumulations (Bosch and Mazor, 1988) the role of oil degassing in fractionating noble gas ratios has been demonstrated. In the Pannonian Basin (Stute et al., 1992) the groundwater circulation system was studied. From the Pakistan Indus Basin (Battani et al., 2000) a complex distillation process was modelled. A comprehensive review on noble gas geochemistry of oil and gas accumulations is given by Prinzhofer (2013). These studies have supported a strong background for model developments on CO₂ migration.

A comprehensive model has been developed to describe CO₂-water interaction in some reservoirs in the Colorado Plateau (USA) using noble gases (Gilfillan et al., 2008). $\delta^{13}\text{C}_{\text{CO}_2}$ and noble gases in several reservoirs have been used to provide a way of quantifying CO₂ loss by dissolution in water or precipitation (Gilfillan et al., 2009). The models have then been used to estimate the rate of dissolution of CO₂ in the Bravo Dome (USA) (Sathaye et al., 2014). The water degassing induced by CO₂ injection and the consequent re-dissolution

of the gas (Gilfillan et al., 2008) explains gas-water interaction in natural gas fields but has not yet been applied to CO₂ injection fields. This would not only provide information on the CO₂-fluid interaction but may also be used to determine the timescale of stripping and re-dissolution of CO₂.

1.4.2 CO₂ injection fields

From the early 2000s attention turned to CO₂ in injection fields with the purpose of developing tracers of the injected CO₂. Carbon isotopes have been extensively studied to assess their utility in tracing CO₂ in the Pembina Cardium field (Alberta Canada) (Johnson et al., 2011). In their work Johnson et al. (2011) showed that the carbon isotopic compositions correlates strongly with the CO₂ concentrations from production wells and are effective for identifying preferential gas flowpaths. A good correlation between CO₂ concentration and $\delta^{13}\text{C}_{\text{CO}_2}$ was also found in the Cranfield (MS USA) CO₂-EOR field (Lu et al., 2012b). $\delta^{13}\text{C}_{\text{CO}_2}$ has also been found to be a useful tracer in the CO2CRC Otway Project (Victoria, Australia) (Boreham et al., 2011).

In all cases above the $\delta^{13}\text{C}_{\text{CO}_2}$ values of the injected gases are within the negative side of the narrow magmatic range (down to ~ -8 ‰) indicating a natural source of the gas (see Figure 1.4.). The $\delta^{13}\text{C}_{\text{CO}_2}$ values of the ‘traditionally’ combusted gas are generally much lighter (from -24 ‰ to -40 ‰; Widory, 2006), which is where the isotopic composition of the CO₂ would be from the oxidation of hydrocarbons (see Figure 1.4.). A recent measurement has also shown that $\delta^{13}\text{C}_{\text{CO}_2}$ of the captured CO₂ is around -20 ‰ after both coal gasification and amine capture techniques (Flude et al., 2015). This significantly different end-member value in comparison to previous studies may suggest the need of re-evaluation of tracing CO₂ in the reservoir by $\delta^{13}\text{C}_{\text{CO}_2}$.

Ionic trapping (synonym for solubility trapping) of CO₂ has been quantified in the Weyburn field by carbon isotopes (Raistrick et al., 2006) and it has been concluded that the technique applied should be applicable to other CO₂ injection fields, regardless of the reservoir type (deep saline or hydrocarbon) if there is a considerable difference in the end-members of the injected and reservoir gas.

Oxygen isotopes ($\delta^{18}\text{O}$) have been used to show CO₂-water interaction in the Weyburn CO₂-EOR field (Saskatchewan, Canada) (Johnson et al., 2009) where the preservation of the fingerprint of the injected gas was found suitable for tracing. Rapid changes in both O and C isotopes from the Ketzin Site (Germany) were explained by the interaction between injected CO₂ and reservoir water (Myrntinen et al., 2010).

Nimz and Hudson (2005) reported that a unique noble gas isotopic composition can be detected from production wells from the Mabee EOR field from West Texas (USA). In their work they proposed that Xe was the most favourable tracer due to the low volume required, cost and availability. Early attempts were also made by Kharaka et al. (2006) in the Frio Formation, Texas (USA), which was exposed to the injection of 1600 tonnes of CO₂. It was found that the water pH decreased rapidly due to CO₂ dissolution, and that the He and Ar concentrations increased from the injection to production wells.

Chemical tracers (e.g. deuterated methane, CD₄), SF₆, perfluorocarbons and heavy noble gases) have been added to injected gas in order to determine breakthrough time. SF₆ has been found to provide the most obvious evidence of breakthrough compared to Kr and CD₄ in the Otway CO₂ Project. It is because Kr had higher background level in the reservoir due to its atmospheric source and the amount of injected CD₄ seemed unsatisfactory (Stalker et al., 2015). It was also concluded that CD₄ could be used as tracer in a high CH₄ background environment. The experiment in the Cranfield (MS, USA) Detailed Area of Study (DAS) site on added Kr and SF₆ revealed significant heterogeneity in fluid flow and that the wells are connected through different pathways (Lu et al., 2012a). Kr was used as a

tracer in the Ketzin experiment and was found that its maximum peak intensity occurred hours before the maximum CO₂ peak (Giese et al., 2009). SF₆ and fluorescent indicator were injected into basalt within the CarbFix Project in Iceland (Matter et al., 2006).

Surface monitoring is equally as important as the subsurface monitoring because the ability to detect a leak from a CO₂ injection field is a key. Combined carbon and noble gas isotope research has been applied in the Weyburn CO₂-EOR field, revealing that there was no evidence of CO₂ migration from the oil field into the groundwater (Gilfillan and Haszeldine, 2011; Gilfillan et al., 2013). The same conclusion has been made by ‘process based’ methods (Romanak et al., 2012, 2013) and also there are recommendations on different geochemical tracers based on the Weyburn experiment (Risk et al., 2015). The isotopic composition of the injected CO₂ was found to be a suitable tracer if its isotopic composition is distinct from the reservoir gas (Mayer et al., 2015), while assessments of geochemical data from the Green River (Utah, USA) suggest combined use of water chemistry, $\delta^{13}\text{C}_{\text{CO}_2}$ and noble gases to study the migration and origin of the gas (Wilkinson et al., 2009).

1.5 Outline of this thesis

This work focuses on geochemical tracing of injected CO₂ at the Cranfield EOR field (MS, USA), the largest non-power plant associated CO₂ injection project currently in operation in the world. It is the first test of how well the naturally occurring noble gases in the injected CO₂ can be used as a low cost alternative to adding tracers.

Chapter 2 describes all aspects of the gas sampling and the analytical technique that was developed at SUERC in order to undertake the study.

Chapter 3 introduces the geology and injection history of the Cranfield EOR site and discusses the ability of existing and new $\delta^{13}\text{C}_{\text{CO}_2}$ data to trace the injected CO₂.

In Chapter 4 the noble gas compositions of the gas end-members are determined using Ne isotope composition of the production well gases. The ability of $^3\text{He}/^4\text{He}$, $^{40}\text{Ar}/^{36}\text{Ar}$ and $^{40}\text{Ar}^*/^4\text{He}$ to trace CO₂ is determined and the fate of the injected CO₂ is discussed.

In Chapter 5 the CO₂/³He ratio, along with the relationship of $^3\text{He}/^4\text{He}$ and $^{40}\text{Ar}^*/^4\text{He}$ and CO₂ concentration is used to identify and quantify the loss of CO₂ from the gas phase. The modelled fractionation of $^{40}\text{Ar}^*/^4\text{He}$ and $\delta^{13}\text{C}_{\text{CO}_2}$ constrain the process by which CO₂ is lost and the storage mechanism is discussed.

In Chapter 6 the non-radiogenic noble gas ratios ($^{20}\text{Ne}/^{36}\text{Ar}$, $^{84}\text{Kr}/^{36}\text{Ar}$ and $^{132}\text{Xe}/^{36}\text{Ar}$) are used to test the role of groundwater and oil. A model of gas stripping from groundwater and oil during CO₂-reservoir fluid contact is developed that can explain the noble gas data and better understand the oil displacement efficiency. The potential for reservoir engineering is discussed.

Chapter 7 synthesizes the results of this work and attempts to assess the potential for naturally occurring noble gases as tracers in commercial CCS projects.

Chapter 2

Gas sampling and analytical technique

2.1 Introduction

In this thesis the determination of the major gases (CO_2 , CH_4), $\delta^{13}\text{C}_{\text{CO}_2}$, and the isotope composition of noble gases in samples of high pressure gas from the Cranfield EOR site is reported. The first part of this chapter introduces the method of sampling gases in the field. The second part describes the analytical procedures. The analysis of noble gas isotopes from high pressure gas samples for this project required the design, construction and optimisation of a vacuum line for extraction and purification of gases from Cu tubes. The design of this was adapted and evolved from that used by Gilfillan et al. (2008) in Manchester, UK. Thus, the bulk of the chapter is devoted to reporting the noble gas measurement procedures.

2.2 Gas sampling technique

Samples were collected from high pressure wellheads or pipelines via sampling ports in internally polished ~70 cm long, ~6 mm internal diameter, refrigeration-grade copper tubes. The copper tube was retained in a metal holder with clamping devices at each end (Figure 2.1). Gas was collected at a pressure of ~0.15 MPa, providing a sample volume between the clamps approximately 10 cm^3 at STP. To collect samples a stainless steel step down regulator with a high pressure input (up to 2.1 MPa) and low pressure output (< 0.2 MPa) was connected to the pipeline or wellhead through a suitable adaptor. In the case of the bulkline, the CO_2 was supercritical, held around 21 MPa and 32°C (see supercritical condition in e.g. Suehiro et al., 1996). In the case of production wells, where oil, water and gas were present, samples had to be taken from the top of the pipeline in order to avoid

sampling liquid. Production wells were operating at pressures between 0.8 MPa and 9.1 MPa. The Cu tube was connected to the regulator through ~50 cm long, high pressure flexible tubing. Another hose was connected to the other end of the copper tube act as an exhaust in order to avoid backflow from air. Gas was allowed to flow through the line for at least 5 minutes then the downstream end was sealed by cold welding using the clamp. The pressure in the tube was adjusted to ~0.15 MPa and the upstream end of the tube was sealed. From production wells only one sample was collected, whereas from injectors and from the bulkline duplicate was taken. After sampling, the copper tubes were shipped back to the UK with clamps intact, retaining an atmosphere tight seal.



Figure 2.1. Sampling of high pressure gases by the Cu-tube method. Regulator is attached to the pipeline through a suitable adaptor. The Cu tube, kept in a metal holder, is attached to the regulator via a high pressure flexible hose. Gas is flushed through for ~5 minutes before clamps are closed. The clamps form a He tight cold welded seal on the copper tubes and the samples were stored in the Cu tubes until analysis.

2.3 Analytical technique

2.3.1 The gas inlet and purification line

The newly built gas inlet and purification system (Figure 2.2) is directly connected to a pre-existing purification line (Figure 2.3) (e.g. Codilean et al., 2008), which is linked directly to the noble gas mass spectrometer. The entire system is constructed of stainless steel tubing. The vast majority of the system is 16 mm internal diameter pipes connected via Cu-gasketed knife-edge seals. Only the ‘stable isotope section’ and some flexi tubes between that and the sample (Figure 2.2) are built from ~6 mm outer diameter pieces, connected by compression fittings. All-metal, bakeable valves are built in with either Cu sealing pad closure or Cu/stainless steel stem tip closure. The system is pumped to less than 10^{-8} mbar by two Pfeiffer Vacuum HiPace 80 turbo-molecular pumps. Pressure is monitored by a Pfeiffer Vacuum PKR 251 Compact Full Range pressure gauge. The pumping line is constructed from 35 mm internal diameter stainless steel pipe. The volume of each section was determined by inert gas expansions and consequent pressure measurements and is known to $\pm 0.5\%$ (1σ). The system is held at $\sim 150^\circ\text{C}$ using heating tapes when not in use in order to remove adhering gases. Analyses are conducted with the line at $\sim 35^\circ\text{C}$.

Cu tubes are connected to the vacuum system by Swagelok compression fitting and the volume between the clamp and the first valve of the vacuum system is pumped to ultra-high vacuum (UHV). The clamp from the Cu tube is removed and the gas is expanded into a $\sim 20\text{ cm}^3$ volume. In some cases a proportion of the sample ($\sim 5\text{ cm}^3$) is stored for stable isotope analysis. In this case the gas is transferred into a glass tube by liquid nitrogen where CO_2 is separated from hydrocarbon gases cryogenically using a procedure modified after Kusakabe (2005) and Robinson and Kusakabe (1975). The separation is undertaken at the freezing point of iso-pentane ($\sim -160^\circ\text{C}$), where the CH_4 fully and C_3H_8 partially remains in the vapour phase, and these gases are then pumped away while the CO_2 remains

absorbed onto the cold finger (Dean, 1998; Levenson, 1974). The isotopic composition of the remaining CO₂ is determined by an isotope ratio mass spectrometer (IRMS) (see 2.3.2.3).

A ~1 cm³ aliquot of gas is expanded into a volume where the pressure is measured by an MKS 615-A Baratron capacitance manometer. Small fractions of the gas are taken from the pressure gauge volume and the major gas composition determined by a Pfeiffer Vacuum 200 quadrupole mass spectrometer (QMS) (see 2.3.2.2). The majority of the gas is then expanded into a VG Scienta ST22 titanium sublimation pump to remove active gases (e.g. H₂, H₂O, CO₂, N₂) and thermally cracks hydrocarbon molecules (e.g. CH₄). It runs sequentially between ~900°C and cold water temperatures until the pressure drops below ~1 mTorr in the manometer. The purified gas is then exposed to a SAES GP50 ZrAl alloy getter (high specific surface adsorbent) held at 250°C, and then expanded into a 500 cm³ reservoir where it is stored for noble gas isotope analysis (Figure 2.3). Concentrations of ⁴He, ²⁰Ne, ⁴⁰Ar and ⁸⁴Kr are determined on the QMS using the remaining gas in the line in order to determine the optimum amount to take from the reservoir to the noble gas mass spectrometer. The heavy noble gases (Ar, Kr, Xe) are trapped on liquid nitrogen-cooled charcoal and ⁴He and ²⁰Ne are measured. After measurements, they are pumped out of the mass spectrometer, the charcoal heated to room temperature and ⁴⁰Ar and ⁸⁴Kr are measured.

The quantitative noble gas analysis is carried out on the gas trapped in the noble gas reservoir. For each noble gas, a separate aliquot of gas is taken out except for Kr and Xe, which are measured from a single aliquot. For helium, an aliquot of gas is taken from the tank and purified by exposure to two SAES GP50 ZrAl alloy getters held at 250°C then liquid nitrogen cooled charcoal for 20 minutes, and then analysis is performed. Samples for Ne analysis were purified as per He, and the Ne is trapped by a cryogenic activated charcoal finger at -243°C for 20 minutes. He is removed by the pump and the Ne released

at -173°C for 15 minutes prior to analysis. For argon analysis a new gas aliquot is taken and purified as per He, and as a consequence Ar remains trapped on the charcoal. He and Ne are removed by the pump and Ar is then desorbed from the charcoal by heating to room temperature for 15 minutes and analysis is then performed. Lastly an aliquot is taken for Kr and Xe. It is cleaned as per the procedure for Ar up to the point of pumping away the He and Ne. Then the liquid nitrogen cooled charcoal is warmed up to -80°C by acetone–dry ice slush for 15 minutes and the gas is analysed. This step releases $\sim 100\%$ of Ar, $\sim 15\%$ of Kr and $\sim 5\%$ of Xe. Then the charcoal is warmed up to $\sim 80^{\circ}\text{C}$ by hot water for 15 minutes that desorbs all remaining heavy noble gases which are then analysed. The sum of the two intensities of Kr and Xe from each run is used in interpretations. Quantity of aliquots in all cases is pre-determined by the QMS.

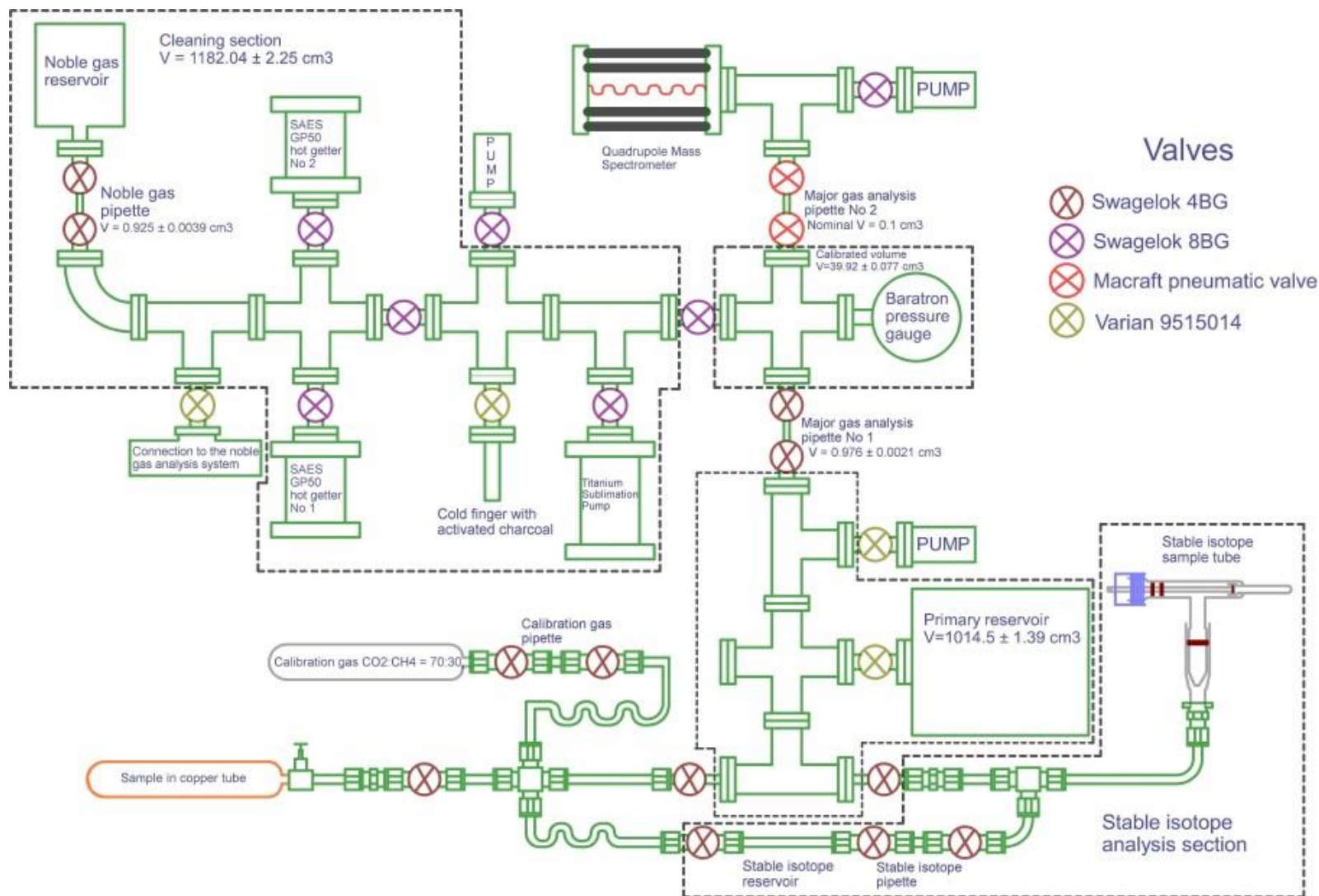


Figure 2.2. Schematic picture of the noble gas extraction line. Green line: Stainless steel piping; Grey line: Glass; Orange line: Copper; Black line: Representation of quadrupole rod; Claret line: Rubber sealing; Red line: Representation of ion beam; Blue line: Teflon; Crossed circles: Valves.

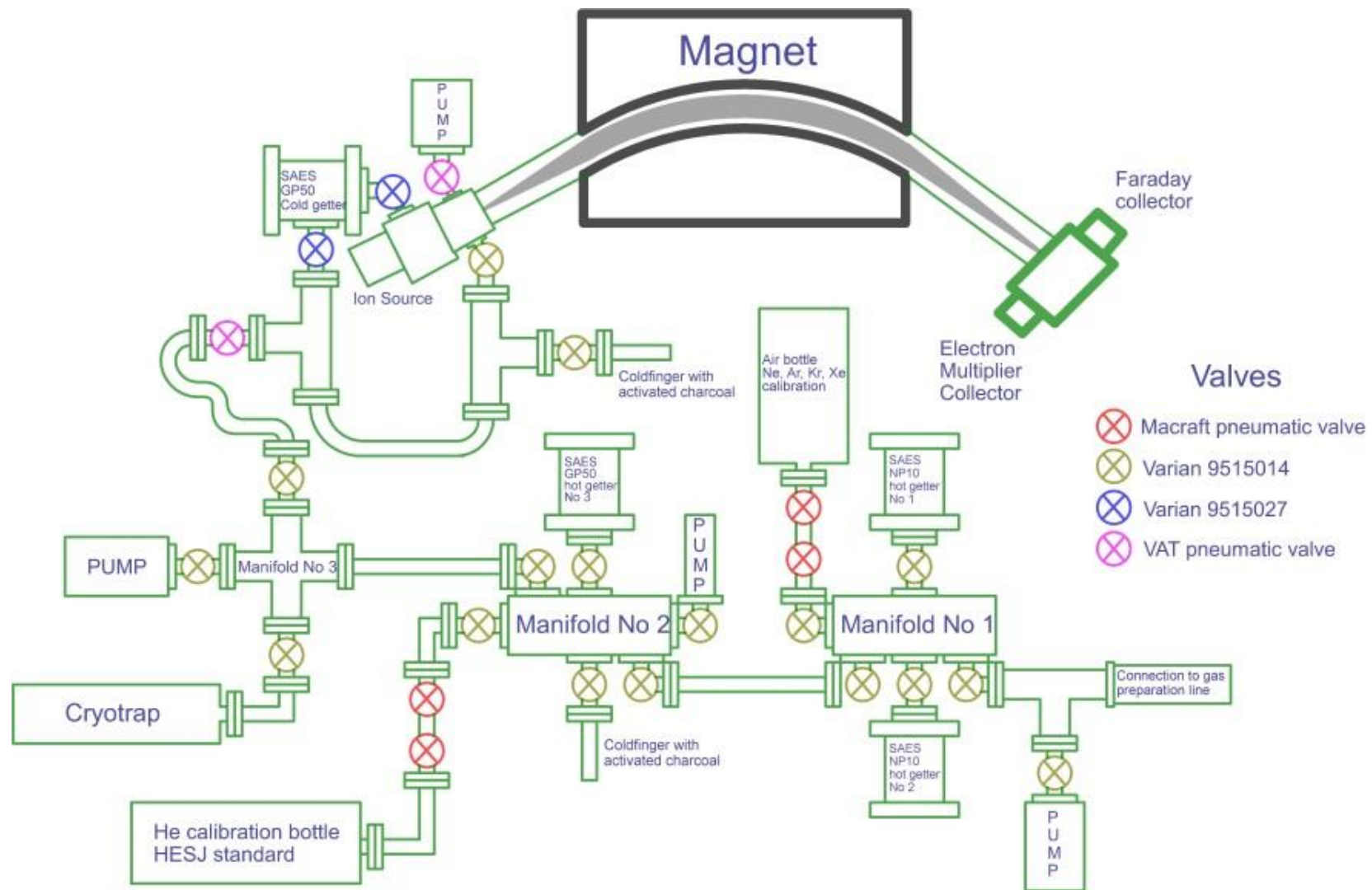


Figure 2.3. Diagram of the pre-existing noble gas purification line. Green line: Stainless steel piping; Black line: Magnet; Grey line: Representation of ion beam. Crossed circles: Valves.

2.3.2 Gas analysis procedure

2.3.2.1 Major gas composition determination

All Cranfield samples are CO₂–CH₄ mixtures with trace concentrations of nitrogen, heavy hydrocarbons, oxygen and hydrogen (Lu et al., 2012b). There may be a small quantity of H₂S as well, originating from Jackson Dome (Zhou et al., 2012). The absolute sensitivity of the QMS for CO₂ and CH₄ is dependent upon their respective concentrations and the total pressure, and is independent of the trace gases (as long as the source parameters were not changed during the analytical period). The instrument was calibrated by determining the CO₂/CH₄ ratio of several different known binary mixtures at different total pressures. Gas pressures were manipulated to ensure all measurements fell within the range of pressure calibration. The results are plotted in Figure 2.4. (see data in Table I.1. in the Appendix). The 44/15 ratio remains largely unchanged within the observed pressure interval if the CO₂ concentration is between 30 and 96%. There is however an observable slope in both, 100% CO₂ and CH₄ concentrations on the diagram.

Calibration gases were supplied by Air Products Inc. The reproducibility of CO₂/CH₄ ratio measurements was $\pm 1\%$ (1σ). Both, CO₂ and CH₄ were measured on the Faraday cup, at mass 44 and 15 respectively, in static mode. Blanks were continuously monitored and found negligible at all times. A 70% CO₂ – 30% CH₄ reservoir was permanently attached to the UHV system and used to check calibrations throughout the analysis period. Initially its 44/15 ratio was accurately determined at a gas concentration of $3 \times 10^{-5} \text{ cm}^3 \text{ STP}$ and was found to be 1.688 ± 0.02 (standard conditions are after Ozima and Podosek, 2001).

Later measurements show no variation at all, implying that the QMS performance was stable with time (Figure 2.5) (see data in Table I.2. in the Appendix). The gas composition of samples was calculated by linear interpolation.

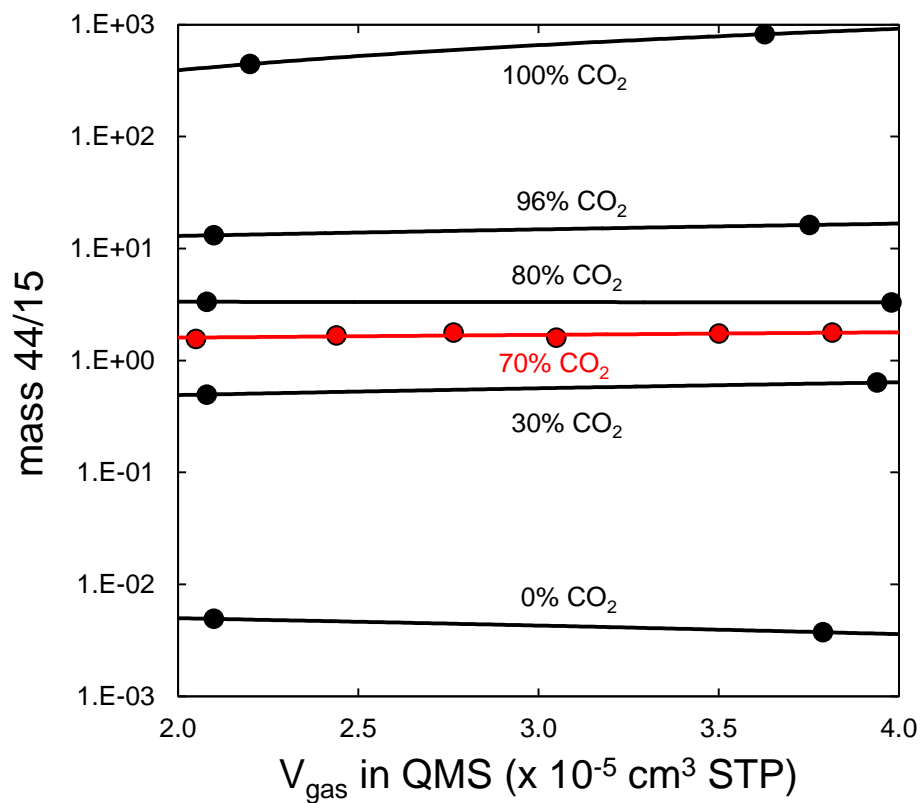


Figure 2.4. Calibration of the mass 44/15 (CO_2/CH_4) ratio on the quadrupole mass spectrometer. Calibration was undertaken with different $\text{CO}_2\text{-CH}_4$ binary mixtures at two different total pressures except for the mixture with 70% CO_2 (red line). That special mixture, permanently attached to the UHV system served the purpose to track changes with time (see Figure 2.5). The composition of a sample between two end-members is calculated by linear interpolation.

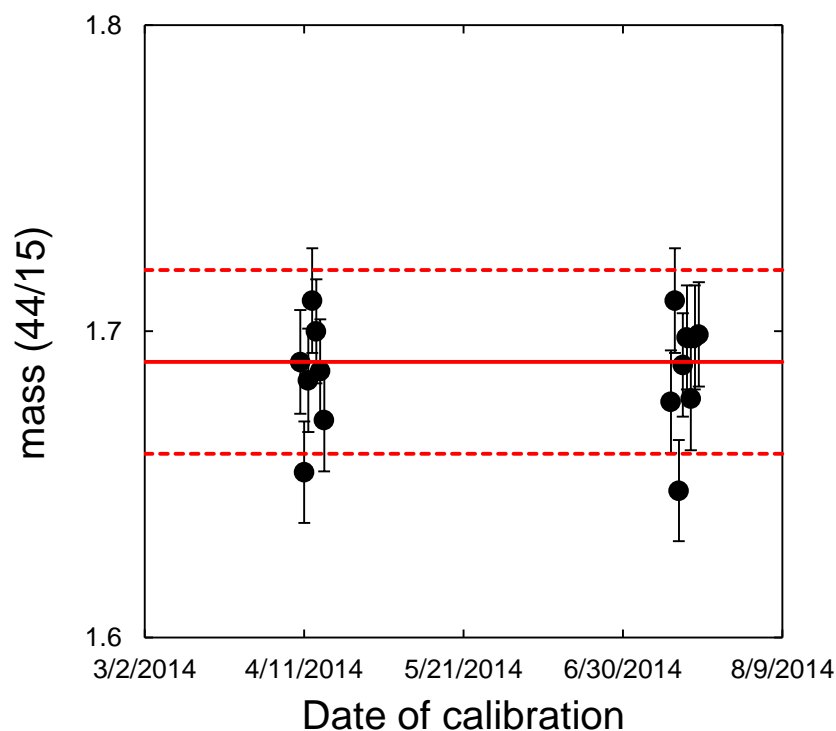


Figure 2.5. The stability of the QMS with respect to 44/15 over time. It was monitored by a binary mixture (70% CO₂ – 30% CH₄). Data are calculated to $V_{\text{gas}} = 3 \times 10^{-5} \text{ cm}^3 \text{ STP}$ gas amount. Red continuous line: original calibration, red dashed line: its 1σ uncertainty. Black: Re-calibration data. Data point's uncertainties are 1σ . Short term variation (days) are within the pre-determined range in both analytical sessions (April and July, 2014). This rules out long term variations (months) and indicates that the QMS is stable over time.

2.3.2.2 QMS determination of noble gas concentrations

Prior to analysing the noble gas isotope composition, concentrations were determined on the QMS in static mode. ⁴He and ²⁰Ne were measured on both Faraday and channeltron detectors, ⁴⁰Ar was measured on the Faraday, and ⁸⁴Kr on the channeltron. The channeltron was operated at 2.0 kV. Blanks were negligible throughout the analytical period, but required significant effort in the early stages. Figure 2.6 illustrates the relationship between the measured ⁸⁴Kr intensity on the QMS relative to the amount of gas let in, and the theoretical ⁸⁴Kr signal on the noble gas mass spectrometer (MAP, see section 2.3.2.4) by

taking one gas aliquot from the noble gas reservoir (see Figure 2.2) (see data in Table I.3. in the Appendix). The data define a straight line as expected but there are severe deviations from it in some cases. This is explained by the QMS not being tuned for noble gas analysis but for the precise determination of CO₂/CH₄ ratio, hence the noble gas measurements on the QMS carry significant uncertainties.

2.3.2.3 Carbon isotope determination

A VG Optima dual inlet isotope ratios mass spectrometer was used in dynamic mode to determine $\delta^{13}\text{C}_{\text{CO}_2}$ relative to PDB international standard (Craig, 1957) based on

Equation 2.1

$$\delta^{13}\text{C} = \left(\frac{(\text{}^{13}\text{C}/\text{}^{12}\text{C})_{\text{sample}}}{(\text{}^{13}\text{C}/\text{}^{12}\text{C})_{\text{standard}}} - 1 \right) 1000 \quad \text{Equation 2.1}$$

according to established procedures (e.g. Bezard et al., 2014). The vacuum system is established by an Edward rotary pump (low vacuum) and by a Balzer turbo molecular pump (high vacuum). Pressure is monitored by a PVG1 Pirani gauge and a VIG24 ion gauge, respectively. The ionization occurs by electron impact, and for detection a Faraday cup is used. The dual inlet system ensures identical flow rates of both the reference gas and the sample removing the need of a calibration curve with respect to total pressure. The gas inlet system is fully automated once samples are attached to the manifold. The internal reproducibility was found ~0.02 ‰. In order to track external reproducibility, aliquots of the calibration gas, permanently attached to the newly built inlet system were prepared frequently and measured by the IRMS.

The mean $\delta^{13}\text{C}_{\text{CO}_2}$ of the calibration gas was found to be -33.3 ‰ and showed 0.2 ‰ reproducibility (1σ). Thereafter the calibration gas was measured prior to each batch of sample and showed only slight shift from the mean value in the short term (days), which

allowed all samples to be corrected (Figure 2.7) (see data in . Long term (months) variation was not observed. The reproducibility of the calibration gas is taken as the uncertainty of all sample measurements.

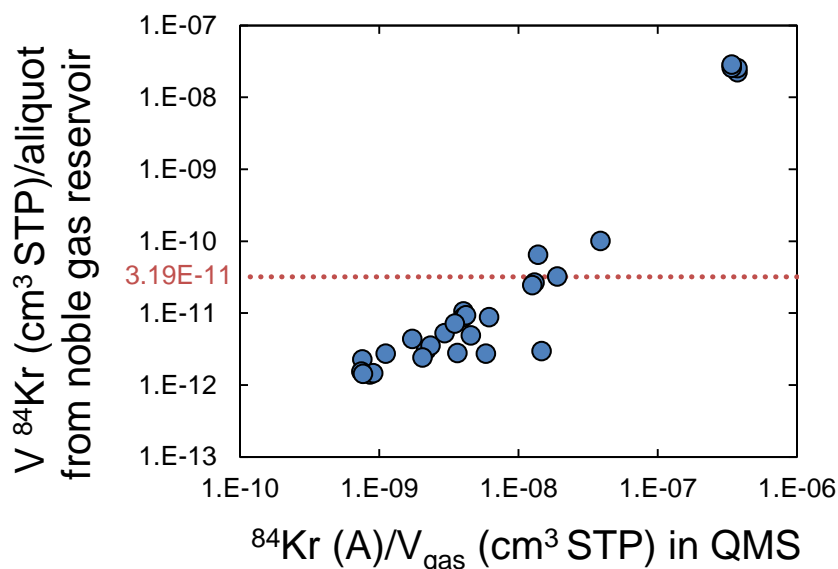


Figure 2.6. The expected amount of ^{84}Kr in the noble gas mass spectrometer and the ^{84}Kr signal/amount of gas in the QMS. The figure contains a wide selection of samples, from magmatic (low ^{84}Kr) to air-like gases (high ^{84}Kr) Blue: samples; Red dashed line: Amount of ^{84}Kr in the calibration bottle. All other major noble gas isotopes measured on the QMS showed similar relationship and allowed the necessary amount of gas let in to the noble gas mass spectrometer to be calculated. Uncertainties are not shown because data do not reflect the result of quantitative measurements. Highest uncertainty is introduced by the QMS measurement due to the set up for other (CO_2/CH_4) analysis and it explains deviation from non-linearity.

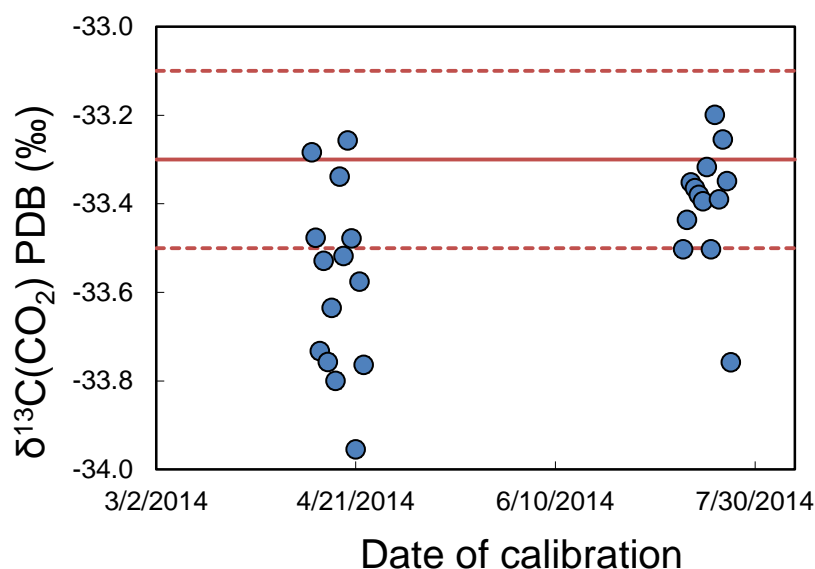


Figure 2.7. The variability of the measured $\delta^{13}\text{C}_{\text{CO}_2}$ of the calibration gas over time. Calibration measurements (blue) varied more than the reproducibility (red dashed line) (0.2 ‰) of the mean value (red continuous line) therefore calibration gas was run with all samples.

2.3.2.4 Noble gas isotope ratio and concentration measurements

Noble gas isotope measurements were carried out by a Mass Analyser Product (MAP) 215-50 mass spectrometer operating, in static mode. It is a dual collector 50° magnetic sector mass spectrometer, equipped with a 10^{11} Ohm resistor Faraday cup and a Burle Channeltron electron multiplier operated in pulse counting mode at 2.5 kV. The source was operated at 3 kV acceleration potential and 300 μA trap current. ^4He , and all Ar isotopes were measured on the Faraday detector while ^3He , ^{20}Ne , ^{21}Ne , ^{22}Ne , ^{84}Kr and ^{132}Xe on the electron multiplier. During He and Ne isotope analysis liquid nitrogen-cooled charcoal was used to remove residual heavy noble gases and active gases from the mass spectrometer. The level of hydrogen was minimised by a cold GP50 getter (Figure 2.3).

The resolving power (~ 600) allowed complete resolution of $^3\text{He}^+$ from $\text{H}_3\text{-HD}^+$. Isobaric interferences at $^{20}\text{Ne}^+$ from $^{40}\text{Ar}^{2+}$ and at $^{22}\text{Ne}^+$ from $^{44}\text{CO}_2^{2+}$ were corrected, in the absence

of the required resolution of as high as 1777 and 6231, respectively. Correction was completed by continuous monitoring of the ratios of $40^+/40^{2+}$ and $44^+/44^{2+}$ with respect to the concentration of hydrogen and by measuring H_2^+ , 40^+ and 44^+ with neon. Isobaric interferences from $^1H^{19}F^+$ and $^1H_2^{18}O^+$ at ^{20}Ne and from $^{63}Cu^{3+}$ at ^{21}Ne (required resolution 1450, 894 and 1212 respectively) were typically less than 0.001% of total ^{20}Ne and 0.01% of total ^{21}Ne (see also Vermeesch et al., 2015).

Mass fractionation during the isotope ratio measurements were determined by repeated determinations of standard gases. Helium isotope determinations were calibrated using the HESJ international standard (20.63 R_A ; Matsuda et al. 2002). Calibration gas was measured prior to each measurement because the calibration data showed significant variation in comparison to each other (Figure 2.8).

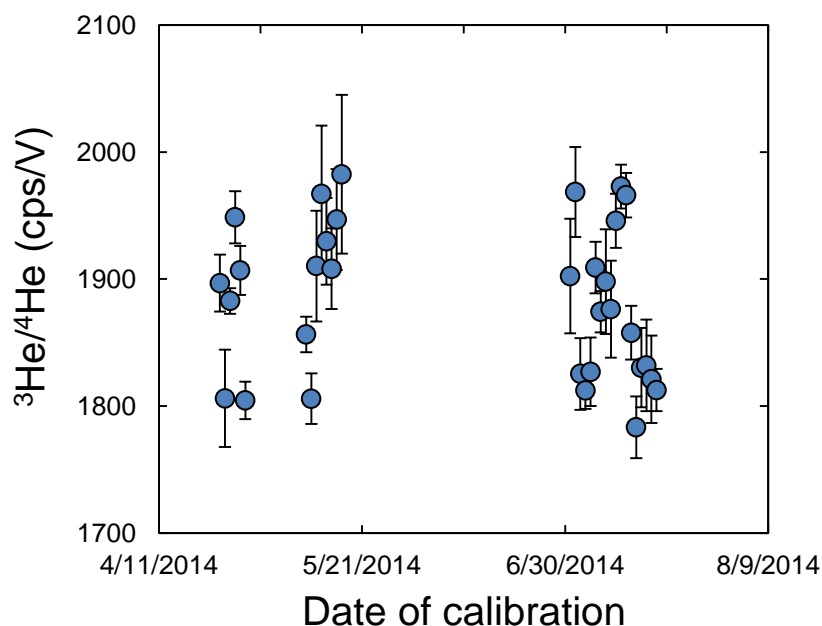


Figure 2.8. He isotopic ratio data of the calibration gas. Data show significant changes with time compared to the reproducibility (0.99%, see text) therefore a calibration was measured before each sample. Uncertainties are 1σ . Cps = counts per second.

This short term variation (days) is explained by the changes in the sensitivity of the multiplier and changes in the ion-source. Both are expected results of continuously exposing the ion source and multiplier to small quantities of hydrocarbon gases. However several consecutive measurement allowed the reproducibility to be determined and was found 0.99% for the $^3\text{He}/^4\text{He}$ ratio. It is a little lower than what was found on the same type of instrument (2.5%; Stuart and Turner 1992) and is explained by the much higher signal of ^3He in our case than in their work where air was used as standard. Long term (months) variation was not observed during the analytical period (see data in Table I.5. in the Appendix).

Mass discrimination of Ne and Ar isotopes were determined using air (Eberhardt et al., 1965; Mark et al., 2011; Ozima and Podosek, 2001). ^{20}Ne and ^{21}Ne , relative to ^{22}Ne is plotted against each other in Figure 2.9 (see data in Table I.6. in the Appendix). The variability of data is typical for the kind of mass spectrometer in the long term (days). All data are significantly off the mass fractionation line. That is most likely the result of an overcorrection on mass 22 (see above) or, less likely kinetic (mass independent) fractionation (personal communication with F. Stuart). Ne calibrations were run less frequently than He. Reproducibility of $^{20}\text{Ne}/^{22}\text{Ne}$ and $^{21}\text{Ne}/^{22}\text{Ne}$ was found 0.40 and 0.94% respectively.

The argon calibration data are shown in Figure 2.10 (see data in Table I.7. in the Appendix). Data are fractionated compared to air. The composition of air is after Mark et al. (2011). Fractionated values overlap with the mass fractionation line. Ar calibration was carried out on a daily basis. Reproducibility of $^{40}\text{Ar}/^{36}\text{Ar}$ and $^{38}\text{Ar}/^{36}\text{Ar}$ was found 0.62% and 0.84% respectively, which is in a good agreement with Renne et al. (2009) from the same type of mass spectrometer.

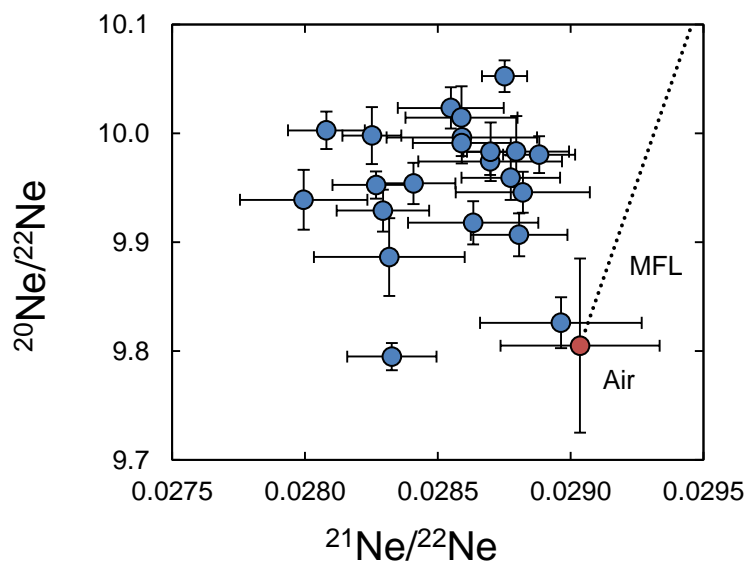


Figure 2.9. Ne isotope data from the calibration bottle compared to air. Data (blue) show fractionation compared to air (red) and they are significantly off the mass fractionation line (MFL). The variation of the data is typical for the MAP 215 mass spectrometer measurements. Uncertainties are 1σ .

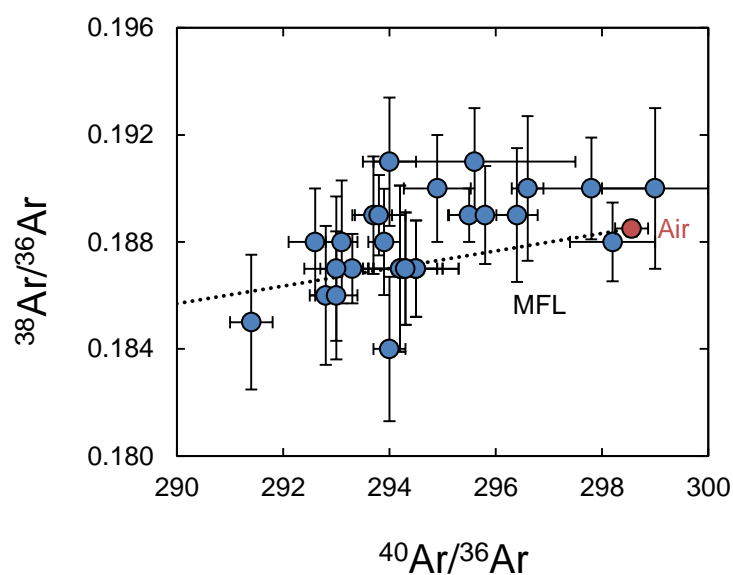


Figure 2.10. Fractionation of Ar isotopes in the calibration gas compared to air. Calibration data (blue) show fractionation compared to air (red) and they mostly overlap with the mass fractionation line (MFL) within uncertainty. Observed data are typical for MAP 215 type noble gas mass spectrometer. Uncertainties are 1σ .

As only one isotope of Kr and Xe were measured the $^{84}\text{Kr}/^{132}\text{Xe}$ ratio was monitored to track changes in the sensitivity of any of the compounds. A series of measurements are shown in Figure 2.11 (see data in Table I.8 in the Appendix). All measured data overlap with each other within 1σ uncertainty, indicating a stable system. All data are much below the air value (after Basford et al., 1973), which is explained by the fact that efficiency of ionization is different for Kr and Xe during the analysis. The reproducibility of the ratio is $\sim 5.1\%$ but not relevant as the individual concentration's uncertainty is the key (see below).

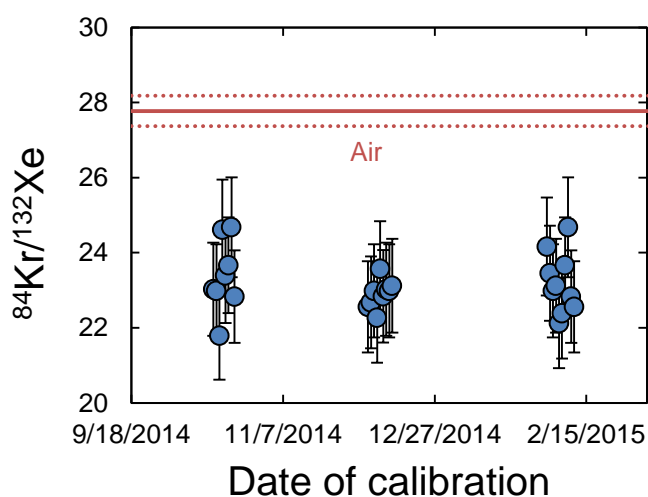


Figure 2.11. The variation of the ratio of ^{84}Kr and ^{132}Xe of the calibration gas. Measured ratios (blue) are mostly within a narrow range, with spikes occurring only occasionally. Air composition (continuous red line) and its 1σ uncertainty (red dashed line) are shown for reference. Data uncertainties are 1σ . Data points are well below the air ratio, which is explained by the different ionization efficiencies of the different elements in the ion source.

The absolute sensitivity of all isotopes was measured prior to each analysis. The absolute concentration of ^4He in the He calibration bottle was based on repeated analysis of cosmogenic ^3He from the CRONUS-P pyroxene international standard. This allowed the ^3He (and consequently ^4He) concentration determination no better than 2.8% (1σ) (Blard et

al., 2015). The air bottle was calibrated with two standards, CREU-1 quartz for cosmogenic ^{21}Ne (Vermeesch et al., 2015) and GA1550 biotite for radiogenic ^{40}Ar (McDougall and Wellman, 2011) in order to check elemental fractionation. Results of both calibrations are shown on Figure 2.12 and demonstrate that the calculated ^{40}Ar concentration from both methods overlap substantially with 2σ uncertainty, therefore fractionation (if it occurred at all) can be considered negligible (see data in Table I.9. in the Appendix). For concentration determinations of all isotopes (except He) the CREU-1 quartz was used, meaning that their uncertainty is not better than 3.6% (1σ).

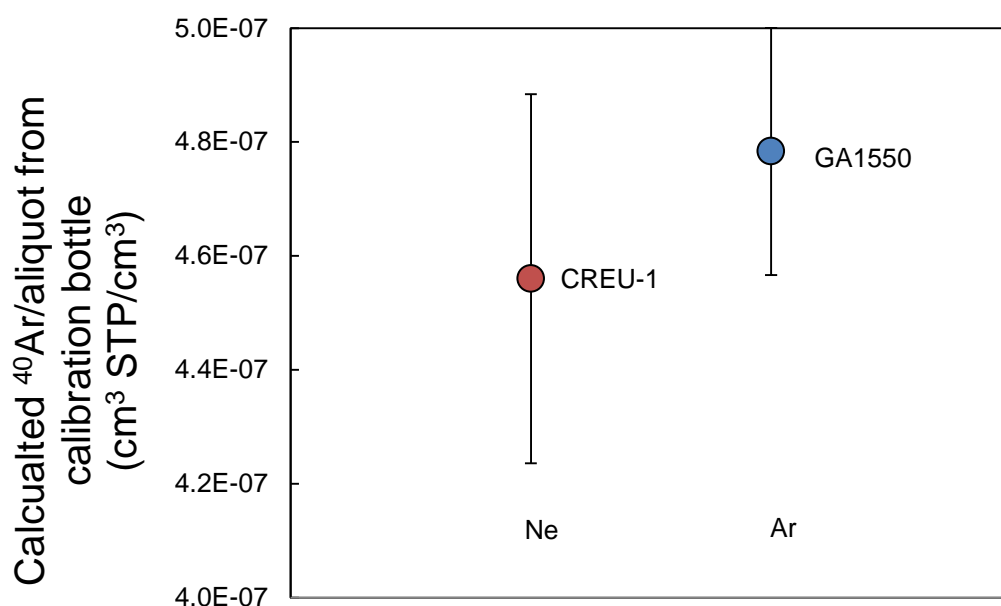


Figure 2.12. The calculated concentration of ^{40}Ar / aliquot from the calibration bottle from two different international standards. Results well overlap with 2σ uncertainty therefore elemental fractionation in the calibration bottle can be ruled out.

Blank measurements were performed on a weekly basis by the same procedure as for samples. Blanks were routinely analysed without connecting a Cu-tube in order to minimise the risk of measuring a sample-derived gas leaking through the crimped tube.

Cu-tube blanks were measured twice during the analytical period and no significant difference was observed compared to the routine method. The blank intensity of all isotopes was typically less than 0.1% of that measured in samples. This is more than an order of magnitude less than the uncertainty of the measurement from any sample and can be considered negligible.

2.4 Commissioning and testing of the new system

The new system and procedures were checked with analysis of two “knowns” i) air and ii) Jackson Dome CO₂ (Zhou et al., 2012 & unpublished data from S. Gilfillan). The composition of Jackson Dome is discussed in detail in 4.2.1.

Air samples were taken by Cu tubes (see 2.2 in this chapter) at 0°C, at 188 m above sea level under 60 % relative humidity in East Kilbride, Scotland. Theoretical noble gas concentrations were calculated from the standard data given for dry air at sea level (see references above) after Kipfer et al. (2002). There is no significant difference between measured and calculated air He, Ne and Ar isotope ratios. Measured concentrations of He, Ne and Xe overlap with 2 σ uncertainty but measured Ar and Kr is higher than air (Table 2.1). This could be explained by an artefact, which could not be tracked due to the small number of measurements (n = 2). Also, very significant sub sampling had to be applied as a result of the large volume of the smallest aliquot that could be let in into the mass spectrometer by the standard procedure for Ne, Ar, Kr and Xe analysis. This results in 98.5% of the aliquot having to be pumped away, which undoubtedly introduces an uncertainty and is not taken into account. The experiment, although it cannot be considered a validation for the system, demonstrates that isotopic ratios can well be reproduced from deep magmatic (Jackson Dome) to air-like gases, but there may be a large increase in the uncertainty when significant sub-sampling is applied. Nevertheless, this is not an issue in

the measurements from Cranfield as the system was designed to have no need for sub-sampling for these samples.

Table 2.1. Comparison between the theoretical and measured composition of air. Concentrations are in ppm and fraction of volume. 2σ uncertainties are in brackets.

	Theoretical composition	Measured composition
^4He	5.11 (10)	5.42 (42)
$^3\text{He}/^4\text{He}$	1.000 (18)	1.02 (15)
^{20}Ne ($\times 10^1$)	1.604 (8)	1.744 (180)
$^{20}\text{Ne}/^{22}\text{Ne}$	9.805 (160)	9.769 (212)
$^{21}\text{Ne}/^{22}\text{Ne}$	0.0290 (6)	0.0286 (12)
^{40}Ar	9068 (20)	10006 (770)
$^{40}\text{Ar}/^{36}\text{Ar}$ ($\times 10^1$)	29.856 (62)	29.78 (38)
$^{38}\text{Ar}/^{36}\text{Ar}$	0.1885 (6)	0.187 (28)
^{84}Kr	0.633 (12)	0.75 (4)
^{132}Xe	0.0234 (6)	0.026 (2)

Chapter 3

The Cranfield EOR field and tracing CO₂ by $\delta^{13}\text{C}_{\text{CO}_2}$

3.1 Introduction

This chapter describes the geology of the Cranfield enhanced oil recovery field and gives an introduction to the history of hydrocarbon extraction. This is followed by a review of the CO₂ injection schedule and its development from the start of injection until the last sampling campaign for this study. Previous geochemical tracing studies at the site, which includes the application of both natural and artificial tracers, are considered. Lastly the CO₂ concentration and $\delta^{13}\text{C}_{\text{CO}_2}$ measurements from this study are shown and put into the context of CO₂ tracing.

3.2 The Cranfield field

The Cranfield oil and gas field is located ~20 km east of the Mississippi river (Figure 3.1) close to the town of Natchez in south western Mississippi, USA. The field varies between 60 and 120 m above sea level and sits on a SE-NW directed normal fault that divides the reservoir into two parts. The oil and gas reservoir, the target reservoir for CO₂ injection, is a circular (diameter is ~6.4 km), four-way anticline of highly permeable fluvial sediments in the Upper Cretaceous Lower Tuscaloosa Formation, locally called the 'D-E' units. The reservoir rock is largely 15-25 m thick unit of conglomerates, sandstones and muddy sandstones that occurs at ~3,000 m below surface level (Hosseini et al., 2013; Lu et al., 2012b). The base and the top of the injection zone unit consists of low permeability terrestrial mudstone (Hovorka et al., 2013). Figure 3.2 shows the stratigraphic column of the Cranfield region after Lu et al. (2013) and shows drill core samples taken from the injection zone (Gilfillan et al., 2011).

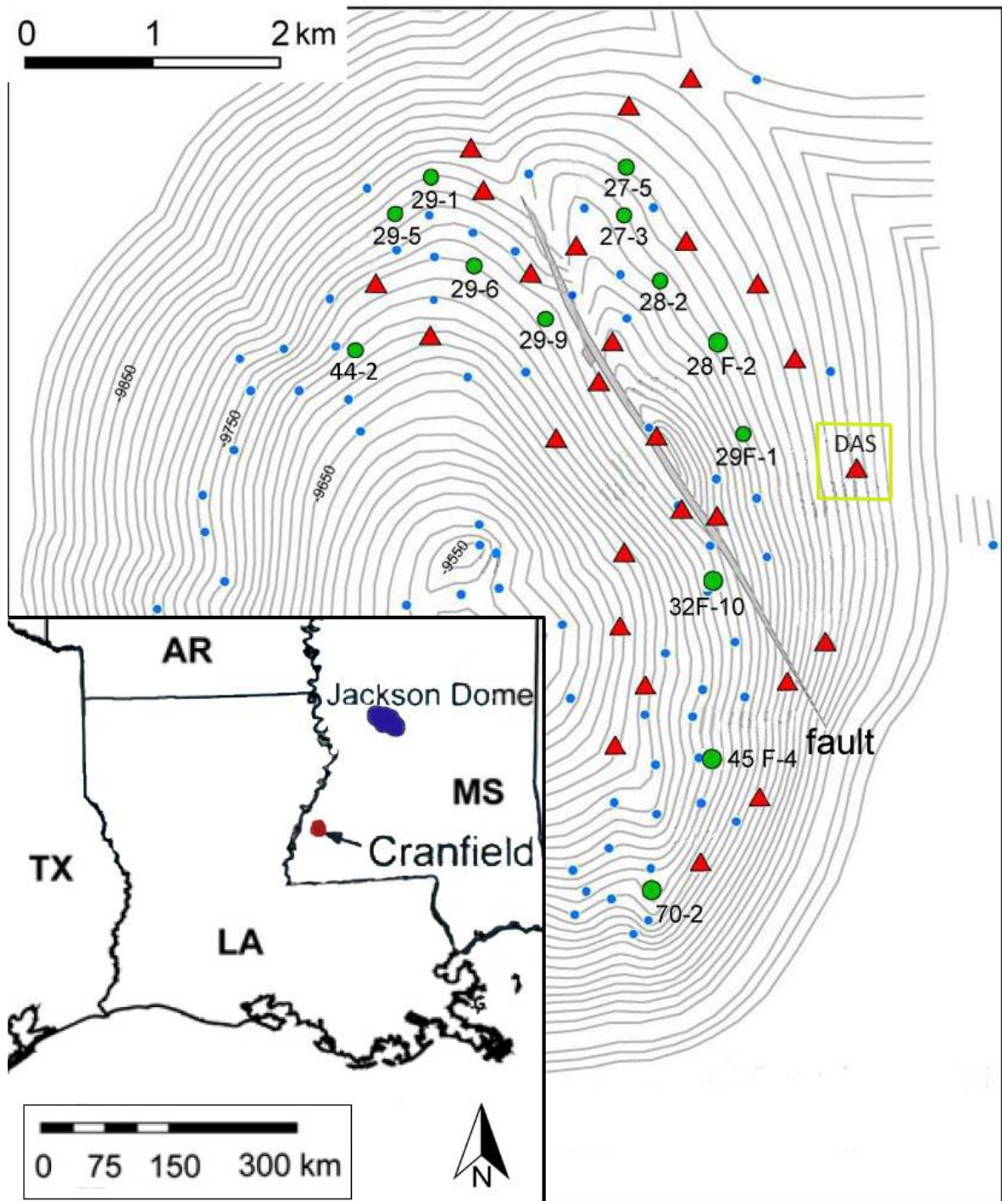


Figure 3.1. The map of the Cranfield EOR field in Mississippi, USA. The contour shows the depth of the oil-water contact (feet). Distribution of injection wells (red triangle) and production wells (green circles) are as per located on the surface. Only those production wells are shown that have been sampled for this study. Unsampled wells are shown as small blue circles. The inset figure shows the location of the Cranfield site relative to the Jackson Dome field, which is the source of the injected CO₂. DAS: Detailed Area of Study (see text). Redrawn after Lu et al. (2012b).

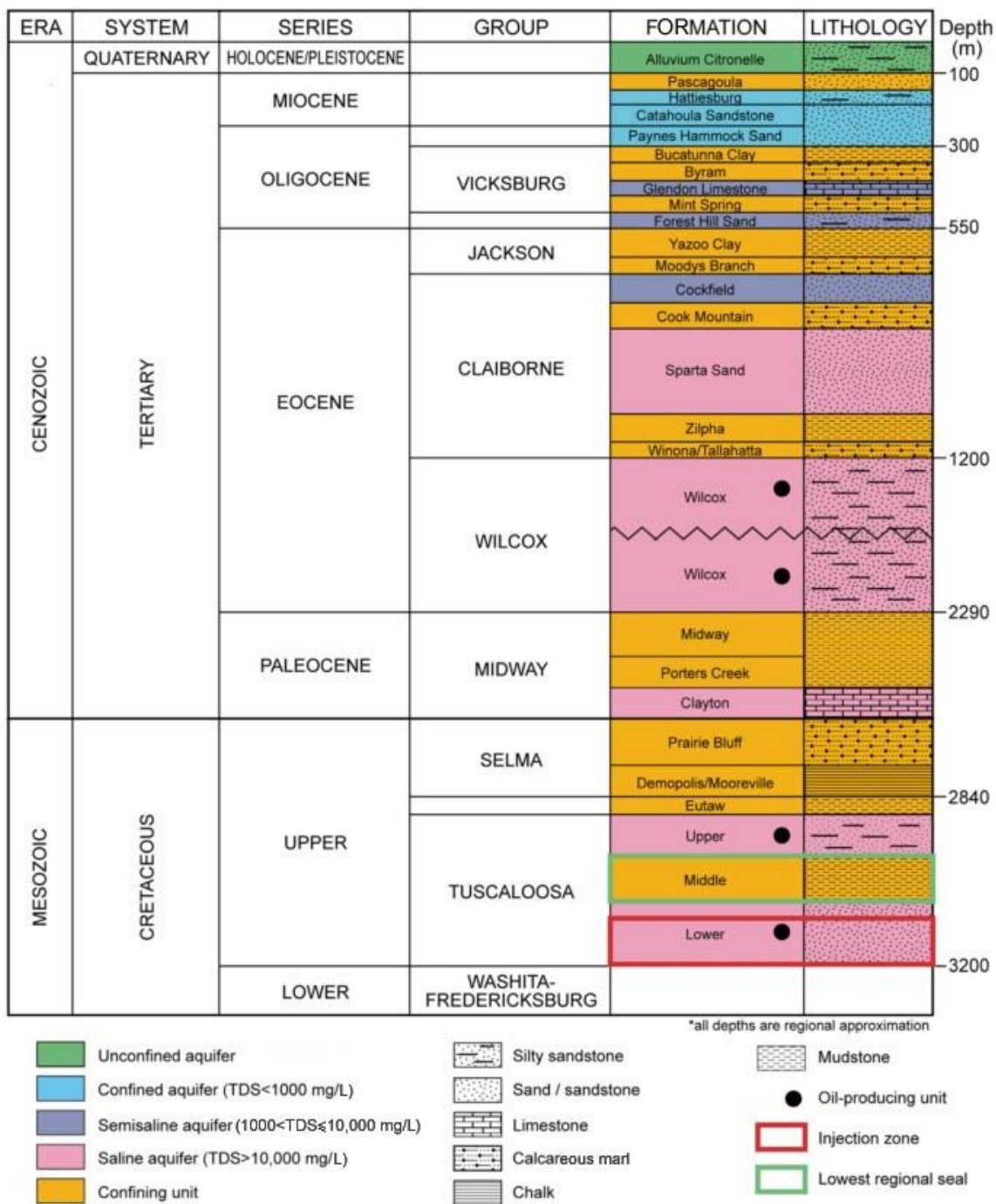


Figure 3.2. Stratigraphic column of the region of Cranfield, MS, USA. Modified after Lu et al. (2013).

Channel deposits are present in core samples taken by Lu et al. (2012b), that are similar to those described by Stancliffe and Adams (1986). These may introduce significant heterogeneity in the fluid flow and provides a major uncertainty in fluid-flow modelling (Hosseini et al., 2013; Lu et al., 2012a).

The reservoir was discovered in 1943 by California Company (Dudley, 1993) and oil and gas production commenced in the following year. The field has an associated gas cap and down-dip oil ring. The field was considered depleted for primary recovery by 1959. After unsuccessful water injection tests for secondary recovery in the NW part of the reservoir in 1958-59, the field was abandoned in 1966.

CO₂ injection for EOR started in July 2008 by Denbury Resources Incorporated. Injection started at the north part of the oil field through 6 injectors (Figure 3.1). The development of injection and production wells has been undertaken in several phases and has followed a clockwise pattern. By the time of the December 2009 sampling campaign for this study (after 18 months of CO₂ injection) the N and NE sections were in operation. In early 2011 24 injectors were in operation and had increased to 29 by March 2012 (45 months of CO₂ injection), when the second sampling campaign took place. That meant the E and SE part of the field was fully covered (Hovorka et al., 2013) and sampled. The amount of injected CO₂ has progressively increased with time. By April 2010 the rate of injection reached one million metric tonnes per annum (Hovorka et al., 2013) and as of January 2015 it was 1.5 Mt/year. This makes Cranfield the world's largest CO₂ injection project for non-power plant CCS projects (Carbon Capture & Sequestration Technologies, 2015).

Gas, water and oil are extracted from the production wells. The oil is removed, the water is disposed onsite and the gas (CO₂ and CH₄) is mixed with incoming CO₂ and re-injected (this is termed recycled gas). Between July 2009 and January 2013 the proportion of recycled gas in the injected gas had increased from ~9 to ~30% (Choi et al., 2013; Hovorka

et al., 2013). By 2013 the total injected gas (including recycled gas) reached 6.8 Mt, from which 4 Mt had been retained in the reservoir (Hovorka et al., 2013).

The high purity (99%) CO₂ used in the process is pumped from the Jackson Dome deposit in central Mississippi (Figure 3.1). The gas is transported via pipeline (referred to as bulkline) ~160 km to Cranfield. The CO₂ is kept under supercritical conditions during transport. The Jackson Dome deposit is one of the world's deepest commercial CO₂ deposits, with the main reservoirs lying at between 4,270 and 5,180 m (Zhou et al., 2012). Approximately 2.8×10^{10} m³ of gas is present in the deposit (Studlick et al., 1987) supplying approximately 1.6×10^6 m³/day for mostly nearby EOR projects (Zhou et al., 2012). The name 'Jackson Dome' refers to a Late Cretaceous igneous intrusion (Baksi, 1997). The regional geology is described in e.g. Studlick et al. (1990) and the local geology is summarized in Zhou et al. (2012). The Jackson Dome gas is 98-99% CO₂ with minor nitrogen, H₂S and methane. A recent noble gas study has shown a strong contribution from the mantle as the origin of the gas with ³He/⁴He ratios between 4.27 and 5.01 R_A (Zhou et al., 2012).

Prior to injection the Cranfield reservoir regained hydrostatic pressure by groundwater recovery over the four decades of abandonment. The continuous CO₂ injection with no water injection means that Cranfield can be viewed as an analogue for injection into a saline aquifer (Hovorka et al., 2013; 2011; Lu et al., 2012b). Saline formations offer the vast majority of available global CO₂ storage capacity (Scott et al., 2013) (see 1.3.1). Therefore in Cranfield a comprehensive monitoring research program has been carried out and that was the central purpose of the U.S. Department of Energy-funded Southeast Regional Carbon Sequestration Partnership (SECARB) project. The research program is a collaboration between the field operator Denbury Resources Incorporated and the Bureau of Economic Geology (Choi et al., 2013; SECARB, 2015). CO₂ monitoring, fluid flow modelling, capacity estimation, sequestration modelling, retaining mechanism constraining

and leak detection research have been undertaken extensively in the past few years (Hosseini et al., 2013; Hovorka et al., 2013; Lu et al., 2012a; Lu et al., 2013; Nicot et al., 2013; Zhang et al., 2013; Zhang et al., 2014).

3.3 Previous geochemical tracing studies from Cranfield

3.3.1 Anthropogenic tracer injection test

As part of the collaborative research program, artificial tracer injection tests were carried out at the easternmost part, on a hydrologically isolated section of the field termed the 'Detailed Area of Study' (DAS) (Figure 3.1). The DAS site consists of one injection well (31F-1) and two observation wells (32F-2 and 32F-3) that are 67 and 109 m away from the injector. CO₂ injection started on the 1st of December 2009 at the rate of 250 t/day (0.09 Mt/year average, see also Chapter 6). This means that the DAS site is rather small compared to the whole field. The injected CO₂ was the same as that used for the main reservoir and it contained ~10% recycled gas at that time (Hovorka et al., 2013). The injection test targeted a zone below the oil/water contact (Gilfillan et al., 2011; Hovorka, 2013; Hovorka et al., 2013).

Two types of tracers have been added to the injected CO₂: SF₆ and noble gases (Kr and Xe) in different stages. Two stages of noble gas injection and three stages of SF₆ injection took place (see also 6.2). The tests have revealed that CO₂ dissolved into the water inducing CH₄ degassing (Gilfillan et al., 2011; Lu et al., 2012a). This, along with the existence of different flow paths resulted in 'boosts' in the concentration of CH₄ (Lu et al., 2012a). Both tracers have responded to changes in the observed CO₂ and CH₄ concentrations in observation wells, indicating a potential for tracing (Lu et al., 2012a).

The possible leakage of injected Kr and Xe into main reservoir that would affect Kr and Xe data measured from samples collected from the main reservoir is thoroughly investigated in 6.2.

3.3.2 Stable carbon isotopes

The isotopic composition of the CO₂ ($\delta^{13}\text{C}_{\text{CO}_2}$) from Cranfield production wells has been reported previously and during CO₂ injection by Lu et al. (2012b). This work measured a pre-injection CO₂ concentration of 4% and $\delta^{13}\text{C}_{\text{CO}_2} = -10.5$ ‰. The $\delta^{13}\text{C}_{\text{CO}_2}$ values from production well gases match well with the theoretical gas mixing relationship (Lu et al., 2012b) indicating a simple two-component mixing between the reservoir and injected gas (Figure 3.3).

The relatively heavy carbon (-10 ‰ to -3 ‰) in CO₂ is rather unusual when the CO₂ concentration is very low in a hydrocarbon field (e.g. Battani et al., 2000); however, it is theoretically possible (Whiticar, 1999). According to Hovorka et al. (2011) the isotopic composition of CO₂ in Cranfield is consistent with biodegradation of thermogenic methane (albeit no stable isotope value is stated in their work).

The reservoir sandstone contains up to 36.8% calcite and 9.8% dolomite (Lu et al., 2012b), which means that some carbonate breakdown is a possible formation mechanism of CO₂. A mixture of CO₂ originated from both, transformation of organic materials and thermal decomposition of carbonate minerals has been revealed in some Carpathian oil accumulations (Kotarba et al., 2014).

3.4 Sampling strategy

Due to the unique noble gas isotopic composition of the injected gas (see above), the ideal sampling strategy would have been started with baseline recording. However, as this was not possible due to logistical issues, samples for this study were instead collected 18 and 45 months after the start of injection in July 2008. The main reason why pre-injection samples were not specifically taken was the different original purpose of the first sampling trip. This issue is addressed and solved later in Chapter 4.

The first sampling campaign took place in December, 2009, at the same time as the artificial tracer injection test into the DAS site commenced. At that time, the artificial injection of Kr and Xe into the DAS site seemed to provide an excellent opportunity to test the applicability of noble gas isotopes (not only Kr and Xe) to trace the movement of injected CO₂ in the reservoir (e.g. Nimz and Hudson, 2005). Beside the DAS site (1 injector and 2 producers), all the 10 production wells in operation along with an injector and the incoming CO₂ were sampled from the main reservoir. In April and May 2010 when again, artificial tracers were injected (see more in 6.2), more samples were taken from the DAS site for noble gases but there was no sampling schedule from the main reservoir for logistic reasons.

The noble gas isotope data from the DAS site did not provide a dataset that could be understood without the understanding of the interaction of the fluids (injected and natural) in the main reservoir during CO₂ injection. To this end another sampling trip was organised in March 2012 that aimed to sample the main reservoir and all 12 production wells in operation, an injector and the incoming CO₂ were sampled then (no DAS site sampling). This work aims to understand the behaviour of noble gases in the main reservoir.

Both sampling campaigns from the main reservoir were carried out under the collaboration between the University of Edinburgh and the Bureau of Economic Geology at the University of Texas at Austin and Denbury Resources Inc.

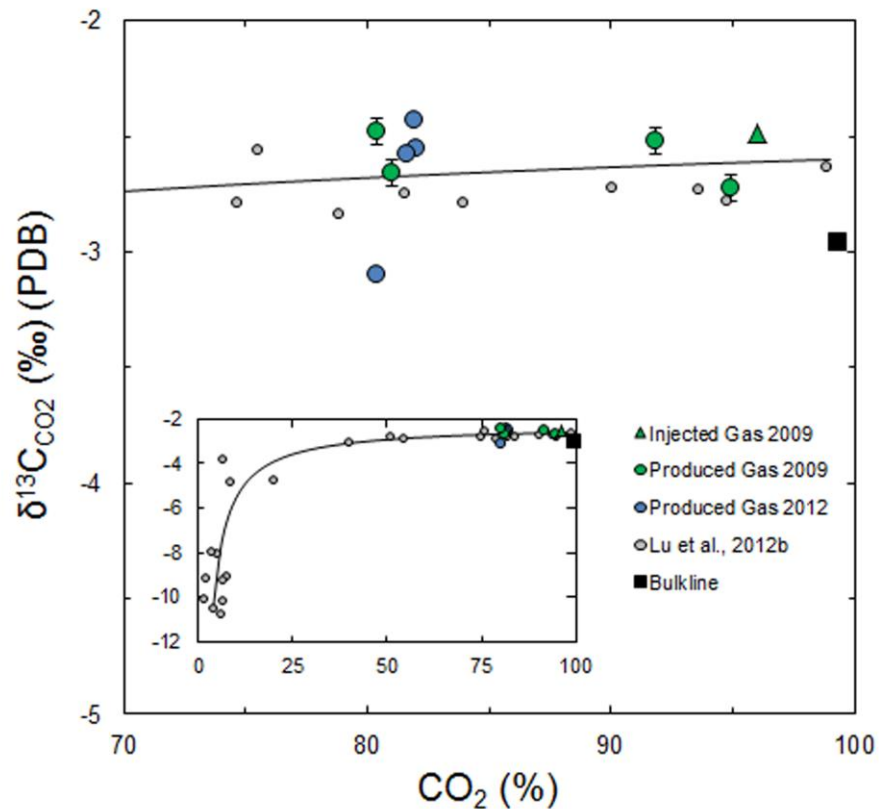


Figure 3.3. Plot of $\delta^{13}\text{C}_{\text{CO}_2}$ (‰) against CO_2 concentration for Cranfield well gases. Data are located around the theoretical mixing curve. The mixing curve end members are: 4% CO_2 and $\delta^{13}\text{C} = -10.5$ ‰ for the natural gas and 99.3% CO_2 and $\delta^{13}\text{C} = -2.6$ ‰ for the bulkline (or Jackson Dome) after Lu et al., (2012b) (inset figure). Their bulkline composition is slightly different from that of this study. 1σ uncertainties are smaller than symbols.

3.5 Recent CO_2 and $\delta^{13}\text{C}_{\text{CO}_2}$ results from Cranfield

The CO_2 concentration and isotopic composition of CO_2 from Cranfield were measured for some samples in this study (Table 3.1) (see extended CO_2 concentration dataset in Table 4.2.)

The bulkline gas is $> 99\%$ CO_2 with a trace amount of CH_4 . The $\delta^{13}\text{C}_{\text{CO}_2}$ value (-2.9 ‰) overlaps the range measured previously -2.6 to -2.95 ‰ (Lu et al., 2012b; Zhou et al., 2012 respectively) (for calculating the average composition of the Jackson Dome see section 4.2.1). The injected gas sampled in 2009 and 2012 significantly differs from the bulkline.

The CO₂ content is lower; 96% in 2009 and 87% in 2012, consistent with the increased proportion of methane-rich produced gas in the injected gas as a result of recycling (see 3.2). The $\delta^{13}\text{C}_{\text{CO}_2}$ was only measured in the 2009 injected gas (-2.5 ‰). It is slightly heavier than the bulkline, but overlaps within the uncertainty of the measured range.

CO₂ concentration measurements from produced gases vary between 80.4% (28-2 from both years) and 94.9% (29-9 2009). The $\delta^{13}\text{C}_{\text{CO}_2}$ values in both 2009 and 2012 sampling are rather constant (-2.4 to -3.1 ‰). When plotted against CO₂ concentration (Figure 3.3) data points plot around the theoretical mixing curve defined by Lu et al. (2012b).

Table 3.1. CO₂ concentration and $\delta^{13}\text{C}_{\text{CO}_2}$ data from Cranfield. For detailed well information see Table 4.3.

Well ID	Well Type	Date of sampling	CO ₂ % ± 0.1	$\delta^{13}\text{C}_{\text{CO}_2}$ ‰ (PDB)
Bulkline	NA	2012	99.3	-2.96
31F-1	Injector	2009	96.0	-2.49
27-3	Producer	2009	81.0	-2.66
28-2	Producer	2009	80.4	-2.48
28-2	Producer	2012	80.4	-3.10
28F-2	Producer	2012	81.9	-2.43
29-6	Producer	2009	91.8	-2.52
29-9	Producer	2009	94.9	-2.72
29-1	Producer	2012	82.0	-2.55
45F-4	Producer	2012	81.6	-2.58

3.6 Tracing CO₂ by $\delta^{13}\text{C}_{\text{CO}_2(\text{gas})}$

The asymptotic nature of the mixing curve (see Figure 3.3) makes $\delta^{13}\text{C}_{\text{CO}_2}$ rather insensitive to changes in the CO₂ concentration in the range of 50 and 100%. In contrast, the extreme slope (or sensitivity in other words) of the curve in the low CO₂ region (0 – 10% CO₂) indicates high potential for tracing CO₂ loss.

The CO₂- $\delta^{13}\text{C}_{\text{CO}_2}$ system could be used to identify processes that cause CO₂ loss from the gas phase, such as dissolution and carbonate mineral precipitation, which are the key mechanisms by which CO₂ could be stored in a reservoir. This is discussed in more detail in Chapter 5. Many data from the original study do not plot on the curve in the low CO₂ region (Lu et al., 2012b). This is evident at other CO₂ injection sites (e.g. Johnson et al. (2011) although the importance of this has been over-looked.

In Chapter 4 & Chapter 5 it will be shown that the low CO₂ samples at Cranfield have lost CO₂ by dissolution into the (high salinity) groundwater. This is qualitatively consistent with the C isotope data of Lu et al. (2012b). The quantification of the CO₂ loss by using only the CO₂- $\delta^{13}\text{C}_{\text{CO}_2}$ system is rather difficult though because it requires determination of the initial CO₂ concentration and $\delta^{13}\text{C}_{\text{CO}_2}$ for each sample. This would require data from the water (or oil) and solid (rock) phase ($\delta^{13}\text{C}_{\text{DIC}}$ and $\delta^{13}\text{C}_{\text{CaCO}_3}$) as well as a precise knowledge of fluid flow to estimate e.g. the amount of CO₂ that could be dissolved under a certain well. Although these data could be obtained it makes CO₂ tracing rather impractical by $\delta^{13}\text{C}$ alone.

3.7 Conclusions

CO₂ concentration and $\delta^{13}\text{C}_{\text{CO}_2}$ data from the Cranfield EOR field are consistent with previous findings, confirming two-component mixing. Due to the shape of the mixing curve the $\delta^{13}\text{C}_{\text{CO}_2}$ is not capable of characterizing the proportion of the injected CO₂ when its concentration is high, whereas it could be a very sensitive tracer in the low concentration region. Dissolution and mineralization, both which are very important processes to discuss in the CCS context could be identified by the CO₂ - $\delta^{13}\text{C}_{\text{CO}_2}$ but the quantification of any of them is complicated and impractical and therefore requires another method.

Chapter 4

Tracing injected CO₂ in Cranfield with noble gas isotopes

4.1 Introduction

In the previous chapter it has been found that $\delta^{13}\text{C}_{\text{CO}_2}$ on its own cannot quantify the amount of injected gas in production (observation) wells over a wide range of CO₂ concentration due to the asymptotic nature of the mixing curve. In the following three chapters the ability of the minor amounts of noble gases that are present in the injected CO₂ to trace its movement and interactions in the Cranfield EOR field is assessed.

Generally, solubility controlled processes and phase equilibria are examined in depth. In solutions, the solubility of noble gases is governed by Henry's law, expressed by Equation 4.1 in a non-ideal system (e.g. Atkins, 1979), where K_i is the Henry constant, Φ_i is the

$$\Phi_i p_i = \gamma_i K_i x_i \quad \text{Equation 4.1}$$

fugacity coefficient, γ_i is the activity coefficient, p_i the pressure in the gas phase and x_i is molar concentration in the liquid phase of a compound 'i'. The meaning of the law is that the concentration of a compound 'i' in the liquid phase is proportional to the partial pressure of that compound in the gas phase in a multicomponent mixture. The Henry constant's unit depends on the unit of the other variables and here is given in GPa. Φ_i can be derived from Φ_i^0 by Lewis-Randall rule (Equation 4.2.) (e.g. Atkins, 1979), where Φ_i^0 is the fugacity coefficient of the pure component. Φ_i^0 is obtained from for example the empirical Virial equation (Equation 4.3. & 4.4)

$$\Phi_i = \Phi_i^0(p, T) x_i \quad \text{Equation 4.2}$$

$$\Phi_i^0(p, T) = \exp\left[\frac{B(T)}{V_m} + (C(T) + B(T)^2/2V_m^2)\right] \quad \text{Equation 4.3}$$

$$\frac{pV_m}{RT} = 1 + \frac{B(T)}{V_m} + C(T)/V_m^2 \quad \text{Equation 4.4}$$

Where R is the gas constant (8.314 J/mol K), T the temperature, p the pressure, V_m the molar volume, B and C are the Virial constants. B, C and Φ as a function of temperature and pressure (or depth) for noble gases, CO₂ and CH₄ can be obtained from Dymond and Smith (1980).

The γ_i activity coefficient in Equation 4.1 can be expressed by Equation 4.5

$$\gamma_i = \exp[Ck_i(T)] \quad \text{Equation 4.5}$$

Where 'C' is the concentration of the salt in a solution and k_i is the Setchenow coefficient. Constants can be obtained from Smith and Kennedy (1983). Henry constants under reservoir conditions for water can be found in Crovetto et al., (1981) and Smith (1985) and for crude oil in Kharaka and Specht (1987).

After the solubilities are known under reservoir conditions, fractionation of e.g. noble gases during phase equilibrium and partitioning can be calculated. In this thesis two basic models, Batch and Rayleigh fractionations are used. The relative fractionation in a gas-water and a water-oil system are given by Equation 4.6 & 4.7 (Batch fractionation) after Bosch and Mazor (1988):

$$\left(\frac{[i]}{[Ar]}\right)_{gas} = \left(\frac{[i]}{[Ar]}\right)_{original} \frac{\frac{V_{gas}}{V_{H2O}} + \frac{1}{K_{Ar}^d}}{\frac{V_{gas}}{V_{H2O}} + \frac{1}{K_i^d}} \quad \text{Equation 4.6}$$

$$\left(\frac{[i]}{[Ar]}\right)_{oil} = \left(\frac{[i]}{[Ar]}\right)_{original} \frac{\frac{V_{oil}}{V_{H2O}} + \frac{K_{Ar,oil}^d}{K_{Ar,H2O}^d}}{\frac{V_{oil}}{V_{H2O}} + \frac{K_{i,oil}^d}{K_{i,H2O}^d}} \quad \text{Equation 4.7}$$

where V is the volume, K the Henry constant and [i] the molar concentration of a noble gas other than Ar.

The Rayleigh fractionation law (dynamic system) can be described by Equation 4.8:

$$\left(\frac{[i]}{[Ar]}\right)_{water} = \left(\frac{[i]}{[Ar]}\right)_{original} P^{\alpha-1} \quad \text{Equation 4.8}$$

where P is the remaining Ar fraction in the liquid phase and α the fractionation coefficient.

α is defined as Equation 4.9 in a gas-water system and as Equation 4.10 in a water-oil system.

$$\alpha = \frac{K_i^{water}}{K_{Ar}^{water}} \quad \text{Equation 4.9}$$

$$\alpha = \frac{K_i^{water} K_{Ar}^{oil}}{K_i^{oil} K_{Ar}^{water}} \quad \text{Equation 4.10}$$

The physical chemistry of noble gases with several case studies is well reviewed by Ballentine et al., (2002).

This chapter firstly deals with the determination of the injected and the natural gas end-members. The inability to sample noble gases of the in-place methane at the site prior to CO₂ injection has required that its noble gas composition is estimated by extrapolation. Later in the chapter, the mixing relationship between the injected and the in-place natural gas is examined.

4.2 Results

4.2.1 Bulkline CO₂

The noble gas isotopic composition of the bulkline CO₂ in Cranfield, sampled in December 2009 was determined at the University of Rochester. Noble gas isotope data of a bulkline sample taken in March 2012 as part of this project are reported in Table 4.1. The 2012 bulkline ³He/⁴He ($5.3 \pm 0.1 R_A$) is slightly higher than the 2009 sample ($4.76 \pm 0.1 R_A$) and the average value of the gas sampled at Jackson Dome ($4.86 \pm 0.05 R_A$; Zhou et al. 2012). The average composition of the Jackson Dome is obtained by averaging the sample called ‘Denkmann’ from Zhou et al., 2012 with the average of all remaining samples from Zhou et al. (2012). The Ne isotopes composition of the 2012 bulkline sample ($^{20}\text{Ne}/^{22}\text{Ne} = 10.82 \pm 0.11$; $^{21}\text{Ne}/^{22}\text{Ne} = 0.0366 \pm 0.0009$) overlaps with the Jackson Dome values ($^{20}\text{Ne}/^{22}\text{Ne} = 10.74 \pm 0.08$; $^{21}\text{Ne}/^{22}\text{Ne} = 0.0355 \pm 0.0012$) within 1 σ uncertainty. The ⁴⁰Ar/³⁶Ar (5043) is higher than the Jackson Dome value (4331) of Zhou et al. (2012). The Ne and Ar isotopes from the 2009 sampling appear to be affected by minor air contamination.

Despite the similarity of isotopic compositions, the noble gas concentrations of both the 2009 and 2012 bulkline samples (Table 4.1) are approximately an order of magnitude lower than those measured in samples of Jackson Dome CO₂ taken from the gas field (Zhou et al., 2012). Mass dependent fractionation of noble gases in the CO₂ cannot account for the bulkline data (Figure 4.1). In the bulkline ²⁰Ne is more depleted, while ³⁶Ar, ⁴⁰Ar and ⁸⁴Kr are more enriched relative to ⁴He in comparison to what mass fractionation of the Jackson Dome can explain. Mass fractionation was calculated after Equation 4.1.

$$\Delta I = I_1 \sqrt{\frac{m_2}{m_1}} \quad \text{Equation 4.11}$$

Where ‘I’ is the certain parameter (e.g. ²⁰Ne/⁴He) of the Jackson Dome value and ‘m₁’ and ‘m₂’ are the masses of the two isotopes. A likely control over fractionation is the solubility:

noble gases may degas from the supercritical CO₂ into the gas phase (atmosphere) at the time of sampling according to Henry's law. Although supercritical CO₂-H₂O system has recently been studied for noble gas partitioning (Warr et al., 2015) there are no partitioning coefficients available for the CO_{2(supercritical)} – CO_{2(gas)} phase system. The depletion in noble gases could also result from solidification of CO₂ (dry ice) within the pipes during sampling. This observation suggests that care must be taken sampling high purity supercritical CO₂ and may require the development of revised sampling methods. In future discussions the average concentration of noble gases of the Jackson Dome CO₂ measured by Zhou et al. (2012) are used, for instance, in determining mixing relationships.

Table 4.1. The average noble gas composition of the Jackson Dome CO₂ compared to two independent measurement of the bulkline gas (UoR in 2009 and SUERC in 2012). Bulkline sample was taken from the pipeline, from supercritical phase. Jackson Dome is after Zhou et al. (2012). The order of magnitude difference in the concentrations between Jackson Dome and bulkline is explained by a significant loss of CO₂ during the sampling of supercritical CO₂ from the bulkline (see text). The Ne and Ar isotopic ratios of the bulkline from 2009 are explained by slight air contamination. Concentrations are ppm and fraction of volumes. NM: Not measured. UoR: University of Rochester. 1σ uncertainties are in parentheses.

	Jackson Dome	Bulkline (UoR)	Bulkline (SUERC)
⁴ He	85.4 (7)	12.06 (10)	10.01 (35)
³ He/ ⁴ He	4.86 (4)	4.76 (2)	5.30 (10)
²⁰ Ne	0.0110 (3)	0.0027 (3)	0.00057 (2)
²⁰ Ne/ ²² Ne	10.74 (8)	10.38 (2)	10.82 (11)
²¹ Ne/ ²² Ne	0.0355 (12)	0.0320 (13)	0.0366 (9)
⁴⁰ Ar (x 10 ¹)	4.32 (18)	0.810 (8)	0.602 (22)
⁴⁰ Ar/ ³⁶ Ar	5043 (26)	1903 (4)	4331 (75)
³⁸ Ar/ ³⁶ Ar	NM	0.231 (1)	0.188 (42)
⁸⁴ Kr	0.000180 (1)	0.000021 (1)	0.000028 (2)
¹³² Xe	NM	0.0000017 (1)	0.0000049 (3)

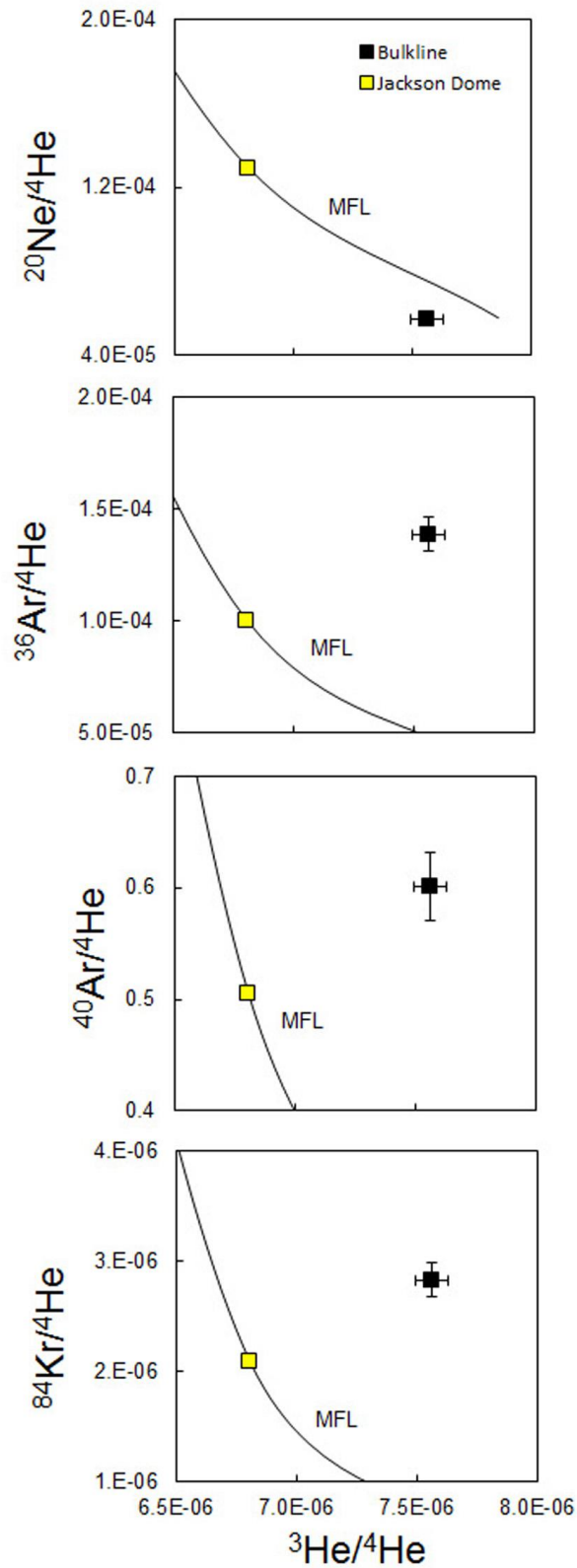


Figure 4.1. The relation of mass fractionation of the Jackson Dome gas and the composition of the bulkline. Mass dependent fractionation cannot explain the bulkline data. Ne shows depletion, while ^{36}Ar , ^{40}Ar and ^{84}Kr enrichment compared to He in the bulkline. MFL: Mass fractionation line.

4.2.2 Injected and produced gas

The He, Ne and Ar isotope data from injection and production well gases are summarised in Table 4.2. Details of all sampled well are summarized in Table 4.3. The He isotope ratio of the injected gas has decreased from $4.73 \pm 0.07 R_A$ to $4.00 \pm 0.06 R_A$ between 2009 and 2012. $^{20}\text{Ne}/^{22}\text{Ne}$ and $^{21}\text{Ne}/^{22}\text{Ne}$ appear to have increased, in the injector from 2009 to 2012 from 10.61 ± 0.1 to 10.69 ± 0.1 and from 0.0349 ± 0.0007 to 0.0372 ± 0.0007 , respectively. Similarly the $^{40}\text{Ar}/^{36}\text{Ar}$ decreased from $2,906 \pm 27$ to $2,763 \pm 107$. These changes are broadly consistent with the increased contribution of recycled gas to the injected gas with time (see 3.2).

The production well data show a wide variation. Typically an increase in the proportion of injected gas with time is observed in the wells that were sampled in 2009 and 2012. This is apparent as increase in $^3\text{He}/^4\text{He}$, $^{20}\text{Ne}/^{22}\text{Ne}$ and $^{40}\text{Ar}/^{36}\text{Ar}$ along with decreases in $^{21}\text{Ne}/^{22}\text{Ne}$ and ^4He , ^{20}Ne and ^{40}Ar concentrations. $^3\text{He}/^4\text{He}$ values vary between $0.2 R_A$ (28F-2 2009) and $4.26 R_A$ (29-9 2009). Well 28F-2 sampled in 2009 shows the lowest $^{20}\text{Ne}/^{22}\text{Ne}$ (9.79), while the highest (10.93) was measured in well 29-6 2009. $^{21}\text{Ne}/^{22}\text{Ne}$ values vary between 0.0388 (29F-1 2009) and 0.0365 (29-9 2009). $^{40}\text{Ar}/^{36}\text{Ar}$ ranges from 609 (27-3 2012) to 3,823 (29-6 2009). $^{38}\text{Ar}/^{36}\text{Ar}$ values are fairly constant in all injection and production wells, usually within uncertainty indistinguishable from the air value. $^4\text{He}/^{20}\text{Ne}$ ratios are at least five orders of magnitude higher than the atmospheric value ruling out any significant contamination from air during sampling or analysis.

Four samples (29-6 2009 & 2012, 29-9 2009 and 29-5 2012) have $^{40}\text{Ar}/^{36}\text{Ar}$ ratios which are significantly higher than the injected gas values. These samples also have high corresponding $^3\text{He}/^4\text{He}$ values.

Table 4.2. Major gas and noble gas isotope data from the Cranfield EOR field. Uncertainties (1σ) in last significant figures are in parentheses. The composition of air is after Eberhardt et al. (1965); Mamyrin et al. (1970); Mark et al. (2011). Relative uncertainties of CO_2 measurements are 1%, while the absolute uncertainty of $\delta^{13}\text{C}_{\text{CO}_2}$ is $\pm 0.2\%$. Noble gas concentrations are $\text{cm}^3 \text{STP}/\text{cm}^3$ after Ozima and Podosek (2001).

Well ID	Year of sampling	Well Type	CO_2 % $\pm 0.1\%$	$^3\text{He}/^4\text{He}$ (R/R_A)	$^{20}\text{Ne}/^{22}\text{Ne}$	$^{21}\text{Ne}/^{22}\text{Ne}$	$^{40}\text{Ar}/^{36}\text{Ar}$	$^{38}\text{Ar}/^{36}\text{Ar}$	^4He ($\times 10^{-4}$)	^{20}Ne ($\times 10^{-9}$)	^{40}Ar ($\times 10^{-5}$)
Bulkline	2012	NA	99.3	5.40 (10)	10.82 (11)	0.0366 (2)	4331 (75)	0.188 (42)	0.100 (4)	0.57 (2)	0.60 (2)
31F-1	2009	Injector	96.0	4.73 (7)	10.61 (10)	0.0349 (7)	2906 (27)	0.185 (14)	0.79 (3)	9.07 (38)	4.27 (16)
32F-4	2012	Injector	87.9	3.99 (6)	10.69 (10)	0.0372 (7)	2763 (10)	0.195 (7)	0.58 (2)	5.00 (21)	3.38 (13)
27-3	2009	Producer	81.0	3.33 (5)	10.33 (13)	0.0382 (11)	1263 (9)	0.188 (6)	1.17 (4)	5.91 (25)	5.36 (20)
27-3	2012	Producer	82.3	3.39 (6)	10.54 (10)	0.0373 (8)	609 (2)	0.186 (4)	0.87 (3)	5.95 (25)	5.98 (22)
29F-1	2009	Producer	3.3	0.38 (1)	9.89 (10)	0.0388 (9)	910 (5)	0.190 (8)	2.83 (10)	13.32 (81)	6.54 (24)
29F-1	2012	Producer	70.5	2.18 (6)	10.30 (10)	0.0383 (7)	1565 (18)	0.187 (10)	1.17 (4)	7.76 (33)	4.26 (16)
29-5	2009	Producer	40.0	1.37 (3)	10.33 (10)	0.0377 (7)	1154 (5)	0.192 (5)	3.14 (9)	17.95 (76)	8.56 (32)
29-5	2012	Producer	85.5	3.92 (6)	10.66 (10)	0.0376 (7)	3126 (12)	0.190 (8)	0.77 (2)	5.71 (24)	3.46 (13)
28-2	2009	Producer	80.4	2.75 (5)	10.46 (10)	0.0374 (7)	1989 (23)	0.189 (8)	0.91 (3)	6.50 (28)	3.75 (14)
28-2	2012	Producer	80.4	2.77 (6)	10.49 (10)	0.0376 (8)	2017 (39)	0.190 (14)	0.94 (3)	6.47 (27)	3.77 (14)
28F-2	2009	Producer	0.9	0.21 (2)	9.79 (9)	0.0383 (8)	839 (6)	0.190 (10)	2.98 (11)	10.57 (45)	5.99 (22)
28F-2	2012	Producer	81.9	3.22 (5)	10.43 (10)	0.0365 (7)	2123 (9)	0.196 (10)	0.87 (3)	7.20 (31)	3.57 (13)
29-6	2009	Producer	91.8	4.18 (9)	10.93 (10)	0.0380 (8)	3671 (32)	0.186 (15)	0.89 (3)	7.15 (30)	4.32 (16)
29-6	2012	Producer	94.9	4.18 (9)	10.71 (10)	0.0370 (7)	3823 (31)	0.186 (24)	0.66 (2)	5.13 (22)	3.08 (11)
29-9	2009	Producer	94.9	4.26 (9)	10.74 (10)	0.0365 (7)	3473 (17)	0.190 (18)	0.82 (3)	6.78 (29)	3.69 (14)
29-9	2012	Producer	82.4	3.46 (7)	10.62 (10)	0.0374 (8)	2306 (36)	0.190 (29)	0.90 (3)	5.70 (24)	3.88 (14)
29-1	2009	Producer	80.7	2.85 (6)	10.45 (10)	0.0373 (8)	2012 (17)	0.190 (13)	1.04 (4)	7.63 (32)	3.99 (15)
29-1	2012	Producer	82.0	3.23 (8)	10.62 (10)	0.0375 (8)	2604 (9)	0.190 (15)	0.95 (3)	6.71 (28)	4.15 (15)
27-5	2009	Producer	46.9	1.71 (4)	10.08 (9)	0.0373 (8)	1348 (11)	0.190 (6)	0.92 (3)	5.26 (22)	4.17 (15)

Well ID	Year of sampling	Well Type	CO ₂ % ± 0.1 %	³ He/ ⁴ He (R/R _A)	²⁰ Ne/ ²² Ne	²¹ Ne/ ²² Ne	⁴⁰ Ar/ ³⁶ Ar	³⁸ Ar/ ³⁶ Ar	⁴ He (x 10 ⁻⁴)	²⁰ Ne (x 10 ⁻⁹)	⁴⁰ Ar (x 10 ⁻⁵)
27-5	2012	Producer	82.5	2.85 (5)	10.56 (10)	0.0376 (8)	2592 (17)	0.180 (16)	1.01 (4)	6.29 (27)	3.64 (13)
44-2	2009	Producer	8.4	0.69 (2)	9.92 (9)	0.0376 (7)	1133 (5)	0.190 (8)	3.12 (11)	14.37 (61)	9.66 (36)
45F-4	2012	Producer	81.6	2.90 (7)	10.51 (10)	0.0375 (8)	2427 (29)	0.200 (20)	0.83 (3)	5.99 (25)	3.77 (14)
32F-10	2012	Producer	80.3	2.91 (6)	10.62 (10)	0.0362 (7)	2156 (14)	0.202 (9)	0.96 (4)	6.46 (27)	3.15 (12)
70-2	2012	Producer	83.4	3.18 (8)	10.51 (9)	0.0371 (7)	2486 (34)	0.184 (16)	0.95 (3)	6.44 (27)	3.61 (13)
AIR	NA	NA	NA	1.000 (9)	9.81(8)	0.0290 (3)	298.6 (3)	0.1885 (3)	0.052 (1)	16452 (36)	930 (1)

Table 4.2. Continued from previous page.

Table 4.3. Details of wells from where samples have been taken for this study.

Well ID	Well Type	Location	Latitude	Longitude	API number
31F-1	Injector	Franklin Co. SEC 31-T7N-R1E	31.563560	-91.141330	23-037-21488-0000
32F-4	Injector	Franklin Co. SEC 32-T7N-R1E	31.551200	-91.145650	23-037-21496-0100
27-3	Producer	Adams Co. SEC 27-T7N-R1W	31.579880	-91.160130	23-001-03394-0001
29F-1	Producer	Franklin Co. SEC 29-T7N-R1E	31.565364	-91.150319	23-037-00046-0001
29-5	Producer	Adams Co. SEC 29-T7N-R1W	31.580939	-91.179189	23-001-00173-0001
28-2	Producer	Adams Co. SEC 28-T7N-R1W	31.576350	-91.157210	23-001-23372-0000
28F-2	Producer	Franklin Co. SEC 28-T7N-R1W	31.572275	-91.153649	23-037-00048-0001
29-6	Producer	Adams Co. SEC 29-T7N-R1W	31.577300	-91.172600	23-001-00198-0001
29-9	Producer	Adams Co. SEC 29-T7N-R1W	31.573561	-91.166689	23-037-00159-0001
29-1	Producer	Adams Co. SEC 29-T7N-R1W	31.583589	-91.176239	23-001-00176-0001
27-5	Producer	Adams Co. SEC 27-T7N-R1W	31.583410	-91.159740	23-001-23380-0100
44-2	Producer	Adams Co. SEC 44-T7N-R1W	31.571200	-91.182660	23-001-23346-0000
45F-4	Producer	Franklin Co. SEC 45-T7N-R1E	31.541440	-91.153430	23-037-00336-0001
32F-10	Producer	Franklin Co. SEC 32-T7N-R1E	31.554860	-91.152940	23-037-00333-0000
70-2	Producer	Adams Co. SEC 70-T7N-R1W	31.537590	-91.155040	23-001-23410-1000

4.3 Defining the natural gas end-member composition

As this PhD started after injection it was not possible to sample the in-place natural gases at Cranfield prior to CO₂ injection commencing. In the absence of pre-injection natural gas, its composition can only be determined by data extrapolation. The Ne isotope composition of the production well gases offers a straightforward way to identify the natural gas composition. Neon in natural gas accumulations is generally a mixture of three isotopically distinct sources: atmosphere, crust and mantle (Ballentine and O'Nions, 1991). The Ne isotopic composition of the three end-members are: $(^{20}\text{Ne}/^{22}\text{Ne})_{\text{air}} = 9.805$, $(^{21}\text{Ne}/^{22}\text{Ne})_{\text{air}} = 0.029$, $(^{20}\text{Ne}/^{22}\text{Ne})_{\text{crust}} = 0.3$, $(^{21}\text{Ne}/^{22}\text{Ne})_{\text{crust}} = 0.52$, $(^{20}\text{Ne}/^{22}\text{Ne})_{\text{mantle}} = 12.5$, $(^{21}\text{Ne}/^{22}\text{Ne})_{\text{mantle}} = 0.06$ (Ballentine, 1997; Ballentine and Burnard, 2002; Eberhardt et al., 1965; Holland and Ballentine, 2006; Kennedy et al., 1990).

Neon in the Jackson Dome CO₂ is a mixture of mantle-derived gas and air-derived gas that was fractionated prior to mixing. The fractionated air component has $^{20}\text{Ne}/^{22}\text{Ne} = 10.46$ and $^{21}\text{Ne}/^{22}\text{Ne} = 0.03$ (Zhou et al., 2012). Figure 4.2 shows the previous measurements of Jackson Dome CO₂ where the grey dashed line shows the mixing trend. The Ne isotopic composition of the gases from all injection and production well gases from Cranfield is shown in Figure 4.2. The data define a clear trend between a point on the Jackson Dome mixing line ($^{20}\text{Ne}/^{22}\text{Ne} = 10.92$; $^{21}\text{Ne}/^{22}\text{Ne} = 0.037$), and a point on the mixing line between air and crustal radiogenic Ne ($^{20}\text{Ne}/^{22}\text{Ne} = 9.62 \pm 0.02$, $^{21}\text{Ne}/^{22}\text{Ne} = 0.0384 \pm 0.001$). These two points represent end-member compositions that have been determined by fitting a best-fit mixing line through the data using general mixing equation and a least square method (Langmuir et al., 1978). The intersection of the best-fit line with the Jackson Dome CO₂ mixing line is indistinguishable from the measured bulkline ($^{20}\text{Ne}/^{22}\text{Ne} = 10.82 \pm 0.11$; $^{21}\text{Ne}/^{22}\text{Ne} = 0.0366 \pm 0.0009$). The intersection with the air–crust line represents the best estimate of the Ne isotope composition of the in-place natural gas. It is

an entirely feasible composition considering the absence of evidence for local Cenozoic magmatism (see 3.2). The identification of these end-member compositions allows the noble gas isotope composition of each component to be determined. A similar technique has been applied for end-member determination by Ballentine et al. (2005).

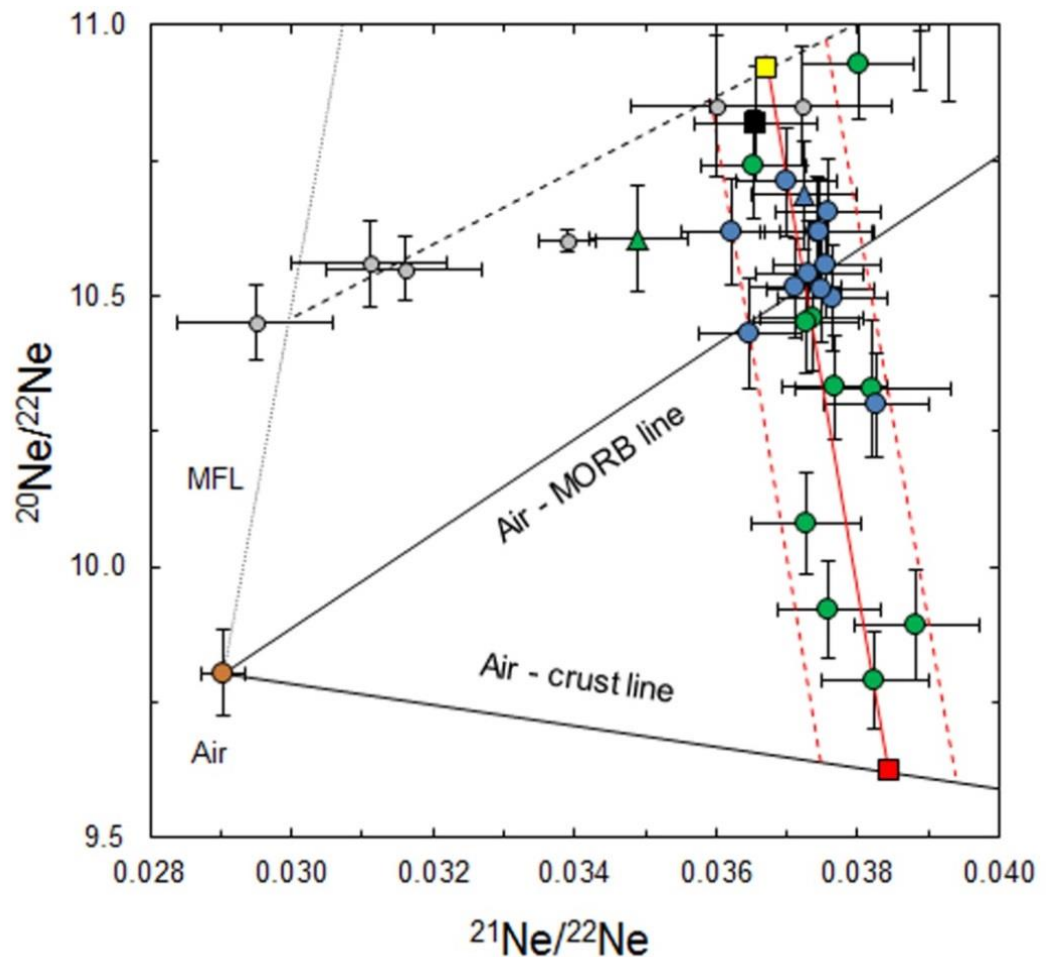


Figure 4.2. Well gas data from Cranfield plotted on the Ne three-isotope plot. The data plot as a binary mixture between injected gas (yellow), (similar to the composition of Jackson Dome CO₂ after Zhou et al., 2012), and natural gas (red), defined by the best fit mixing line (red line). The calculated composition of the natural gas is: $^{20}\text{Ne}/^{22}\text{Ne} = 9.62 \pm 0.02$ and $^{21}\text{Ne}/^{22}\text{Ne} = 0.0384 \pm 0.001$. Red dashed lines represent the 1σ uncertainty of the best fit line. Black square: bulkline, triangle: injected gas, circle: produced gas, green: 2009, blue: 2012, grey circles: Jackson Dome CO₂ data from Zhou et al. (2012). MFL: Mass fractionation line. MORB: Mid-Ocean Ridge Basalt. Uncertainties are 1σ .

The $^3\text{He}/^4\text{He}$ of the injection and production well gases is plotted against $^{20}\text{Ne}/^{22}\text{Ne}$ ratios on Figure 4.3A. Extrapolating to the $^{20}\text{Ne}/^{22}\text{Ne}$ of the natural gas end-member, the best-fit mixing curve defines the $^3\text{He}/^4\text{He}$ of $0.05 \pm 10\% R_A$. This is slightly in excess of the value of radiogenic He from the continental crust ($\sim 0.02 R_A$; Andrews (1985) and is lower than the lowest measured $^3\text{He}/^4\text{He}$ from well 28F-2 2009 ($0.2 R_A$). The degree of the curvature of the line is determined by $^4\text{He}/^{22}\text{Ne}_{\text{Jackson Dome}}/^4\text{He}/^{22}\text{Ne}_{\text{natural gas}}$ (0.488). Integrating this value with the $^4\text{He}/^{22}\text{Ne}$ measured in Jackson Dome CO_2 (12,452; Zhou et al. (2012) implies that the $^4\text{He}/^{22}\text{Ne}$ of the natural gas is $25,524 \pm 1942$. The $^4\text{He}/^{22}\text{Ne}$ measured from the lowest CO_2 sample is $28,178 \pm 1556$ (28F-2 2009), which is consistent with the calculated value. The hyperbolic nature of the mixing relationship means that the $^3\text{He}/^4\text{He}$ of the in-place natural gas end-member is rather poorly defined. The ^4He concentration of the natural gas end-member is assumed to be close to that of the lowest CO_2 sample (28F-2 2009; $3 \times 10^{-4} \pm 2 \times 10^{-5} \text{ cm}^3 \text{ STP/cm}^3$).

When the $^{40}\text{Ar}/^{36}\text{Ar}$ values are plotted against $^{20}\text{Ne}/^{22}\text{Ne}$ (Figure 4.3B) the $^{40}\text{Ar}/^{36}\text{Ar}$ data are broadly consistent with mixing between a high $^{40}\text{Ar}/^{36}\text{Ar}$ injected gas and in-situ natural gas with lower $^{40}\text{Ar}/^{36}\text{Ar}$. The best-fit line defines the $^{40}\text{Ar}/^{36}\text{Ar}$ of the in-situ natural gas to be 836 ± 75 . This is considerably higher than the atmospheric $^{40}\text{Ar}/^{36}\text{Ar}$ value (298.6; Mark et al. (2011) and requires that the in-situ natural gas contains radiogenic ^{40}Ar . The concentration of ^{36}Ar of the in-situ reservoir gas ($7 \times 10^{-8} \text{ cm}^3 \text{ STP/cm}^3$) is taken from well 28F-2 2009 (the lowest CO_2 sample). The gradient of the mixing line is defined by $^{36}\text{Ar}/^{22}\text{Ne}_{\text{Jackson Dome}}/^{36}\text{Ar}/^{22}\text{Ne}_{\text{natural gas}} = 0.2$. Combining this with the measured $^{36}\text{Ar}/^{22}\text{Ne}$ of the Jackson Dome gas (8.36), the $^{36}\text{Ar}/^{22}\text{Ne}$ of the in-situ natural gas is calculated to be 41.7.

Air-derived noble gases are present in variable concentrations as a third component that tends to mask the mixing trend in Ne-Ar isotope systematics. The extremely high $^4\text{He}/^{20}\text{Ne}$

of the produced gases ($10^4 - 10^5$) rules out direct air contamination. The source of the atmospheric component in the Cranfield reservoir is examined in detail in Chapter 6.

The production of ^{36}Ar in the crust and mantle is insignificant and it can be assumed that all ^{36}Ar in the Cranfield gases ultimately originates from the atmosphere. The atmospheric ^{40}Ar contribution can be removed by Equation 4.12:

$$^{40}\text{Ar}^* = ^{40}\text{Ar}_{\text{measured}} - \left(^{36}\text{Ar}_{\text{measured}} \left(\frac{^{40}\text{Ar}}{^{36}\text{Ar}} \right)_{\text{air}} \right) \quad \text{Equation 4.12}$$

where the radiogenic ^{40}Ar (from both crust and mantle) is denoted $^{40}\text{Ar}^*$. This is commonly normalised to radiogenic ^4He to trace the source and interaction history of ancient and modern fluids in the crust (Stuart and Turner, 1992).

A plot of $^{40}\text{Ar}^*/^4\text{He}$ vs. $^{20}\text{Ne}/^{22}\text{Ne}$ reveals a coherent mixing trend between the high $^{40}\text{Ar}^*/^4\text{He}$ injected gas and the low $^{40}\text{Ar}^*/^4\text{He}$ reservoir gas (Figure 4.3C). Using the end-member $^{20}\text{Ne}/^{22}\text{Ne}$ yields $^{40}\text{Ar}^*/^4\text{He} = 0.09 \pm 0.01$ in the natural gas end-member.

There is a coherent trend between $^{20}\text{Ne}/^{22}\text{Ne}$ and $^{20}\text{Ne}/^{36}\text{Ar}$ that mimics the isotope ratios (Figure 6.4). The distribution of data points along the mixing curve is similar to that of $^{40}\text{Ar}/^{36}\text{Ar}$ versus CO_2 plot (Figure 4.3B) where both 2009 and 2012 samples from well 27-3 plot significantly below the curve. The lowest $^{20}\text{Ne}/^{36}\text{Ar}$ (28F-2 2009; 0.148) is close to the value recorded by air saturated water (ASW) (0.163). The abundances of the non-radiogenic noble gases (^{20}Ne , ^{36}Ar , ^{84}Kr and ^{132}Xe) are dealt with in Chapter 6.

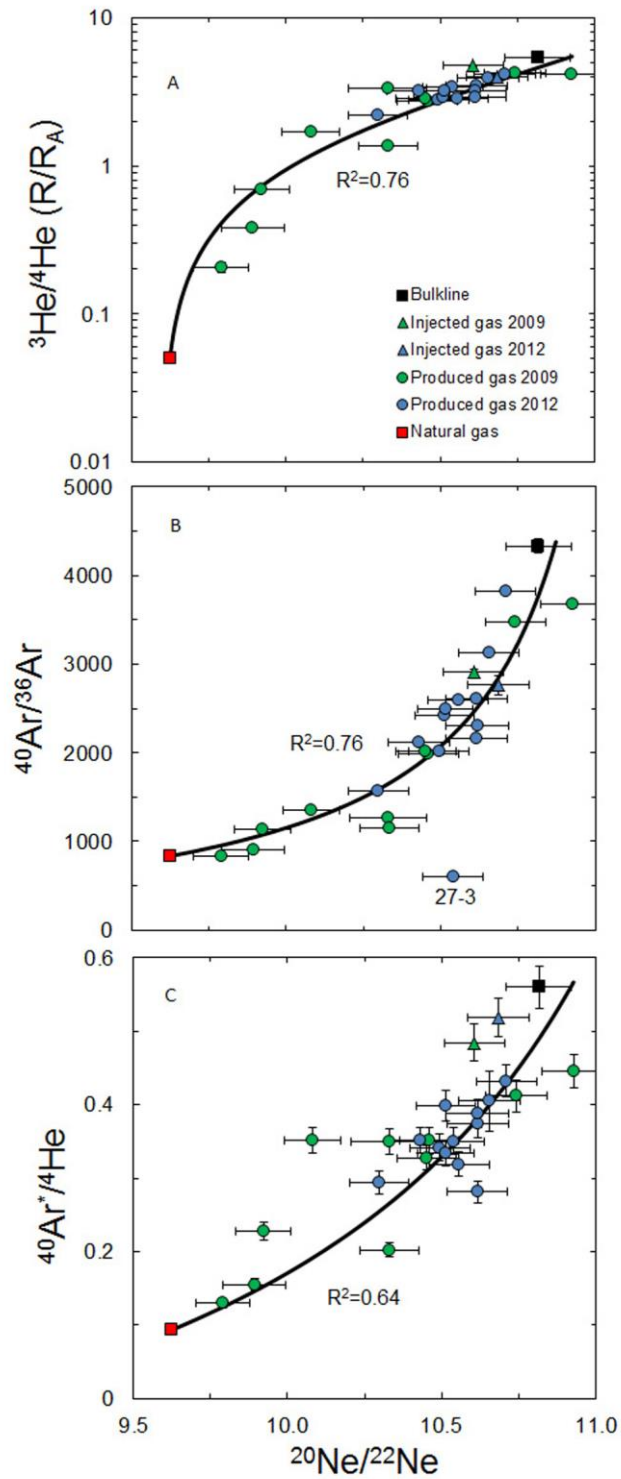


Figure 4.3. $^{20}\text{Ne}/^{22}\text{Ne}$ of Cranfield well gases plotted against He and Ar isotopic ratios. A: $^3\text{He}/^4\text{He}$, B: $^{40}\text{Ar}/^{36}\text{Ar}$ and C: $^{40}\text{Ar}^*/^4\text{He}$. In all cases the composition of the natural gas end-member is determined by the previously determined $^{20}\text{Ne}/^{22}\text{Ne}$ of natural gas end-member (9.62) and the best fit line defined by the data. The bulkline is for illustration only. On figure B, data from well 27-3 was rejected when fitting the line. Uncertainties are 1σ .

4.4 Noble gas isotope composition of the in-place natural gas

The He, Ne and Ar isotope ratios of the in-situ natural gas are consistent with an origin in the shallow crust, and provide no evidence of significant mantle-derived volatiles. The He concentration ($\sim 3 \times 10^{-4} \text{ cm}^3 \text{ STP/cm}^3$) overlaps with the range measured in natural methane deposits that have not been affected by leakage of mantle volatiles (e.g. Ballentine et al., 1991; Kotarba et al., 2014). The $^{40}\text{Ar}^*/^4\text{He}$ is significantly lower (0.09 ± 0.01) than the average production ratio in the continental crust (~ 0.2 ; Torgersen et al. (1989) and is the result of the preferential release of ^4He from minerals at lower temperature than ^{40}Ar by diffusion and/or ejection of α -particles. Again this is typical of oil field gases (Ballentine et al., 1996).

The $\text{CH}_4/^{36}\text{Ar}$ is indicative of the degree of gas–groundwater contact and gas transportation mechanism in the reservoir (Ballentine and O'Nions, 1994; Elliot et al., 1993). The $\text{CH}_4/^{36}\text{Ar}$ from well 28F-2 2009 is $1.4 \pm 0.05 \times 10^7$. Under reservoir conditions (3km, 100°C , 32 MPa, 2M salinity; Lu et al., 2012b) the concentration of CH_4 in brine is $\sim 2.1 \text{ cm}^3 \text{ STP/cm}^3$. This calculation is based on laboratory experiments and empirical equations after (Price et al., 1981). If the ^{36}Ar originates from groundwater recharge (see Chapter 6) and the groundwater is taken as seawater after Lu et al., (2012b) the ^{36}Ar concentration in the brine is $8.8 \times 10^{-7} \text{ cm}^3 \text{ STP/cm}^3$ (Smith and Kennedy, 1983). This gives $\text{CH}_4/^{36}\text{Ar}$ of 2.4×10^6 . This is considerably lower than value from 28F-2 2009. The higher value in well 28F-2 2009, which is indicative of the Cranfield reservoir end-member suggest that not all the CH_4 originates from the groundwater. This excess methane is unlikely to have been transported in the water phase (e.g. Ballentine and O'Nions, 1994). A more likely explanation is that the excess methane in the natural gas originates from the large amount of heavy hydrocarbons by decomposition and degassing, similar to that of noble gas degassing in natural hydrocarbon accumulations (e.g. Bosch and Mazor, 1988). This means

that some of the CH₄ is transported in the reservoirs in the hydrocarbon phase. If this is the case the presence of CH₄ in the gas phase may be affected by the efficiency of oil displacement during EOR activity in certain wells (see Chapter 6). Such an abnormal CH₄ concentration has been observed in production well 27-5 and discussed in 5.2.2.

4.5 Tracing injected CO₂

The coherent relationship between the He, Ne and Ar isotope compositions of the production well gases (Figure 4.3) implies that they may be promising tracers of the injected CO₂. The helium isotopic composition of well gases is plotted against the CO₂ concentrations in Figure 4.4A. Mixing curves are drawn between the 2009 and 2012 injected gases and the in-situ natural gas end-member (³He/⁴He = 0.05 R_A, see above). The curvature of the mixing lines is dependent on the ⁴He concentration in the injected gas and the in-situ natural gas.

The 2009 and 2012 mixing lines overlap as the evolution of the injected gas (see section 3.2) fairly well mirrors the gas mixing underground. Except from the five lowest CO₂ samples from 2009, all data plot within the area defined by the mixing curves, implying that they are consistent with the predicted binary mixing. This demonstrates that ³He/⁴He fingerprints the CO₂ and has the potential to be used as a tracer CO₂ from CCS sites where the difference between the helium isotopic composition of the injected and in-place gases is significant.

Figure 4.4B shows the ⁴⁰Ar/³⁶Ar of the well gases plotted against the CO₂ content, along with theoretical mixing lines. The curvature of mixing lines is defined by the ⁴⁰Ar/³⁶Ar of the natural gas (836) from the Ar-Ne relationship and data from injectors. The concentration of ³⁶Ar has been determined above. The systematic mixing relationship observed for ³He/⁴He vs. CO₂ is not as apparent in ⁴⁰Ar/³⁶Ar-CO₂ space. The five low CO₂

samples that plot above the mixing line in case of He, also plot above the curves. Samples from well 27-3 taken in both sampling campaigns plot significantly below the mixing curve. These may be due to the addition of small amount of atmosphere derived Ar that would lower $^{40}\text{Ar}/^{36}\text{Ar}$ ratios.

The $^{40}\text{Ar}^*/^4\text{He}$ ratio allows the effect of small addition of air-derived Ar to be removed (Equation 4.1). In Figure 4.4C the $^{40}\text{Ar}^*/^4\text{He}$ is plotted against CO_2 concentrations along with theoretical mixing lines. Generally, the data follow the mixing lines to a greater extent than Ar isotopes. As with He and Ar isotope data, the low CO_2 samples plot above the mixing line.

The five low CO_2 concentration gases from 2009 are the general exception to the systematic mixing relationships identified in both CO_2 vs. $^3\text{He}/^4\text{He}$ and $^{40}\text{Ar}^*/^4\text{He}$. In both cases, the data plot significantly above the theoretical mixing lines. The internal consistency of the noble gas isotope data suggests that this is unlikely to be the result of the addition of a third noble gas component. The simplest and most likely explanation is that it mirrors the loss of CO_2 from the gas phase during the early (18 months after injection) phase of CO_2 injection. The amount of CO_2 sequestered and the sequestration mechanism are investigated in Chapter 5.

Some of the remaining data points are also located slightly off the mixing curve on Figure 4.4. Those may indicate that a small proportion of CO_2 has been lost from the gas phase. This may comply well with the fact that there is a small but observable changes in the $\text{CO}_2/^3\text{He}$ ratios in some high CO_2 concentration samples in comparison to the Jackson Dome value (see e.g. Figure 5.3, page 101). Although the possibility of a minor CO_2 loss in those samples is not exploited in this work, this indicates that noble gases could be a sensitive means for CO_2 tracing.

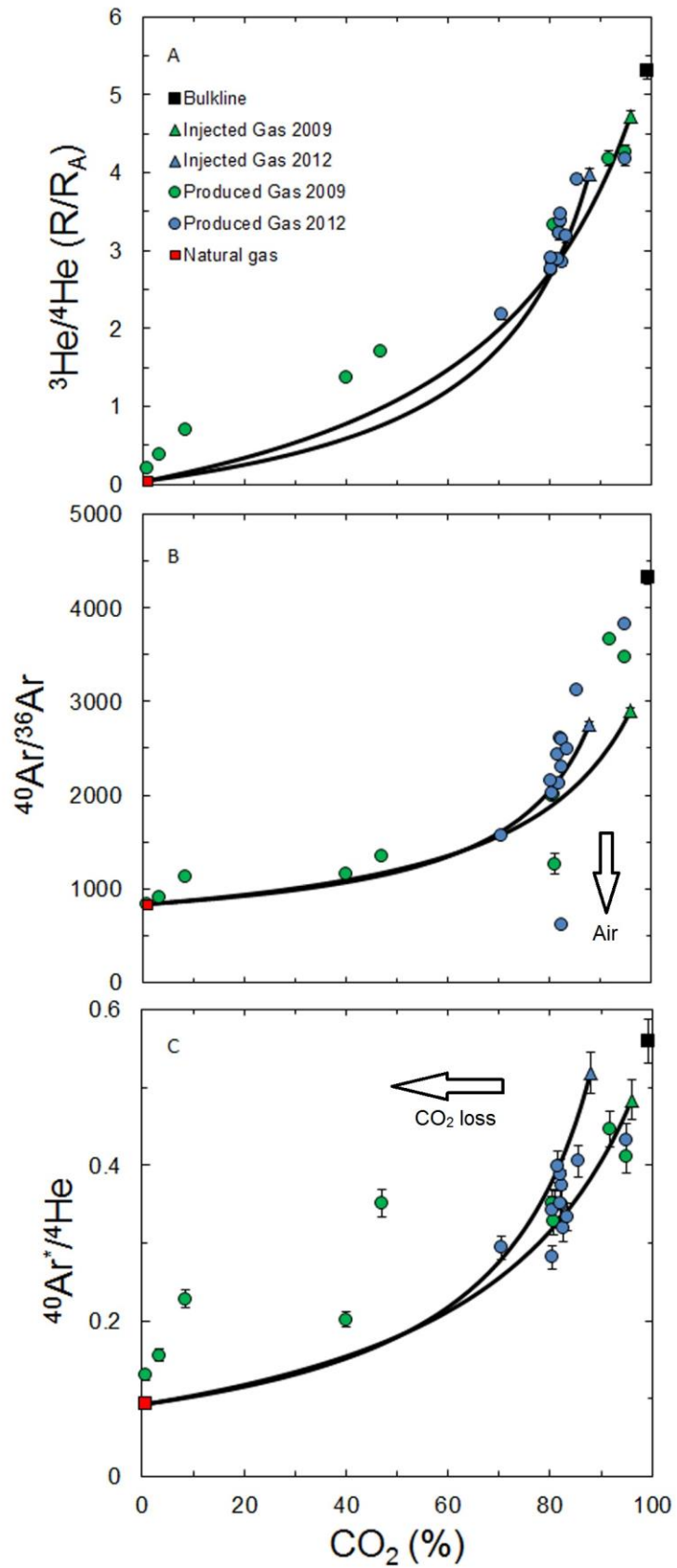


Figure 4.4. The CO₂ content of Cranfield well gases plotted against He and Ar isotopic ratios. A: $^3\text{He}/^4\text{He}$, B: $^{40}\text{Ar}/^{36}\text{Ar}$, C: $^{40}\text{Ar}^*/^4\text{He}$. Mixing lines are drawn between natural gas end-member determined by Ne isotopes in Figure 4.3. Uncertainties are 1σ .

4.6 Conclusions

The unique noble gas isotope composition of the Jackson Dome CO₂ injected in the Cranfield CO₂-EOR field facilitates testing how well He, Ne and Ar isotopes can be used to trace injected gas. The isotopic composition of well gases from Cranfield defines binary mixtures between injected gas and the in-place natural gas. This allows the noble gas isotopic composition of the reservoir gas to be determined. $^3\text{He}/^4\text{He}$ and $^{40}\text{Ar}^*/^4\text{He}$ of produced gas samples plot on theoretical mixing lines with CO₂ content suggesting that, the noble gas isotopes track the presence of the injected CO₂. In general the noble gas ratio(s) are much more sensitive to CO₂ concentration changes over the whole range of CO₂ concentration than $\delta^{13}\text{C}_{\text{CO}_2}$. Also in the noble gas system there is potentially flexibility to adjust the tracer to a certain need. The five samples with the lowest proportion of CO₂ sampled in 2009 sit above the theoretical mixing lines. The most likely explanation is that a significant proportion of CO₂ has been lost from the gas phase. This loss is discussed further in Chapter 5.

Chapter 5

Storage mechanism of the injected CO₂ in the Cranfield field

5.1 Introduction

In the previous chapter it has been shown how the He, Ne and Ar isotope data from five production well gases at the Cranfield EOR site sampled in 2009 appear to record the loss of some amount of CO₂ from the gas phase. Here two methods are used to quantify the extent of CO₂ loss and demonstrate how the noble gas isotopes can be used to distinguish the fate of the CO₂. The mechanism responsible for the CO₂ loss is investigated using variation in the CO₂/³He as well as noble gas and carbon isotope compositions, and with production well data. The storage mechanism of the CO₂ is discussed and compared with the findings of previous studies.

5.2 Quantifying CO₂ loss from the gas phase

5.2.1 ³He/⁴He and ⁴⁰Ar*/⁴He vs. CO₂

The majority of the production well gases sampled in 2009 and 2012 are consistent with the simple two component mixing in ³He/⁴He-CO₂ and ⁴⁰Ar*/⁴He-CO₂ diagrams (see section 4.5). Therefore the CO₂ concentration of any free gas sample can be calculated from the ³He/⁴He and ⁴⁰Ar*/⁴He value.

In this section the loss of CO₂ is quantified in each well. For gases that have lost CO₂, the off-set between the predicted and measured CO₂ represents the absolute change in concentration. The proportion of lost CO₂ is calculated from Equation 5.1:

$$CO_{2\text{ loss}}(\%) = \frac{[CO_2]_{\text{predicted}} - [CO_2]_{\text{measured}}}{[CO_2]_{\text{predicted}}} 100 \quad \text{Equation 5.1}$$

However, the process responsible for CO₂ loss may result in the fractionation of noble gas element ratios such as ⁴⁰Ar*/⁴He, in which case the equation above cannot fully quantify the relative loss. This could slightly affect the predicted CO₂ concentration. Relative CO₂ loss is calculated on the basis of the relationships of ³He/⁴He-CO₂ and ⁴⁰Ar*/⁴He-CO₂. Additionally the theoretical CO₂, obtained from the ³He/⁴He-CO₂ relationship is used to estimate a theoretical ⁴⁰Ar*/⁴He on the bases of ⁴⁰Ar*/⁴He – CO₂ mixing relationship (Table 5.1). The newly calculated ⁴⁰Ar*/⁴He value allows estimation of the CO₂ loss if ³He/⁴He had not fractionated during the loss, which is certain. The predicted CO₂ content of the five low CO₂ well gases using ³He/⁴He and both, measured and predicted ⁴⁰Ar*/⁴He are shown in Table 5.2. The proportion of the injected CO₂ lost from the gas phase calculated for the measured ³He/⁴He ratios is between 30% (27-5 2009) and 93% (28F-2 2009). From the measured ⁴⁰Ar*/⁴He ratios the range is 22% to 96% and from the predicted ⁴⁰Ar*/⁴He ratios the range is 44% to 97%. It should be noted that the contribution of these wells to the total produced CO₂ is yet unknown.

Uncertainties in the proportion of CO₂ loss are dependent upon two factors: 1) the uncertainty in the CO₂, ³He/⁴He and ⁴⁰Ar*/⁴He measurements, and 2) the uncertainty of both the natural gas and the injected gas end-members (ratios and concentrations) that define the mixing curves (see 4.3.1). The propagated uncertainties reveal that the proportional loss of CO₂ calculated by the three different methods (³He/⁴He and two ⁴⁰Ar*/⁴He) overlaps within 2σ uncertainty in case of well 28F-2, 29F-1 and 44-2 (Table 5.2). The large difference between the calculated relative loss, obtained from the method ⁴⁰Ar*/⁴He_{predicted} and the two remaining may be explained by the high ⁴He (3.14 x 10⁻⁴ cm³ STP/cm³) concentration (and therefore the inconsistency in the ⁴⁰Ar*/⁴He ratio in comparison to others). This is higher than the ⁴He content of the end-member natural gas

(see 4.4) and may be explained by heterogeneity of the concentration of ^4He in the natural gas. Explanation is given for the observed differences in well 27-5 in 5.2.2.

Table 5.1. Measured and theoretical $^{40}\text{Ar}^*/^4\text{He}$ of well gases that have lost CO_2 . Calculation is based on the $^3\text{He}/^4\text{He}$ - CO_2 and $^{40}\text{Ar}^*/^4\text{He}$ - CO_2 system. Uncertainties are 1σ in brackets.

Well	Measured $^{40}\text{Ar}^*/^4\text{He}$	Theoretical $^{40}\text{Ar}^*/^4\text{He}$
28F-2	0.130 (7)	0.142 (13)
29F-1	0.155 (8)	0.190 (16)
44-2 2009	0.228 (12)	0.261 (19)
29-5 2009	0.202 (9)	0.361 (15)
27-5 2009	0.352 (18)	0.381 (30)

Table 5.2. The percentages of CO_2 loss from the 2009 well gas samples based on $\text{CO}_2/{}^3\text{He}$ and noble gas ratios. $^{40}\text{Ar}^*/^4\text{He}$ ‘measured’ refers to the use of measured ratio, while ‘predicted’ refers to the calculated $^{40}\text{Ar}^*/^4\text{He}$ on the basis of the $^3\text{He}/^4\text{He}$ – CO_2 and $^{40}\text{Ar}^*/^4\text{He}$ relationship. 2σ uncertainties are in parentheses.

Well	$\text{CO}_2/{}^3\text{He}$	CO_2 - ${}^3\text{He}/^4\text{He}$	CO_2 - $^{40}\text{Ar}^*/^4\text{He}_{(\text{measured})}$	CO_2 - $^{40}\text{Ar}^*/^4\text{He}_{(\text{predicted})}$
28F-2 2009	96 (2)	93 (4)	96 (4)	97 (3)
29F-1 2009	91 (4)	84 (4)	90 (4)	93 (6)
44-2 2009	89 (4)	77 (4)	85 (6)	87 (8)
29-5 2009	71 (12)	30 (8)	22 (8)	51 (4)
27-5 2009	NA	28 (6)	42 (4)	44 (3)

5.2.2 CO₂/³He

Previous studies have demonstrated that CO₂/³He of natural gases is a powerful tracer of the history of crustal natural gases that were derived from magmatic sources (e.g. Marty et al., 1989). Figure 5.1 shows the CO₂/³He of the Cranfield gases plotted against the CO₂ concentration. The injected gases show a slight increase in CO₂/³He from 2009 (1.84×10^9) to 2012 (2.71×10^9), which overlap the range of Jackson Dome CO₂ ($1.1 \times 10^9 - 4.6 \times 10^9$) Zhou et al. (2012) and magmatic gases in general ($10^9 - 10^{10}$, Marty and Jambon (1987). Mixing curves are drawn between the natural gas (black circle on Figure 5.1, CO₂/³He = 1.9×10^9) and the extreme Jackson Dome values (small yellow squares on Figure 5.1). The natural gas composition has been calculated by using the concentration of ⁴He and ³He/⁴He from section 4.3 (3×10^{-4} cm³ STP/cm³ and 0.05 R_A) and the pre-injection CO₂ concentration of 4% after Lu et al. (2012b). CO₂/³He values of the production well gases vary between 9.65×10^7 (28F-2 2009) and 4.01×10^9 (29-5 2012), the majority of which fall on the mixing trend. Gases from both injector wells, all the production wells in 2012, and the high CO₂ wells from 2009 have lower CO₂ concentrations that reflect the dilution of the injected CO₂ by the in-place reservoir CH₄. The four 2009 gas samples with the lowest CO₂ content (and the lowest ³He/⁴He and ⁴⁰Ar*/⁴He) have CO₂/³He that are considerably lower than injected gases. This is consistent with the loss of CO₂ from the gas phase and cannot be explained by mixing with the in-place natural gas.

The gas sample from well 27-5 taken in 2009 is an exception. Although the ³He/⁴He-CO₂ and ⁴⁰Ar*/⁴He-CO₂ relationships shows that it suffered CO₂ loss (Figure 4.4A & C) this is not apparent from the CO₂/³He ratio which overlaps the range in Jackson Dome and injected gases. The CO₂/³He – [CO₂] relationship indicates that there has been significant dilution of the CO₂ but no significant change in the CO₂/³He ratio. Well 27-5 was the most prolific oil producer of all the Cranfield wells. The gas/oil (G/O) and gas/water (G/W) ratio is lower than observed in all other oil producing wells (including those sampled in 2012).

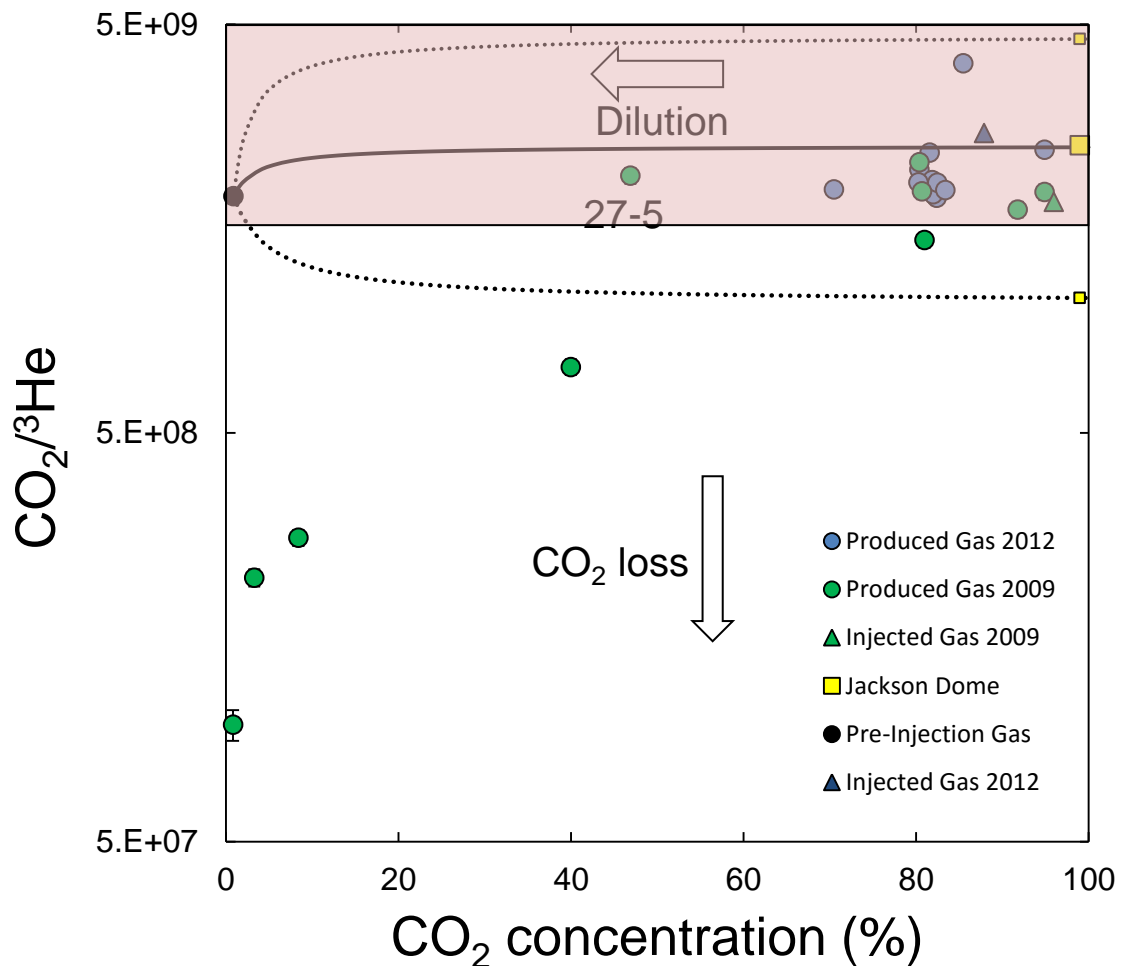


Figure 5.1. Plot of $\text{CO}_2/{}^3\text{He}$ against CO_2 concentration for Cranfield well gases. The pink surface is showing the range of global magmatic $\text{CO}_2/{}^3\text{He}$ (Marty and Jambon, 1987). Mixing curves are drawn between the natural gas and mean Jackson Dome $\text{CO}_2/{}^3\text{He}$ (continuous line) and minimum and maximum Jackson Dome $\text{CO}_2/{}^3\text{He}$ (dotted lines). The effect of dilution by the in-place natural gas (pure CH_4), addition and loss of CO_2 are shown by arrows. Four 2009 production well gases appear to have lost a significant amount of CO_2 . These are the same samples that show CO_2 loss according to ${}^3\text{He}/{}^4\text{He}$ and ${}^{40}\text{Ar}^*/{}^4\text{He}$ data (Figures 4.4A & C). Yellow square represents the average measured in Jackson Dome CO_2 , small squares its extreme values (Zhou et al., 2012). 1σ uncertainties are smaller than symbols.

In 2009 G/O = 9.2, while the average field value is 86, with an individual well exceeding 256 (well 29-6) in December 2009. Similarly, the G/W = 3.9, average field value is 10.4 with the maximum value of 32 (well 28-2), in 2009 (personal communication with field operator) (see well data in Table I.10. in the Appendix). The degassing of He-poor CH₄ from the oil is the likeliest explanation for observed data in well 27-5.

In order to quantify the loss of CO₂ from the four low CO₂/³He well gases, the measured CO₂/³He with the average of Jackson Dome CO₂/³He (2.5×10^9 ; Zhou et al., 2012) and 4.2.1) are compared. The proportional loss of CO₂ calculated using Equation 5.1 can be seen in Table 5.2. It ranges from 71% (well 29-5) to 96% (well 28F-2). Uncertainties are propagated using the measured CO₂ and ³He concentration data from each well and the standard deviation of the Jackson Dome CO₂/³He value ($\sigma = 5 \times 10^8$) using the two extreme values (see above). Except for well 29-5, the data agree with the CO₂ loss calculated using the methods described in section 5.2.1 (Table 5.2). The high degree of CO₂ loss calculated for well 29-5 (71%) compared to the ³He/⁴He and ⁴⁰Ar*/⁴He based methods (30%, 22% and 51% respectively) may be explained by heterogeneity in ⁴He/CH₄ ratio of the natural gas.

5.2.3 Quantifying the total CO₂ loss

Using the amount of CO₂ lost in each well provides a means to estimate the percentage of cumulative injected CO₂ that has been lost. The injected gas is a mixture of the produced gas and the incoming Jackson Dome gas (Choi et al., 2013). The composition of the cumulative produced gas (before mixing with the Jackson Dome CO₂ to form the injected gas composition, see Figure 6.1) could not be measured. However it is estimated that by December 2009 the CO₂ made up 82.5% of the produced gas, which is equivalent to 0.35 Mt produced CO₂ (see calculation in 6.2 for more details). This estimate is based on the amount of produced gas at the time of sampling, weighted by the concentration of CO₂ as a

proportion of the total produced gas. The calculation uses production well data as if no CO₂ loss had happened.

The theoretical total amount of produced CO₂ can be estimated in the same way. In this case the CO₂ concentrations from those four wells (therefore the amount of produced CO₂ in each well) where CO₂ loss was identified are replaced with the predicted value based on the ³He/⁴He - CO₂ relationship (Table 5.3). The calculation with these modified data reveal 78% CO₂, equivalent to be 0.36 Mt produced CO₂, suggesting that ~0.01 Mt has been lost from the free gas phase. Until December 2009 1.4 Mt of new CO₂ (excluding recycled) was injected in Cranfield (Hovorka et al., 2013), which means that approximately 0.7% of the injected Jackson Dome gas has been lost from the gas phase. This is in comparison to the gas that had been retained until December 2009 based on this calculation (1.4 – 0.35 = 1.05 Mt) (see also Hovorka et al., 2013) is negligible (0.09%) and is considered a maximum value (see 6.2).

Table 5.3. The observed and calculated CO₂ concentration and amount of gas produced where CO₂ loss has been found. The calculation is based on the ³He/⁴He and CO₂ relationship where the theoretical CO₂ is the most certain. The theoretical gas amount in each well allows the cumulative CO₂ loss to be estimated (see text).

Well	Measured CO ₂ %	Measured gas (x 10 ⁻⁶ Mt/day)	Theoretical CO ₂ % from ³ He/ ⁴ He	Theoretical injected gas (x 10 ⁻⁶ Mt/day)
28F-2 2009	0.9	3	11.8	43
29F-1 2009	3.3	5	21.8	31
44-2 2009	8.4	4	36.5	17
29-5 2009	40	3	57.5	4

5.3 Mechanism of CO₂ loss

5.3.1 He and Ar isotope constraints

The possibility that the CO₂ injected into the Cranfield field has dissolved into a fluid phase can be tested by exploiting the differential solubility of the noble gases and CO₂ in a likely fluid phase. The relative solubility of noble gases in water (Xe>Kr>Ar>Ne>He) (Smith and Kennedy, 1983) means if dissolution has occurred the lighter noble gases will be enriched in the gas phase. Noble gases was first applied in fluid interaction studies in the 1960s (Zartman et al., 1961) and has subsequently been used to constrain gas migration (e.g. Battani et al., 2000), oil bank estimation (e.g. Ballentine et al., 1996) as well as CO₂ migration mechanism (e.g. Gilfillan et al., 2008).

The CO₂/³He and ⁴⁰Ar*/⁴He of the Cranfield injection and production wells are plotted in Figure 5.2 along with theoretical mixing lines between the Jackson Dome CO₂ (Zhou et al., 2012) and the in-place reservoir gas (see 4.4). The majority of the well gas data plot within the mixing zone.

The four data points that have lost CO₂ plot significantly below the mixing line. Dissolution into a fluid will result in a decrease in ⁴⁰Ar*/⁴He of the gas phase due to the greater solubility of Ar in water than He (Zartman et al., 1961). The theoretical CO₂ concentration of each sample was calculated on the basis of CO₂-³He/⁴He relationship (see 4.5 and Table 5.3) and used to determine a theoretical ⁴⁰Ar*/⁴He according to the mixing equation between CO₂ and ⁴⁰Ar*/⁴He (Table 5.1). Fractionation curves (dashed line) are drawn from the initial values with increasing amount of dissolution (decreasing the gas/water ratio). Henry constants (K) for CO₂ and noble gases were calculated for reservoir conditions: 3 km depth, ~100°C, 32 MPa, ~2M salinity (Lu et al., 2012b). They were found to be K_{CO₂} = 0.88 and K_{He} = 18.5 GPa and K_{Ar} = 12.3 GPa. Calculations have been

made after Ballentine et al. (2002) and references therein (see data in Table I.11. in the Appendix).

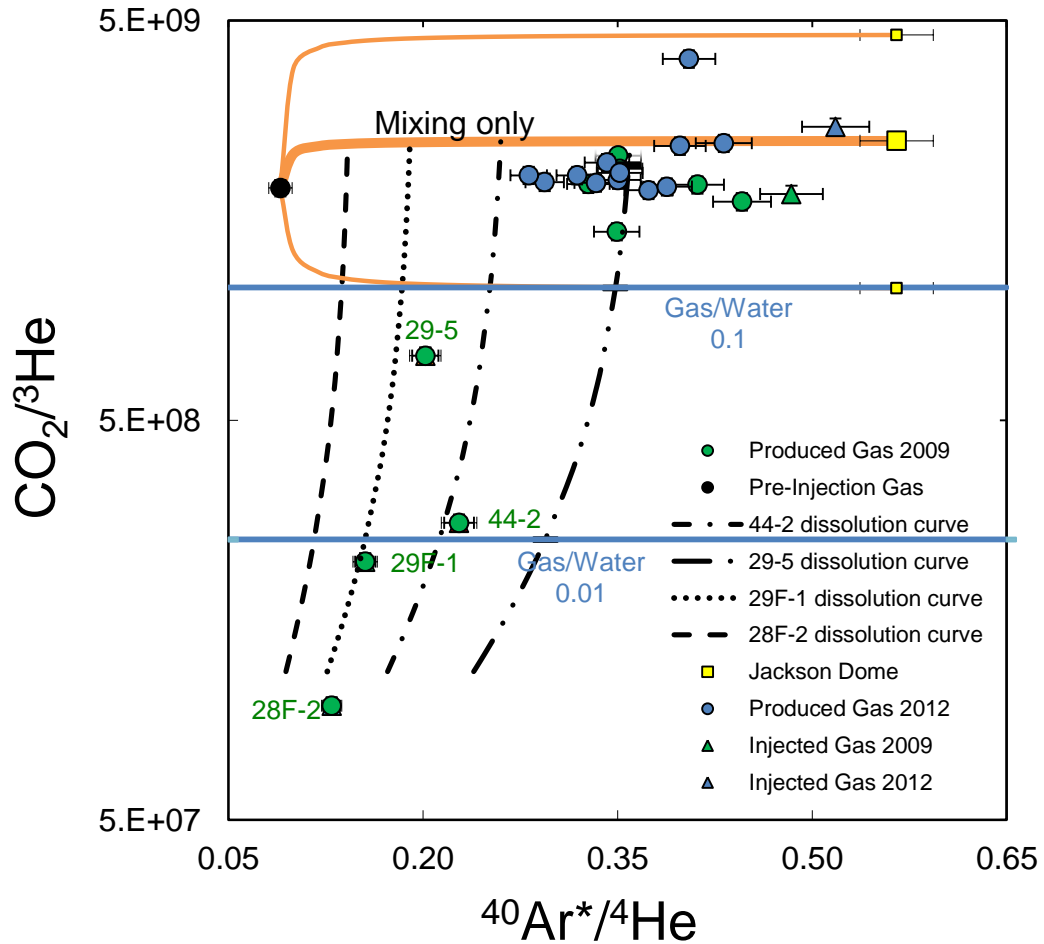


Figure 5.2. Plot of $\text{CO}_2/{}^3\text{He}$ against ${}^{40}\text{Ar}^*/{}^4\text{He}$ for Cranfield well gases. The mixing between natural gas end-member and Jackson Dome is shown as thin orange lines, with best estimate shown as thick orange line. The extreme values of the Jackson Dome $\text{CO}_2/{}^3\text{He}$ are indicated as small yellow squares. Samples significantly below the mixing region show CO_2 loss. Curved lines show the batch fractionation curves for water dissolution in different gas/water (G/W) ratios. Their starting point is the calculated theoretical ${}^{40}\text{Ar}^*/{}^4\text{He}$ (see text) value for each sample. Except well 29-5 all data can be explained by solubility controlled processes (see text). Uncertainties are 1σ .

The measured $^{40}\text{Ar}^*/^4\text{He}$ of gases from wells 44-2, and 29F-1 sit on the predicted dissolution curve, supporting the contention that the low CO_2 content of these samples is due to dissolution into water. Gas from well 29-5 has a lower $^{40}\text{Ar}^*/^4\text{He}$ than predicted and is explained by the high ^4He concentration (see section 5.2.1).

The measured $^{40}\text{Ar}^*/^4\text{He}$ from well 28F-2 lies to the right of the theoretical fractionation curve. A possible hypothesis can be given to explain this: The $^{40}\text{Ar}^*/^4\text{He}$ of the natural gas may vary throughout the reservoir. For instance well 28F-2 is on the east side of the fault that dissects the field, while 44-2 is on the west side (Figure 3.1). Well 28F-2 has a higher degree of water degassing (i.e. more noble gases have entered to the gas phase from the water phase) than 44-2 (see e.g. Figure 6.5). If it is in connection with a higher $^{40}\text{Ar}^*/^4\text{He}$ fluid and the dominant mechanism is the gas stripping as opposed to dissolution, the $^{40}\text{Ar}^*/^4\text{He}$ ratio will decrease from the initial value (e.g. 0.2) but would never reach the fractionation line until dissolution becomes more important than stripping. To test this hypothesis precise baseline data would be needed from both parts of the reservoir as well as non-radiogenic noble gas data from well 29F-1. That well is the neighbour of 28F-2 hence the initial $^{40}\text{Ar}^*/^4\text{He}$ would be expected to be the same (e.g. 0.2). As 29F-1 lies on the fractionation curve on Figure 5.2 it would be expected to show near zero water degassing on Figure 6.5. The competitive stripping and dissolution is similar to that of described by Gilfillan et al. (2008).

Although the Jackson Dome composition could be slightly different due to its natural variability (small yellow squares on Figure 5.2) it has little effect on the shape of the fractionation curve.

The noble gases are considerably more soluble in oil than in water and the relative solubility is the same than in water (Kharaka and Specht, 1988; Smith and Kennedy, 1983). Consequently the residual gas phase after dissolution in oil would be more depleted in the heavy noble gases than if the gas was dissolved in water. The resulting fractionation

curves would be less vertical than in Figure 5.2. Therefore only data point that plot to the left of the water dissolution fractionation curve could be explained by the presence of oil. No data (except 27-5, explained above) plot to the left of the water curve therefore significant dissolution in oil can be ruled out. This is also supported by well data because except for 29F-1, the wells did not produce any oil by the time of sampling. See also Chapter 6.

5.3.2 Carbon isotopes

The fractionation of $\delta^{13}\text{C}_{\text{CO}_2}$ and $\text{CO}_2/{}^3\text{He}$ has previously been used to distinguish between CO_2 precipitation to carbonate minerals and dissolution into the water (Gilfillan et al., 2009). This technique has been applied in natural gas fields (Dubacq et al., 2012; Zhou et al., 2012) but to date it has not been used in a CO_2 injection field.

Lu et al. (2012b) have reported the $\delta^{13}\text{C}$ of CO_2 from several production well gases that were sampled during the 2009 campaign at the same time as samples for noble gas isotopes were collected for this study. This includes one of the four well gases that suffered CO_2 loss (29F-1; $\delta^{13}\text{C} = -4.81 \text{ ‰}$). This can be combined with the $\text{CO}_2/{}^3\text{He}$ from this study in order to test the CO_2 dissolution model.

The effect of dissolution into groundwater and mineral precipitation on $\text{CO}_2/{}^3\text{He}$ and $\delta^{13}\text{C}_{\text{CO}_2}$ is shown in Figure 5.3. The plotted data use the $\text{CO}_2/{}^3\text{He}$ data from this study and $\delta^{13}\text{C}_{\text{CO}_2}$ values measured at SUERC (symbols as per Figure 5.2) or from Lu et al. (2012b) (small grey circles). Where $\delta^{13}\text{C}_{\text{CO}_2}$ has been measured in both laboratories the data tend to overlap within 1σ uncertainty. The starting point for the fractionation curves is the average Jackson Dome CO_2 (yellow square; $\text{CO}_2/{}^3\text{He} = 2.5 \times 10^9$, $\delta^{13}\text{C}_{\text{CO}_2} = -2.96 \text{ ‰}$; Zhou et al. (2012). The large variation in Jackson Dome $\text{CO}_2/{}^3\text{He}$ is demonstrated by the small yellow square which represents the minimum value $\text{CO}_2/{}^3\text{He}$ (Zhou et al., 2012). The Jackson

Dome CO₂/³He is combined with δ¹³C_{CO₂} from Lu et al. (2012b) (-2.6 ‰) and shown as a grey square. The data typically have CO₂/³He ratio that are within the Jackson Dome range but well 29F-1 is significantly below any Jackson Dome value and the δ¹³C_{CO₂} is much lower than all others.

The dotted line shows the predicted trend for carbonate precipitation according to the Rayleigh fractionation equations for the CO₂–calcite system after Deines et al. (1974), using equations after Gilfillan et al. (2009). The change in the CO₂/³He ratio as a function of the fraction of the CO₂ precipitated is given by Equation 5.2.

$$\left(\frac{CO_2}{^3He}\right)_{after\ precipitation} = \left(\frac{CO_2}{^3He}\right)_{Jackson\ Dome} \left(1 - \frac{(CO_2)_{precipitated}(\%)}{100}\right) \quad \text{Equation 5.2}$$

The continuous lines show the trend expected by dissolution into water at different pH under reservoir conditions (see above). Calculations have been made assuming that CO₂ forms either H₂CO₃ or HCO₃⁻ but negligible CO₃²⁻ (Gilfillan et al., 2009) (see data in Table I.12. in the Appendix).

The proportion of H₂CO₃ or HCO₃⁻ is pH dependent and can be calculated by Equation 5.3

$$pH = pKa + \log \frac{[HCO_3^-]}{[H_2CO_3]} \quad \text{Equation 5.3}$$

where pK_a is 6.3 (Fritz and Fontes, 1980). Henry constants for He and CO₂ for the calculations are those calculated in 5.3.1.

The low CO₂ sample (well 29F-1) plots significantly below the mineral precipitation line which tends to rule out significant transformation of CO₂ into carbonate minerals. It plots between the dissolution lines defined by pH 6 and 7. This supports the evidence from noble gases that the local groundwater is the sink of the injected CO₂. This reservoir pH estimation is not far from that measured by Lu et al. (2012b) (pH = 5.8), however their value has been measured on the surface and is expected to be somewhat higher under reservoir conditions (see Lu et al. (2012b)). The quantification of the degree of dissolution

is difficult to obtain because of the variability of the Jackson Dome gas $\text{CO}_2/{}^3\text{He}$ and $\delta^{13}\text{C}_{\text{CO}_2}$.

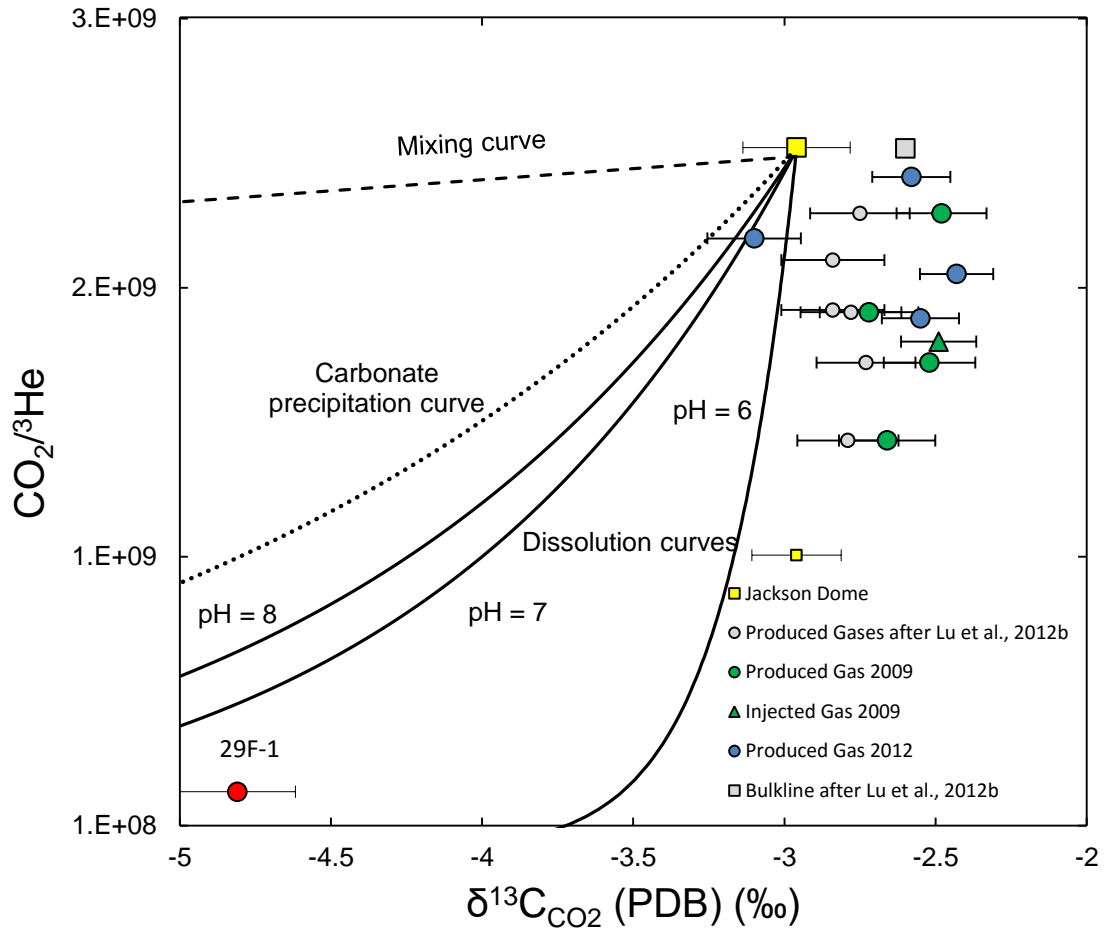


Figure 5.3. The plot of $\text{CO}_2/{}^3\text{He}$ versus $\delta^{13}\text{C}_{\text{CO}_2}$ for Cranfield well gases. The dashed line shows the theoretical mixing. The dotted line shows the fractionation trend for carbonate precipitation, while continuous lines plot fractionation expected for dissolution in water at different pH values (Gilfillan et al., 2009). Sample 29F-1 (red circle) plots in the dissolution field. Uncertainties are 1σ .

5.4 Storage of injected CO₂

On balance it seems that the CO₂ loss is best explained by dissolution into the saline groundwater. The lack of evidence for mineral trapping is consistent with the predicted low pace of carbonate formation (Bachu et al., 2007). In contrast, other siliciclastic reservoirs have shown that up to 18% of the CO₂ in the Bravo Dome (Gilfillan et al., 2009), and up to 27% in the Jackson Dome (Zhou et al., 2012) has been trapped in mineral form. CO₂ dissolution into groundwater is more common than mineral precipitation in natural gas fields even on long time scales (Battani et al., 2000; Bosch and Mazar, 1988; Gilfillan et al., 2009; Zhou et al., 2012). CO₂ dissolution has been demonstrated by a sharp decrease in the pH of brine from the Frio experimental site where 1600 tonnes of CO₂ were injected (Kharaka et al., 2006). Solubility trapping has also been found to have an important role in storing CO₂ from the beginning of injection (see Figure 1.3).

The majority of the CO₂ injected at Cranfield over the 3 year period of this study appears to have remained as a free gas phase with no significant gas loss. In the majority of the production well gas samples the noble gas isotopic and elemental ratios can be explained by mixing between injected and reservoir gases. This means that neither mineral nor solubility trapping processes have resulted in the storage of a significant volume of CO₂. Whether some of the CO₂ is retained by residual trapping (see 1.3.1) is something that isotope geochemistry cannot model on current knowledge. Due to the nature of that trapping mechanism the CO₂/noble gas ratio should be more or less unchanged, as it is similar to stratigraphic trapping. Although some degree of the occurrence of residual trapping cannot be ruled out it is expected to become significant only after CO₂ injection has stopped (e.g. Lu et al., 2013).

Conclusions made on how the majority of CO₂ is stored in Cranfield are fully consistent with the work carried out by Lu et al. (2013). They concluded that the CO₂ was dominantly

trapped as a free gas, on the basis of seismic data and core analysis at Cranfield. The Cranfield reservoir is a four-way anticline, which is an ideal condition for structural trapping. The Cranfield reservoir water has high salinity and is saturated with CH₄ (Lu et al., 2012b), making it difficult to dissolve CO₂. The reservoir fluid geochemistry remained mostly unchanged for major anions and cations, during the 14 months of injection (Lu et al., 2012b). The abundance of reactive minerals is low (Lu et al., 2012b; Lu et al., 2013). Also, the 3.6 Mt of injected gas (excluding recycled) by early 2012 is an extremely high amount.

The storage mechanism may be a function of the relative CO₂ flux compared to the volume (and type) of reservoir fluids. The number of injection and production wells, the complexity of the injection schedule (Choi et al., 2013) and the absence of injection data means reconstructing the CO₂ flux at any well at the time of sampling at Cranfield is rather imprecise.

However Table 5.4 shows an attempt to calculate the amount of injected CO₂ that could have reached the production wells. These calculations use the injection data from the wells that directly surround each production well (usually from three to five injectors). The data reflect the injected CO₂ on the day of sampling in 2009 (personal communication with field operator), or the day closest to the time of sampling (MSOGB, 2015). The volume of injected CO₂ was weighted by the reciprocal of the relative linear distance between each injector and the producer, and a weighted average amount of injected CO₂ was calculated. This does not take into account changes in fluid flow, caused by heterogeneity in, for example, the permeability of the rocks between the injectors and producers.

Table 5.4. The average amount of injected gas around the production wells and the amount of produced oil in 2009 production wells. Wells are categorized into low and high flux production wells. 28F-2, 29F-1, 44-2 and 29-5 show low flux (see text). In case of the first two it is explained by the low amount of injected gas. In case of 44-2 and 29-5 the lack of oil is the indicator, which suggests geological heterogeneity. Source: MSOGB (2015).

Well	CO ₂ %	Injected CO ₂ ; m ³ STP/day (x 10 ³) around the well	Produced oil m ³ /day
28F-2	0.9	65.7	0
29F-1	3.3	86.9	10.8
44-2	8.4	203.5	0
29-5	40.0	142.6	0
27-5	46.9	151.8	57.8
29-1	80.7	107.4	13.0
29-9	94.9	148.9	7.8
27-3	81.0	176.0	22.1
28-2	80.4	180.1	32.8
29-6	91.8	149.1	7.5

The volume of injected CO₂ ranges from 65.7 to 203.5 m³. The lowest volume of injected gas was around wells 28F-2 and 29F-1 (65.7 and 86.9 respectively). The two other wells that have shown CO₂ loss (44-2 and 29-5) do not show low injected volumes (203.5 and 142.6 respectively). However, they had not produced oil by December 2009, implying a low CO₂ flux to the well. This may be governed by the presence of low permeability rocks that limits the CO₂–oil contact and is supported by core analysis that showed large permeability variations within the reservoir sandstone, from <1 and 1900 mD (Lu et al., 2013). In all other cases the high amount of injected gas from surrounding injectors is accompanied by significant oil production, therefore the CO₂ flux is relatively high in comparison to the four discussed.

5.5 Conclusions

The proportion of CO₂ loss can be best estimated by the combined use of CO₂/³He – CO₂ and ³He/⁴He – CO₂ systems. It was quantified to be ~0.1% of the total injected gas. According to the fractionation of CO₂/³He and ⁴⁰Ar*/⁴He, solubility controlled processes are responsible for the observed CO₂ loss. This is supported by the fractionation of δ¹³C_{CO2}. The majority of wells that did not show loss of gas are consistent with a stratigraphic (or residual) trapping mechanism that was found to be the most important storage mechanism in Cranfield previously (Lu et al., 2013) and expected within the timescale of CO₂ injection (Bachu et al., 2007). The different trapping mechanism observed spatially and temporary are consistent with the differences in the average CO₂ flux under production wells.

Chapter 6

Examining the interaction of injected CO₂, brine and oil in the Cranfield fluid reservoir using non-radiogenic noble gases

6.1 Introduction

In the previous chapters the mixing between injected and reservoir gas has been examined using the radiogenic noble gas isotopes. The Ne-Ar isotope systematics led to the conclusion that a small contribution of atmosphere-derived gases is present in the Cranfield reservoir fluids (section 4.3). The atmosphere is the dominant reservoir of non-radiogenic noble gas isotopes in the Earth, and recharge of air saturated water (ASW) is the dominant mechanism for introducing these gases into the shallow crust. The large mass range of the dominant non-radiogenic noble gas isotopes (²⁰Ne, ³⁶Ar, ⁸⁴Kr and ¹³²Xe) means that ASW patterns are fractionated significantly by physical processes such as variation in atmosphere equilibration temperature, evaporation and equilibrium with other fluids (e.g. Kennedy et al., 2002).

Natural gases, both CH₄-rich and CO₂-rich, typically have non-radiogenic noble gas patterns that are consistent with derivation from an air saturated water source (e.g. Pinti and Marty, 1995). Variation of ²⁰Ne/³⁶Ar, ⁸⁴Kr/³⁶Ar and ¹³²Xe/³⁶Ar ratios in natural gases can be used to identify the degree of gas–water interaction (e.g. Battani et al., 2000) and even gas-water–oil interaction (Bosch and Mazor, 1988).

In this chapter the ²⁰Ne/³⁶Ar, ⁸⁴Kr/³⁶Ar and ¹³²Xe/³⁶Ar ratios of the gas end-members in the Cranfield reservoir are identified, and the data from production wells are used to test the mixing models identified in Chapters 4 and 5, with the specific intention of trying to track the interaction history between injected CO₂, brine and oil.

As part of the SECARB (see 3.2) large-scale CO₂ injection tests, a large volume of atmospheric Kr and Xe was injected into the Cranfield reservoir in late 2009 and early

2010 in the hydrologically-isolated ‘Detailed Area of Study’ (DAS) site (Lu et al., 2012a) (Figure 3.1). The possibility that the injected Kr and Xe migrated from the DAS site into the main reservoir is a complication that must be assessed beforehand to determine whether the heavy noble gases constrain sources and mixing history.

6.2 The influence of injected Kr and Xe at the DAS site

This section investigates whether there has been any significant leak of heavy noble gases from the DAS site into the main reservoir. To this end a three-component mixing system is set up: Bulkline gas, main reservoir prior to injection (well 28F-2, see section 4.2.1) and the gas injected at the DAS site (see Table 6.1). The Kr/Xe ratios of the production wells from the main reservoir are compared to the proposed end-members in order to assess the extent of leakage.

Noble gas tracers were injected into the DAS site on 3rd December 2009 and 15th April 2010 (Gilfillan et al., 2011; Lu et al., 2012a). The injected gas was approximately 50% N₂, 40% Kr and 10% Xe (Gilfillan et al., 2011). As the isotopic composition of the injected Kr and Xe is identical to air (see Table I.13 in the Appendix), the ⁸⁴Kr/¹³²Xe ratio of the injected gas is 27.8 (unpublished data, S. Gilfillan). This is significantly higher than the range of values measured in production gases from the main Cranfield reservoir from both years (9.09 –14.13) (Table 6.2).

The first injection of Kr and Xe at the DAS site occurred 2 days before the production wells from the main reservoir were sampled in 2009 for this study. The breakthrough of the injected ⁸⁴Kr in the observation well at the DAS site, 68 m from the injector (well 31F-1), took 15 days (Gilfillan et al., 2011). Gases sampled from the main reservoir production wells in December 2009 for this study are several hundreds of meters away from the DAS

injection well. Therefore it is highly unlikely that the injected Kr and Xe are present in any of the 2009 production well gases.

A substantial time (827 days) had elapsed between tracer injection and the March 2012 sampling campaign. Given the rate of movement through the DAS site, the injected Kr and Xe could have reached many of the wells in the main reservoir if it is not hydrologically isolated. As a result the injected DAS site gas is only possible in the 2012 production well samples.

6.2.1 $^{84}\text{Kr}/^{132}\text{Xe}$ in the DAS site in March 2012

In order to assess the extent, if any, of the injected DAS site gas in the main reservoir the Kr and Xe concentration of the leaking gas must be determined. It has three sources of Kr and Xe: i) the artificial gas added to the CO₂ stream, ii) the injected Jackson Dome CO₂ (Zhou et al., 2012) and iii) the pre-injection reservoir gas.

i) Approximately 1.49 m³ STP of atmospheric Kr was injected on 3/12/2009. This equates to 0.852 m³ STP of ^{84}Kr . During the second injection phase 0.574 m³ Kr, so 0.327 m³ STP of ^{84}Kr , were injected (Gilfillan et al., 2011; Lu et al., 2012a). The total injected ^{84}Kr was therefore 1.18 m³ STP by March 2012.

ii) The Jackson Dome CO₂ carried $1.78 \times 10^{-10} \text{ cm}^3 \text{ STP/cm}^3 \text{ Kr}$ (Zhou et al., 2012). The DAS CO₂ injection started in December 2009 and the average injection rate until March 2012 was ~0.09 Mt/a (personal communication with J. Lu). This means that ~0.2 Mt CO₂ (~1 x 10⁸ m³ STP) was injected by March 2012. Using the ^{84}Kr concentration of the Jackson Dome CO₂ from Zhou et al. (2012) the total amount of injected ^{84}Kr is calculated to be 0.02 m³ STP.

The injected CO₂ in the DAS site is identical to that injected into the main reservoir. The recycling of production well gas means the injected gas is continuously being enriched in

⁸⁴Kr because (i) the high concentration in the reservoir gas (well 28F-2, $2.6 \times 10^{-9} \text{ cm}^3 \text{ STP/cm}^3$) compared to Jackson Dome ($1.8 \times 10^{-10} \text{ cm}^3 \text{ STP/cm}^3$), and (ii) it is not extracted (there is no production well). Although the degree of Kr enrichment could be calculated in the case of pure gas mixing, it is unknown whether i) only mixing is responsible for the changes of the concentration of ⁸⁴Kr and ii) whether the reservoir gas enriches the injected gas and does not itself leak from the DAS site, investigation of which is the purpose of this section. It is unlikely that the calculated ⁸⁴Kr ($0.02 \text{ m}^3 \text{ STP}$) would change significantly as there is no obvious source or sink, and it is negligible compared to the artificially injected ⁸⁴Kr ($1.18 \text{ m}^3 \text{ STP}$), so such a small change would not change the interpretation in section 6.2.2.

iii) The amount of the naturally occurring ⁸⁴Kr in the DAS site needs to be estimated. This can be done by estimating the amount of natural Kr in the main reservoir.

To this end the following model is established. By Equation 6.1 & 6.2 (see Figure 6.1)

$$C_3 = \frac{M_1 C_1 - M_s C_1 + M_2 C_2}{M_1 C_1 - M_s C_1 + M_2 C_2 + M_2 (1 - C_2)} \quad \text{Equation 6.1}$$

$$C_4 = \frac{2M_1 C_1 - M_s C_1 + M_2 C_2}{2M_1 C_1 - M_s C_1 + M_2 C_2 + M_2 (1 - C_2)} \quad \text{Equation 6.2}$$

Where ‘C’ is concentration in % and ‘M’ is mass in Mt.

The Jackson Dome CO₂ (M₁), with CO₂ concentration (C₁), mixes with an unknown amount of reservoir gas (M₂) after injection, which is a mixture of CO₂ and CH₄ with CO₂ concentration (C₂, 4%) (see Chapter 4). The mixed gas (M₃), reduced by the amount of stored gas, retained in the reservoir (M_s) is extracted through production wells (M₃ = M₁+M₂-M_s) has a CO₂ concentration (C₃). The produced gas (M₃) is mixed with the incoming Jackson Dome gas (M₁) and results in the injected gas, of which the concentration was measured (C₄). The reinjection facility does not separate CO₂ from CH₄

thus the recycled gas is a CO₂-CH₄ mixture (Choi et al., 2013). The illustration of the model can be seen in Figure 6.1.

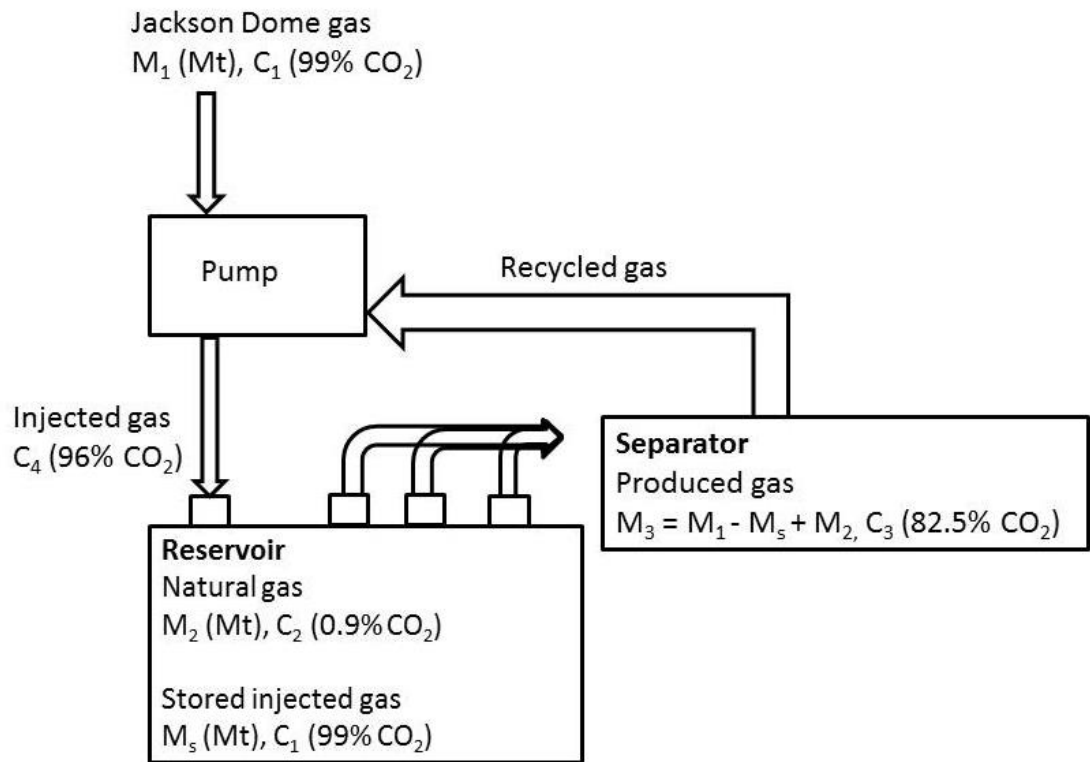


Figure 6.1. Schematic picture of the gas cycle in Cranfield. For the model see text.

This calculation assumes that all the initial reservoir gas remained in the gas phase and was extracted, i.e. there was no CO₂ loss by dissolution or mineral precipitation (see section 5.3). The model is used for December 2009, when all the production wells in operation were sampled. This allows the average composition of the recycled gas (C_3), to be estimated. All producers contribute to the recycled gas according to the amount of gas produced and the CO₂ concentration.

Using the individual well data, the total amount of gas extracted up to December 2009 was 0.4 Mt (personal communication with field operator). This is a maximum estimate because some wells started operating after the start of injection in July 2008. This value is close to the 0.2 Mt estimated by Hovorka et al. (2013). The average CO₂ concentration of the

recycled gas (C_3) can be calculated to be 82.5% by weighting the CO_2 concentration of individual wells by the amount of gas produced, measured at the time of sampling. By using the composition of the injected gas in 2009 (96%) the boundary condition that $C_1 = 100\%$ and the total injected gas amount by December 2009 ($M_1 = 1.4$ Mt) and the total recycled gas ($M_3 = 0.2$ Mt) after Hovorka et al. (2013), the pre-injection gas (M_2) can be estimated to be 0.08 Mt.

The composition of the recycled gas is influenced by processes other than mixing such as dissolution, which is an important sink of the CO_2 in some wells (see section 5.3). The most significant uncertainty is the assumption that all the reservoir gas was extracted. Nevertheless, this provides an approximate constraint on the amount of reservoir gas prior to injection. This is equivalent to 2.2×10^8 m³ STP total gas in the main reservoir.

The DAS site is smaller than the main reservoir. The mass of the gas can be estimated by using the relative volumes of the DAS site and main reservoirs. Since the average depth is the same in both reservoirs (~3 km) (Lu et al., 2012a, b) the surface area can be used for calculation. The main reservoir is approximately circular with a diameter of 6.4 km (Lu et al., 2012b), giving a surface area of 32.2 km². The DAS site area is 1 km² (Carter and Spikes, 2013). Using the estimated amount of gas in the main reservoir (0.08 Mt) this would mean 0.003 Mt and therefore 2×10^6 m³ STP gas prior to injection in the DAS site. Using the concentration of ⁸⁴Kr of well 28F-2 to represent the Kr concentration in the natural gas (2.6×10^{-9} cm³ STP/cm³) this means 0.004 m³ STP of ⁸⁴Kr.

The total ⁸⁴Kr in March 2012 in the DAS site ($1.18 + 0.02 + 0.004$ m³ STP) is 1.204 m³ STP. The concentration of ⁸⁴Kr in the DAS site can be calculated by $V_{Kr}/V_{total\ gas}$ where $V_{total\ gas}$ is the sum of reservoir and injected gas ($1 \times 10^8 + 2 \times 10^6$) and is $\sim 1 \times 10^8$ m³ STP. Consequently the concentration of ⁸⁴Kr is 1.2×10^{-8} cm³ STP/cm³.

Calculating the Xe from the DAS site is hampered by the lack of a measured value in the Jackson Dome CO_2 . However in case of ⁸⁴Kr the contribution of that source is only 1.6%

of the total ^{84}Kr present in the DAS site by March 2012 and is therefore negligible. Here it is assumed that the ^{132}Xe concentration in the Jackson Dome CO_2 be proportionately small, considering the source of the gas (see Zhou et al., 2012).

The remaining two sources of Xe in the DAS site (artificial injection and naturally occurring prior to injection) can be calculated. The cumulative amount of Xe injected into the DAS site in the two injection events (see above) was $0.14 \text{ m}^3 \text{ STP}$ (Gilfillan et al., 2011; Lu et al., 2012a). By using the concentration of Xe of the natural gas end-member (28F-2 2009, $1.2 \times 10^{-10} \text{ cm}^3 \text{ STP/cm}^3$) and the total gas amount in the DAS site prior to injection ($2 \times 10^6 \text{ m}^3 \text{ STP}$) the baseline amount of Xe can be estimated to be $0.0002 \text{ m}^3 \text{ STP}$, which can also be considered negligible. The concentration of ^{132}Xe in the DAS site by March 2012 can be calculated by $V_{\text{Xe}}/V_{\text{total gas}}$ where the total ^{132}Xe is 0.14 m^3 and the total gas is 2×10^6 (natural gas) + 1×10^8 (Jackson Dome) = $\sim 1 \times 10^8 \text{ m}^3 \text{ STP}$. The concentration of ^{132}Xe therefore is calculated to be $1.4 \times 10^{-9} \text{ cm}^3 \text{ STP/cm}^3$. As is apparent from the calculations, the predominant Kr and Xe source in the DAS site is the artificial tracer injection test. The concentrations of both isotopes are an order of magnitude higher in the DAS site than in the main reservoir and two order of magnitude higher than that of the bulkline gas.

Table 6.1. Kr and Xe concentrations of the three main components in the Cranfield reservoir. Concentrations are $\text{cm}^3 \text{ STP/cm}^3$.

	^{84}Kr	^{132}Xe
DAS site by March 2012	1.2×10^{-8}	1.4×10^{-9}
Main reservoir prior to injection	2.6×10^{-9}	1.2×10^{-10}
Bulkline	2.8×10^{-11}	4.9×10^{-12}

6.2.2 Assessing the potential leak from the DAS reservoir

The Kr and Xe concentration of the three main gas components in the main Cranfield reservoir are in Table 6.1 and shown in Figure 6.2 along with the injection and production well data from the main reservoir. The composition of the gas in the main reservoir prior to injection is taken to be represented by well 28F-2 (orange circle on Figure 6.2). If there has been no DAS site leakage the data would be expected to fall on the mixing line between the main reservoir gas and Jackson Dome CO₂ in Figure 6.2. Leakage of Kr- and Xe-rich gas from the DAS site would be expected to generate gases from 2012 that plot at considerably higher concentrations of Kr and Xe than the natural gas, plotting between the bulkine-DAS injection and natural gas-DAS injection mixing lines.

All the 2012 injection and production well gas data plot within the envelope defined by the three mixing lines, indicating that all three sources may have contributed (Table 6.2).

However, there are several reasons why this is unlikely to be the case. The 2012 production well gas samples have Kr/Xe ratios that are indistinguishable from the 2009 production well data – in Figure 6.2 they plot along a trend that overlaps that described by the 2009 samples. As the 2009 data cannot be due to leakage of DAS injected gas this is difficult to explain by leakage. Furthermore, the highest Kr/Xe is from a production well 27-5 that was sampled in 2009. Also, leakage from DAS site would likely be most evident in the production wells closest to the DAS site. Instead, the highest Kr and Xe concentration are found in well 70-2 2012 that is the farthest from the DAS site.

These observations appear to show that significant leakage from the DAS site can be ruled out. This is consistent with studies that demonstrate the DAS site to be isolated from the main reservoir at Cranfield (Hovorka, 2013). That the production well gases do not have Kr-Xe composition indicating simple two component mixing in Figure 6.2 imply that a process other than mixing has occurred in the main reservoir.

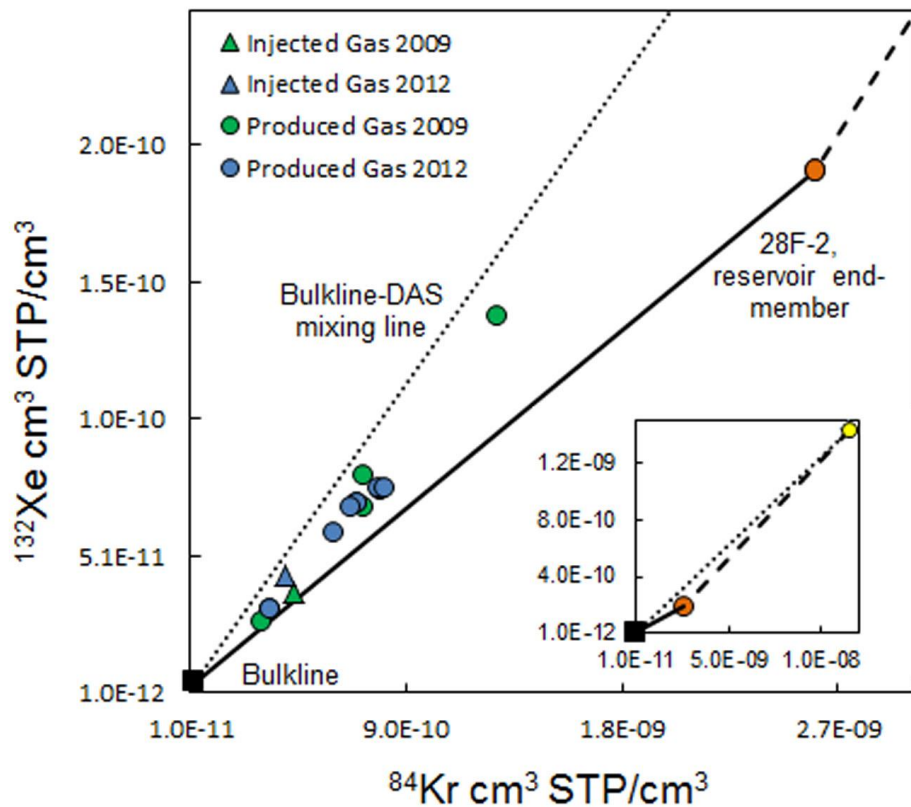


Figure 6.2. The concentration of ^{132}Xe and ^{84}Kr in Cranfield injection and production well gases. In case of a simple gas mixing between injected (bulkline, black square) and reservoir (well 28F-2, orange circle) in the main reservoir, the data would lie on the black mixing line. If there was no CO_2 injection into the main reservoir but into the DAS site only, data would be on the dashed line between the main reservoir gas and gas injected at the DAS site (yellow circle in embedded figure). The bulkline – DAS mixing line is represented by dotted line. Data plot within the area defined by the three end-members. The 2009 data show the same trend as 2012 data and do not require DAS noble gases. Uncertainties are 1σ .

6.3 Non-radiogenic noble gas data: mixing with air-saturated water

Having ruled out contamination of injected gases from the DAS site and identified the need for process(es) other than mixing in the reservoir, the non-radiogenic noble gases can be used to identify the source and interaction history of the fluids during CO₂ injection. In common with previous studies (e.g. Bosch and Mazar, 1988) the non-radiogenic noble gases (²⁰Ne, ⁸⁴Kr and ¹³²Xe) are normalised to ³⁶Ar in future discussions (Table 6.2).

The ²⁰Ne/³⁶Ar of the Jackson Dome CO₂ is 1.29 ± 0.06 (Zhou et al., 2012). The ²⁰Ne/³⁶Ar of the injected gas decreased from 0.617 to 0.409 between 2009 and 2012. The ²⁰Ne/³⁶Ar of the production well gases range from 0.148 (28F-2 2009) to 0.637 (well 29-6 from both campaigns). ²⁰Ne/³⁶Ar data are generally lower than the air value (0.526), while some exceed it.

The ⁸⁴Kr/³⁶Ar of the Jackson Dome CO₂ is 0.021 ± 0.001 (Zhou et al., 2012). The ⁸⁴Kr/³⁶Ar of the injection well gases increased with time, from 0.030 to 0.044 from 2009 to 2012. Among production well gases well 29-9 2009 has the lowest value (0.030) and 70-2 2012 has the highest (0.056). ⁸⁴Kr/³⁶Ar data are all higher than the air value of 0.021.

The ¹³²Xe/³⁶Ar in injectors changed from 0.0025 to 0.0048 between 2009 and 2012.

Production well gases vary between 0.0024 (well 44-2 2009) and 0.0053 (well 28-2 2012).

All values are higher than the air value of 0.00075. Xe was not measured in Jackson Dome CO₂ by Zhou et al. (2012) but in order to model mixing between reservoir and injected gas with ¹³²Xe/³⁶Ar the ratio of the Jackson Dome CO₂ needs to be estimated.

Table 6.2. The non-radiogenic isotopic composition of CO₂ well gases from Cranfield. Noble gas concentrations are cm³ (STP)/cm³. 1σ uncertainties are in parentheses. The values for Jackson Dome are after Zhou et al. (2012) but the Xe was estimated (see text). Air composition is after Ozima and Podosek (2001). ASW is calculated as atmosphere that equilibrated with zero salinity groundwater at 16°C and 50 m altitude, and contains a 10 % excess of Ne (Aeschbach-Hertig et al., 1999; Kipfer et al., 2002). For well data see Table 4.3.

Well ID	Year	Well Type	CO ₂ % ±0.1	⁸⁴ Kr x 10 ⁻¹⁰	¹³² Xe x 10 ⁻¹¹	²⁰ Ne/ ³⁶ Ar	⁸⁴ Kr/ ³⁶ Ar	¹³² Xe/ ³⁶ Ar
Bulkline	2012	NA	99.3	0.284 (12)	0.489 (26)	0.411 (24)	0.020 (1)	0.0035 (2)
Jackson Dome	NA	NA	99.0	1.782 (39)	1.271 (100)	1.291 (32)	0.020 (1)	0.0014 (2)
Injector	2009	Injector	96.0	4.356 (181)	3.743 (196)	0.618 (35)	0.030 (2)	0.0025 (2)
Injector	2012	Injector	87.9	4.045 (168)	4.384 (230)	0.547 (31)	0.044 (3)	0.0048 (3)
28-2	2009	Producer	80.4	7.278 (303)	6.835 (358)	0.345 (20)	0.039 (2)	0.0036 (2)
28-2	2012	Producer	80.4	13.81 (57)	13.34 (69)	0.255 (14)	0.054 (3)	0.0053 (3)
28F-2	2009	Producer	0.8	25.82 (99)	19.19 (99)	0.148 (40)	0.036 (2)	0.0027 (2)
28F-2	2012	Producer	81.9	7.026 (292)	6.989 (366)	0.428 (24)	0.042 (2)	0.0042 (3)
29-6	2009	Producer	91.8	3.439 (143)	3.103 (163)	0.607 (35)	0.030 (2)	0.0026 (2)
29-6	2012	Producer	94.9	3.411 (142)	3.101 (162)	0.637 (36)	0.042 (2)	0.0038 (2)
29-9	2009	Producer	94.9	3.041 (126)	2.691 (141)	0.637 (36)	0.030 (2)	0.0025 (2)
29-1	2009	Producer	80.7	7.273 (303)	8.000 (419)	0.384 (22)	0.037 (2)	0.0040 (3)
29-1	2012	Producer	82.0	6.056 (252)	5.952 (312)	0.422 (24)	0.038 (2)	0.0037 (2)
27-5	2009	Producer	46.9	12.77 (53)	13.83 (72)	0.170 (15)	0.041 (3)	0.0045 (3)
27-5	2012	Producer	82.5	6.723 (279)	6.865 (359)	0.448 (25)	0.048 (3)	0.0049 (3)
44-2	2009	Producer	8.4	24.06 (98)	17.03 (89)	0.201 (20)	0.034 (2)	0.0024 (2)
45F-4	2012	Producer	81.6	7.929 (329)	7.502 (393)	0.386 (22)	0.051 (3)	0.0048 (3)
32F-10	2012	Producer	80.3	7.897 (328)	7.567 (396)	0.443 (25)	0.054 (3)	0.0052 (3)
70-2	2012	Producer	83.4	8.141 (338)	7.551 (395)	0.443 (26)	0.056 (3)	0.0052 (3)
AIR	NA	NA	NA	6498 (5)	234 (3)	0.526 (3)	0.021 (0)	0.0007 (0)
ASW	NA	NA	NA	NA	NA	0.163	0.039	0.0025

To this end the $^{84}\text{Kr}/^{36}\text{Ar}$ is plotted against $^{132}\text{Xe}/^{36}\text{Ar}$ of injected and produced gases in Figure 6.3. The data define a near straight line, which is broadly consistent with the previously identified binary mixing between the injected CO_2 and reservoir gas (see section 4.3). The $^{84}\text{Kr}/^{36}\text{Ar}$ of the Jackson Dome CO_2 is identical to that of air (Zhou et al., 2012). The Jackson Dome $^{132}\text{Xe}/^{36}\text{Ar}$ can be estimated from the intersection of the best-fit line with the air value in Figure 6.3. In this way the $^{132}\text{Xe}/^{36}\text{Ar}$ is estimated to be 0.0014 ± 0.0001 . Using the published ^{36}Ar concentration (Zhou et al., 2012) the ^{132}Xe concentration in Jackson Dome CO_2 is $1.3 \times 10^{-11} \text{ cm}^3 \text{ STP}/\text{cm}^3$.

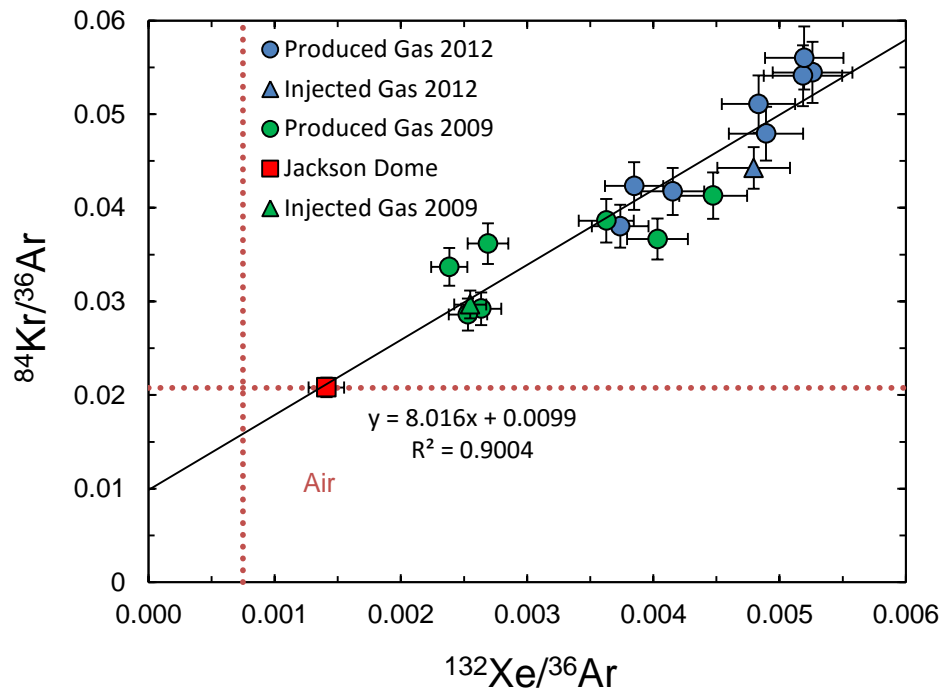


Figure 6.3. $^{84}\text{Kr}/^{36}\text{Ar}$ and $^{132}\text{Xe}/^{36}\text{Ar}$ of gases from injection and production wells from Cranfield. The best fit line to all injection and production gas samples seems to represent the previously identified mixing. The $^{84}\text{Kr}/^{36}\text{Ar}$ of the Jackson Dome is known to be air (red dotted line and see text in section 5.2). Extrapolation of the best fit line to the $^{84}\text{Kr}/^{36}\text{Ar}$ of Jackson Dome thus defines the $^{132}\text{Xe}/^{36}\text{Ar}$ Jackson Dome CO_2 (red rectangle) and was found to be 0.0014 ± 0.0001 . Uncertainties are 1σ .

The fact that the production well $^{84}\text{Kr}/^{36}\text{Ar}$ and $^{132}\text{Xe}/^{36}\text{Ar}$ ratios are higher than air rules out the direct contamination by air, for instance during sampling, as the source of the non-radiogenic gases. The pattern observed in $^{20}\text{Ne}/^{36}\text{Ar}$, $^{84}\text{Kr}/^{36}\text{Ar}$ and $^{132}\text{Xe}/^{36}\text{Ar}$ is generally consistent with the fractionation generated by the dissolution of atmosphere-derived noble gases in fluids such as groundwater or oil. This pattern is typical of hydrocarbon gases (e.g. Kennedy et al., 2002), and models have been developed that explain the noble gas abundance pattern of natural gases as a result of stripping of noble gases from air saturated water (ASW) (e.g. Battani et al., 2000; Gilfillan et al., 2008). The injection of CO_2 into a hydrocarbon field might be an obvious mechanism for the presence of highly fractionated noble gases in the gas phase. During EOR operation the CO_2 will dissolve in water and oil and the pre-existing noble gases in those fluids may be removed. In section 4.4 I demonstrated how the $^{20}\text{Ne}/^{22}\text{Ne}$ of the production well gases can be used to determine the He and Ar isotopic composition of the in-place reservoir gas. By plotting the non-radiogenic noble gas data in this way it can be used to assess how well the pre-injection reservoir gas fits ASW-derived noble gases.

The $^{20}\text{Ne}/^{36}\text{Ar}$ data generally follows the mixing curve (Figure 6.4A). Several samples have $^{20}\text{Ne}/^{36}\text{Ar}$ values that are below the mixing line. These samples have low $^{40}\text{Ar}/^{36}\text{Ar}$ (section 4.3) indicative of a small amount of air. The three 2012 production well samples with $^{20}\text{Ne}/^{36}\text{Ar}$ values that are higher than the injected gas from 2012 have higher $^3\text{He}/^4\text{He}$ ratios than the injected gas, implying a higher contribution from the Jackson Dome component than would be expected according to mixing alone. The fit of the $^{20}\text{Ne}/^{36}\text{Ar}$ data to the mixing curve indicates that ASW is a realistic source of Ne and Ar in the natural gas. The $^{20}\text{Ne}/^{36}\text{Ar}$ ratio of the ASW component is likely to be spatially and temporally variable as the reservoir contains a mixture of meteoric water and brine, with the latter dominating near the oil-water contact.

Mixing between an ASW-derived in-place natural gas and injected Jackson Dome CO₂ is much less apparent in the case of ⁸⁴Kr/³⁶Ar (Figure 6.4B) and ¹³²Xe/³⁶Ar (Figure 6.4C). The ⁸⁴Kr/³⁶Ar of the 2009 production well gases are close to the predicted mixing curve, but all the 2012 production well gases plot above the theoretical mixing line and, with the exception of the gas from production well 44-2 2009, the ¹³²Xe/³⁶Ar of the wells sampled in 2009 and 2012 plot above on the mixing curve. There is no clear relationship between the extreme ²⁰Ne/³⁶Ar samples and ⁸⁴Kr/³⁶Ar or ¹³²Xe/³⁶Ar values.

While ASW-derived noble gases may be extracted from groundwater by dissolution of the injected CO₂ (Gilfillan et al., 2008), the heavy noble gas data do not support a simple two-component mixing with injected Jackson Dome CO₂. The data require either the presence of a third source of non-radiogenic noble gases (e.g. from the pre-injection natural gas) and/or that some processes have fractionated the gas mixtures.

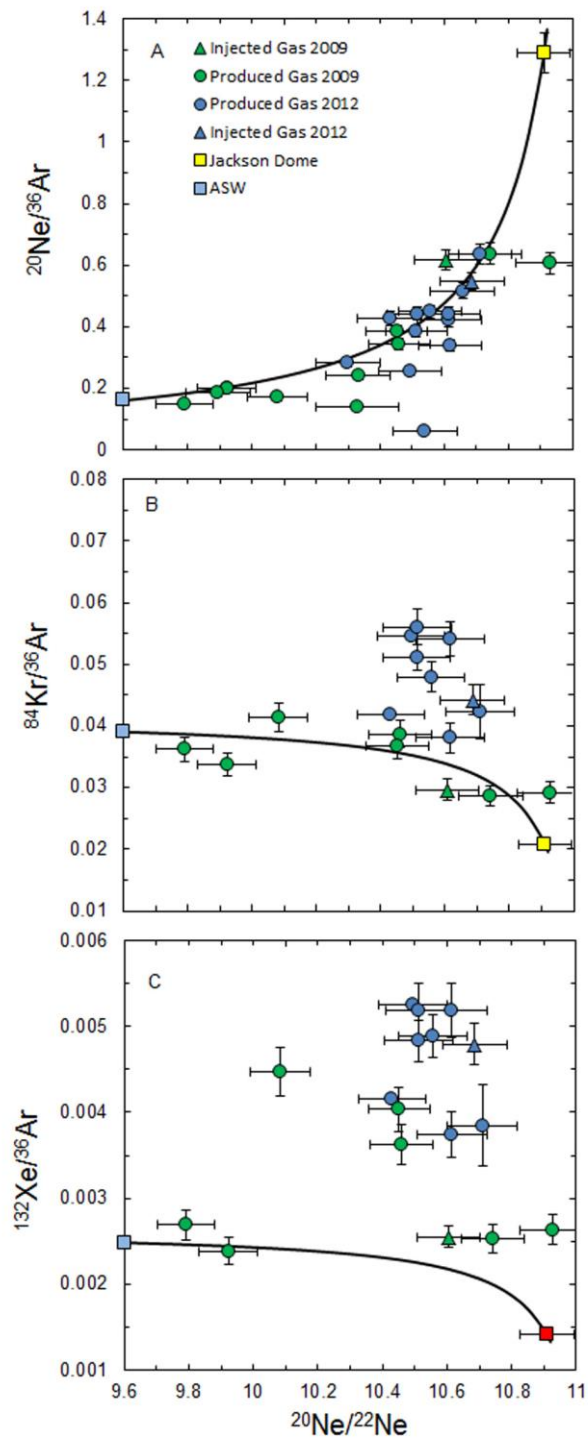


Figure 6.4. The non-radiogenic noble gas ratios plotted against $^{20}\text{Ne}/^{22}\text{Ne}$ for gases from Cranfield. Mixing curves are drawn between Jackson Dome (yellow rectangle; Zhou et al. (2012) and air-saturated water (ASW) compositions (see text). (A) $^{20}\text{Ne}/^{36}\text{Ar}$ mostly follows the mixing curve that confirms ASW composition a suitable end-member. Kr (B) and Xe (C) data do not sit on the curve indicating either the presence of a third end-member or a more complicated process than mixing that causes severe fractionation. Green: 2009, blue: 2012, circle: production well, triangle: injection well. Uncertainties are 1σ .

6.4 Partial degassing of groundwater

6.4.1 The composition of non-radiogenic noble gases prior to injection in the gas phase

While the gas phase may acquire ASW-like noble gases due to dissolution of injected CO₂ into groundwater (e.g. Gilfillan et al., 2008) the noble gas composition of the pre-injection natural gas composition may complicate the simple binary mixing scenario (see section 4.3). Here the composition of that natural gas is quantified and used to interpret data from production well gases.

Air-derived noble gases enter the reservoir through groundwater. When the water is in contact with the gas phase (CH₄) in the reservoir, noble gases will partition between the two phases according to Henry's law. As a general rule the heavier noble gases are more soluble in water; ¹³²Xe > ⁸⁴Kr > ³⁶Ar > ²⁰Ne (Smith and Kennedy, 1983). Consequently the gas phase will have higher ²⁰Ne/³⁶Ar and lower ⁸⁴Kr/³⁶Ar and ¹³²Xe/³⁶Ar than ASW. In order to calculate the pre-injection composition of noble gases in the gas phase after the natural degassing of ASW groundwater the gas/water (G/W) ratio needs to be determined for the pre-injection Cranfield reservoir.

The pre-injection G/W ratio can be estimated in the same way as concentration data (see 4.4). Well 28F-2 2009 represents the natural gas end-member and the G/W in this well represents the reservoir composition, although at a different pressure. The measured G/W in that production well was ~6 and the pressure was 1.3 MPa (personal communication with field operator). The reservoir pressure before CO₂ injection was 32 MPa (Lu et al., 2012b). From Boyle-Mariotte Law (e.g. Atkins, 1979) (Equation 6.3), the reservoir gas/water ratio is calculated to be 0.25 before injection.

$$p_1V_1 = p_2V_2$$

Equation 6.3

Henry constants for reservoir conditions for Ne and Ar are given in section 5.2.1 and for Kr and Xe they are 10.39 and 8.36 GPa, respectively (Ballentine et al., 2002 and references therein). According to the batch fractionation equation (Bosch and Mazor, 1988) the reservoir gas has $^{20}\text{Ne}/^{36}\text{Ar} = 0.183$, $^{84}\text{Kr}/^{36}\text{Ar} = 0.0333$ and $^{132}\text{Xe}/^{36}\text{Ar} = 0.0021$ (see data in Table I.14 in the Appendix).

Complications in the phase equilibrium can emerge in a three phase system such as water, gas and oil as is present in Cranfield. Air-derived noble gases are unlikely to dissolve into the oil phase directly. More likely the noble gases in the oil originate from the water by oil-water contact and concurrent partitioning of noble gases (e.g. Ballentine et al., 1996). It will be shown in section 6.5.1 that the pre-injection oil/water ratio is low and therefore the degree of extraction of noble gases from the water by oil leaves the water phase nearly intact with respect to noble gas composition. Consequently the investigation of the water-gas system remains valid.

In the following sections the heavy noble gas data are compared to the expected fractionation trend for partial degassing of groundwater.

6.4.2 $^{84}\text{Kr}/^{36}\text{Ar}$

The $^{84}\text{Kr}/^{36}\text{Ar}$ of 2009 samples is plotted against $^{20}\text{Ne}/^{36}\text{Ar}$ in Figure 6.5. The red dotted lines show the composition of air (Ozima and Podosek, 2001), while the blue dotted lines define the composition of ASW (see above). The Jackson Dome CO₂ (yellow rectangle, composition of the injected gas at time zero) has atmospheric $^{84}\text{Kr}/^{36}\text{Ar}$ but $^{20}\text{Ne}/^{36}\text{Ar}$ is much higher (1.29; Zhou et al., 2012). The batch fractionation line (dotted line) defines the evolution of the noble gas composition in the gas phase degassed from groundwater. It starts from the pre-injection composition ($^{20}\text{Ne}/^{36}\text{Ar} = 0.183$ and $^{84}\text{Kr}/^{36}\text{Ar} = 0.0333$, see 6.4.1 and Table I.11.) and reaches ASW when the G/W ratio approaches infinity.

The mixing line between gas from the fully degassed water and Jackson Dome CO₂ is shown as a continuous line. The dashed line defines mixing between the natural gas and Jackson Dome CO₂. Data that would plot within the area defined by the batch fractionation line and the two mixing lines are consistent with partial degassing of water.

Gases from two wells (28F-2 and 44-2) lie on the batch fractionation line. This requires contact between the injected gas and the water, suggesting that the water–CO₂ contact is ongoing and therefore degassing of the ASW may still be taking place. These are the two samples that have lost CO₂ for which heavy noble gases were measured (see section 5.2.2).

Gases from three wells (28-2, 29-1 and 27-5) plot on the ASW–Jackson Dome CO₂ mixing curve within uncertainty. These samples appear to have acquired their Ne, Ar and Kr by complete degassing of ASW. Data from well 27-5 also suggest that no CO₂ loss has happened through dissolution (see 5.2.2).

Gases from injection well and production wells 29-6 and 29-9 respectively overlap the mixing line defined by the reservoir noble gas end-members. The injected gas is the mixture of all the produced gases and Jackson Dome CO₂ therefore its composition is determined by the degree of contribution of each production wells. Since the latter is unknown, the injected gas composition is not discussed any further. As the well 29-9 and 29-6 gases have high ²⁰Ne/³⁶Ar they plot away from the batch fractionation line. The location of these samples on the mixing line means that the amount of injected CO₂ is much higher than in the case of e.g. well 44-2, evidence for a less efficient ASW degassing than the one above. Well gases 29-6 and 29-9 show the highest CO₂ concentrations of all production wells, and the noble gas data are also distinct. These samples exhibit the highest ³He/⁴He, ²⁰Ne/²²Ne, ⁴⁰Ar/³⁶Ar and ⁴⁰Ar*/⁴He ratios (see e.g. 4.5). This is consistent with the injected CO₂ flowing through the reservoir with little contact with the formation water, and supports the hypothesis that the in-place natural gas has Ne, Ar and Kr in relative proportion that is consistent with partially degassed groundwater.

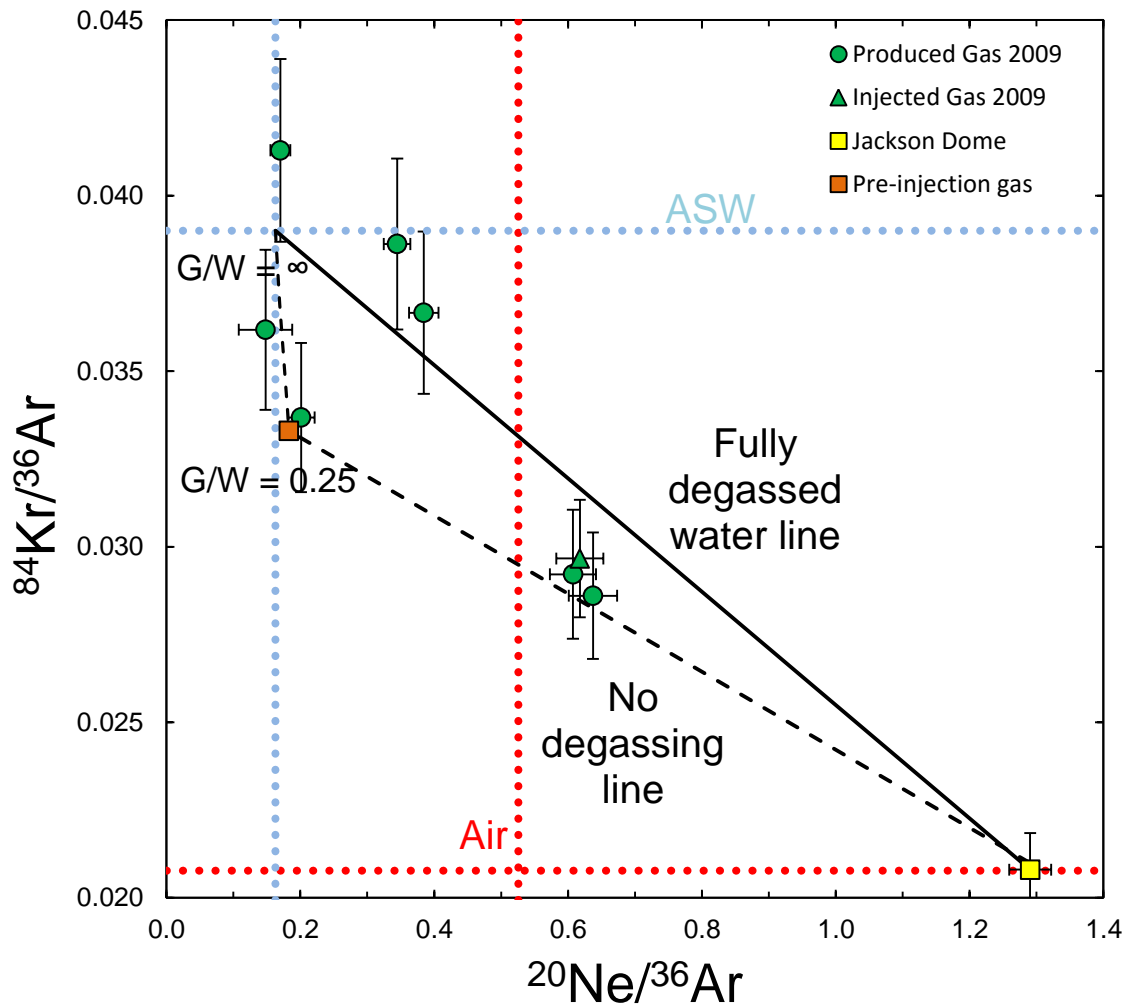


Figure 6.5. The plot of $^{84}\text{Kr}/^{36}\text{Ar}$ against $^{20}\text{Ne}/^{36}\text{Ar}$ for well gases from 2009. Samples from 2009 are explained by different degree of noble gas stripping from water. The dotted line is the batch fractionation line for water degassing starting from the natural gas composition (orange square, $G/W = 0.25$) (see text) and reaching ASW compositions when degassing has completed. The mixing between Jackson Dome CO_2 and the natural gas (no degassing, dashed line) and the gas after the water fully degassed (continuous line) makes the degassing process evident in the field. Groups of production wells show different stage of degassing. Samples on the fractionation line show intense and ongoing CO_2 -water contact. Samples on the straight line show full degassing. Samples on the zero degassing (dashed) line show little degassing and the closer the sample is to the Jackson Dome value the more unlikely is degassing (mobilizing). Injected gas: triangle. Uncertainties are 1σ .

6.4.3 $^{132}\text{Xe}/^{36}\text{Ar}$

The $^{132}\text{Xe}/^{36}\text{Ar}$ ratios of 2009 samples are plotted against $^{20}\text{Ne}/^{36}\text{Ar}$ in Figure 6.6. Using the technique described above, mixing curves are drawn between undegassed, and fully degassed water and the Jackson Dome CO_2 composition. The $^{132}\text{Xe}/^{36}\text{Ar}$ of the Jackson Dome CO_2 is obtained from Figure 6.3. Interestingly, the majority of the 2009 gases plot well above the curve that would indicate fully degassed water, except for those from well 44-2. Also, the three distinct groups that have been identified based on the Kr/Ar data are still observable. The two wells gases that have lost CO_2 (28F-2 and 44-2) are the closest to the batch fractionation line. The three that require fully degassed water (28-2, 29-1 and 27-5) plot together. The injection well and the production wells 29-6 and 29-9 that did not show significant interaction with the groundwater also have similar Xe/Ar ratios. The high Xe/Ar concentrations than required by the ASW – Jackson Dome mixing line is discussed in section 6.5.3.

6.5 Partial degassing of oil

6.5.1 The composition of non-radiogenic noble gases prior to injection in the oil phase

As shown in Figure 6.4 the $^{84}\text{Kr}/^{36}\text{Ar}$ and $^{132}\text{Xe}/^{36}\text{Ar}$ are not consistent with simple binary mixing between the injected gas and ASW. All 2012 $^{84}\text{Kr}/^{36}\text{Ar}$ and most 2009 and 2012 $^{132}\text{Xe}/^{36}\text{Ar}$ data are much higher than ASW values. No data from 2012 would fit into the water degassing model. Highly fractionated noble gases have previously been explained by oil degassing (e.g. Bosch and Mazor, 1988) and more recently have been summarized in e.g. Prinzhofer (2013). Here an attempt is made to explain observed noble gas data by the partial degassing of the oil phase induced by CO_2 injection.

Noble gases in oils most likely originates from a water phase by phase equilibrium (e.g. Ballentine et al., 1996). In order to quantify the noble gas ratios in the oil phase after

equilibrium, the oil/water (O/W) ratio needs to be estimated for the Cranfield reservoir prior to CO₂ injection. Well 28F-2-2009 is thought to be representative of the pre-injection Cranfield reservoir and had not produced oil (i.e. less than the 0.04 m³/day detection limit). The produced water (76 m³/day; personal communication with field operator) means the oil/water ratio was <0.001.

By using the estimated O/W value the fractionation of noble gases between the water and oil phase can be calculated in a similar way as in case of the CO₂-water system. The solubility of noble gases in crude oil for gravity degree (API) = 34° (light oil) have been calculated from after Kharaka and Specht (1988), which is the best representation of the Cranfield oil (API = 39°, Hosseini et al., 2013). Calculated Henry constants under reservoir conditions are 373.9, 136.8, 48.5 and 25.1 atm kg/mol for oil and 2039, 1141, 788 and 568 atm kg/mol for water for Ne, Ar, Kr and Xe respectively (see also above). This means that solubility of noble gases in oil is higher than in water (see also 5.3.1).

As a result of the oil-water equilibrium, and assuming ASW noble gases in the water, the oil phase would have $^{20}\text{Ne}/^{36}\text{Ar} = 0.107$, $^{84}\text{Kr}/^{36}\text{Ar} = 0.075$ and $^{132}\text{Xe}/^{36}\text{Ar} = 0.007$. The relatively low oil/water ratio means that the noble gas composition of water will be largely unchanged: $^{20}\text{Ne}/^{36}\text{Ar} = 0.162$, $^{84}\text{Kr}/^{36}\text{Ar} = 0.0387$ and $^{132}\text{Xe}/^{36}\text{Ar} = 0.0024$ (see data in Table I.15. & 16. in the Appendix). In the following sections the calculated noble gas isotopes ratios are used to explain observed data from production well gases.

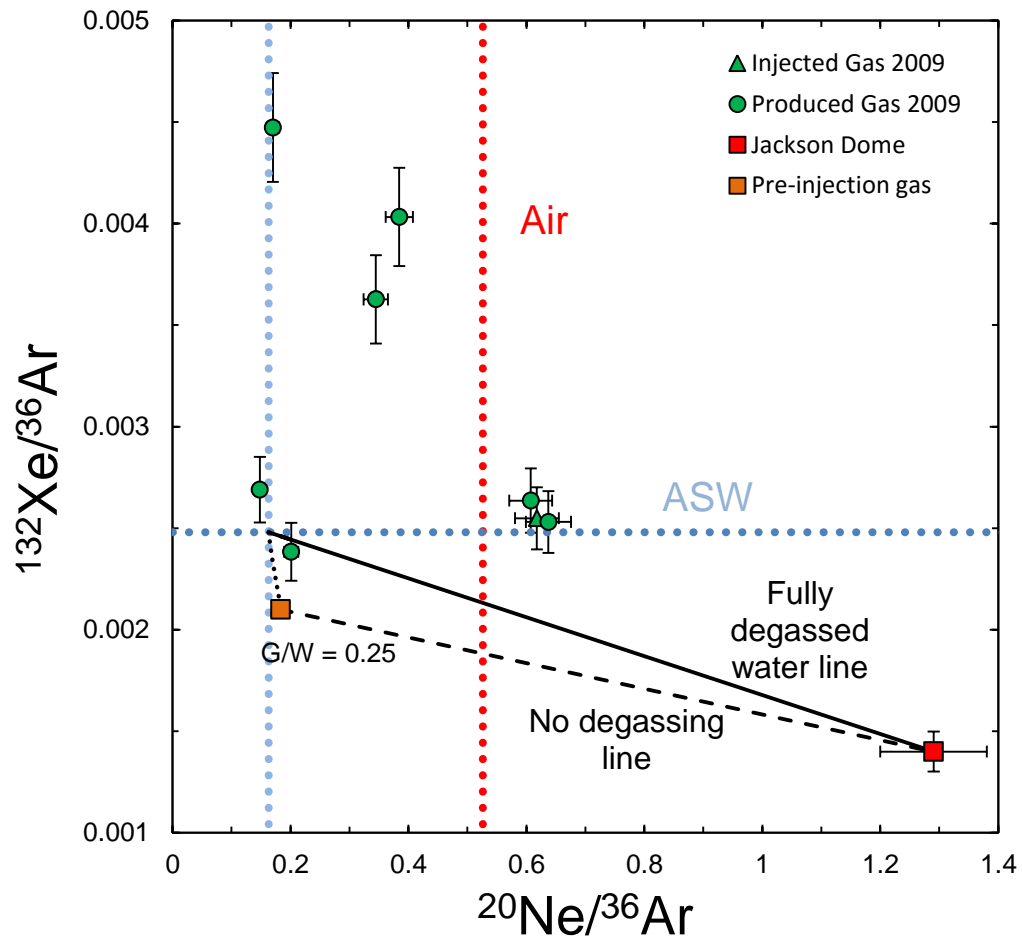


Figure 6.6. The plot of $^{132}\text{Xe}/^{36}\text{Ar}$ against $^{20}\text{Ne}/^{36}\text{Ar}$ for well gases from 2009. Definition of the curves see text and Figure 6.5. The three groups of production well gases (green circles) are the same than defined by Kr data but all data show much higher $^{132}\text{Xe}/^{36}\text{Ar}$ values than would be expected according to the identified degassing. This means an excess of Xe is in the water. The excess Xe most likely originates from the organic phase (oil) (see also text). Red square: estimated Jackson Dome (see text). Symbols are as per Figure 6.5. Uncertainties are 1σ .

6.5.2 $^{84}\text{Kr}/^{36}\text{Ar}$

The $^{84}\text{Kr}/^{36}\text{Ar}$ of the 2012 well gas samples are plotted against $^{20}\text{Ne}/^{36}\text{Ar}$ in Figure 6.7, and all data are plotted in Figure 6.8. The batch fractionation line (dash dotted line) defines the gas phase degassed from oil. Mixing between ASW and Jackson Dome CO_2 is represented by a continuous line. Mixing between gas released from oil and Jackson Dome CO_2 is shown by the dash-double dotted line.

As with the gas-water system for the 2009 data these three lines delineate a region that represents mixing between the three noble gas components. The majority of the data are located within the area showing partial oil degassing. The smallest fractionation of $^{84}\text{Kr}/^{36}\text{Ar}$ is shown by well 29-1. Two well gases (32F-10 and 70-2) plot close to the fully degassed oil line and may be explained by the time elapsed since the start of EOR operation until those wells started producing. They are from the E-SE part of the field which was the last section to be subjected to CO_2 injection and was only exposed to CO_2 flooding shortly before the March 2012 sampling. This could indicate:

- 1) Oil degassing by continuous CO_2 injection reached near complete degassing by the time these two wells started producing, implying that oil degassing (active CO_2 – oil contact) and oil production are unrelated and the oil degassing is a regional event.
- 2) The initial O/W is different in that part of the reservoir, which caused different noble gas composition in the oil phase during phase equilibrium. This will result in a different composition in the gas phase in the case of complete degassing, which will generate a line with a different slope.

Here the first explanation is preferred because the second is a very unlikely scenario. This allows the partial degassing to be quantified in each well (Figure 6.7). The calculation assumes that the degree of degassing is proportional to the relative distance of a sample from the ASW–Jackson Dome and the fully degassed oil – Jackson Dome mixing lines.

In general the effective CO₂-oil contact is more difficult to establish (e.g. it takes longer and therefore more gas is needed) than the CO₂-water contact. This may be in connection to an unsuccessful water injection test in the 1950s (Lu et al., 2012b). This is similar to the difficulties of degassing water in case of well 29-6 and 29-9.

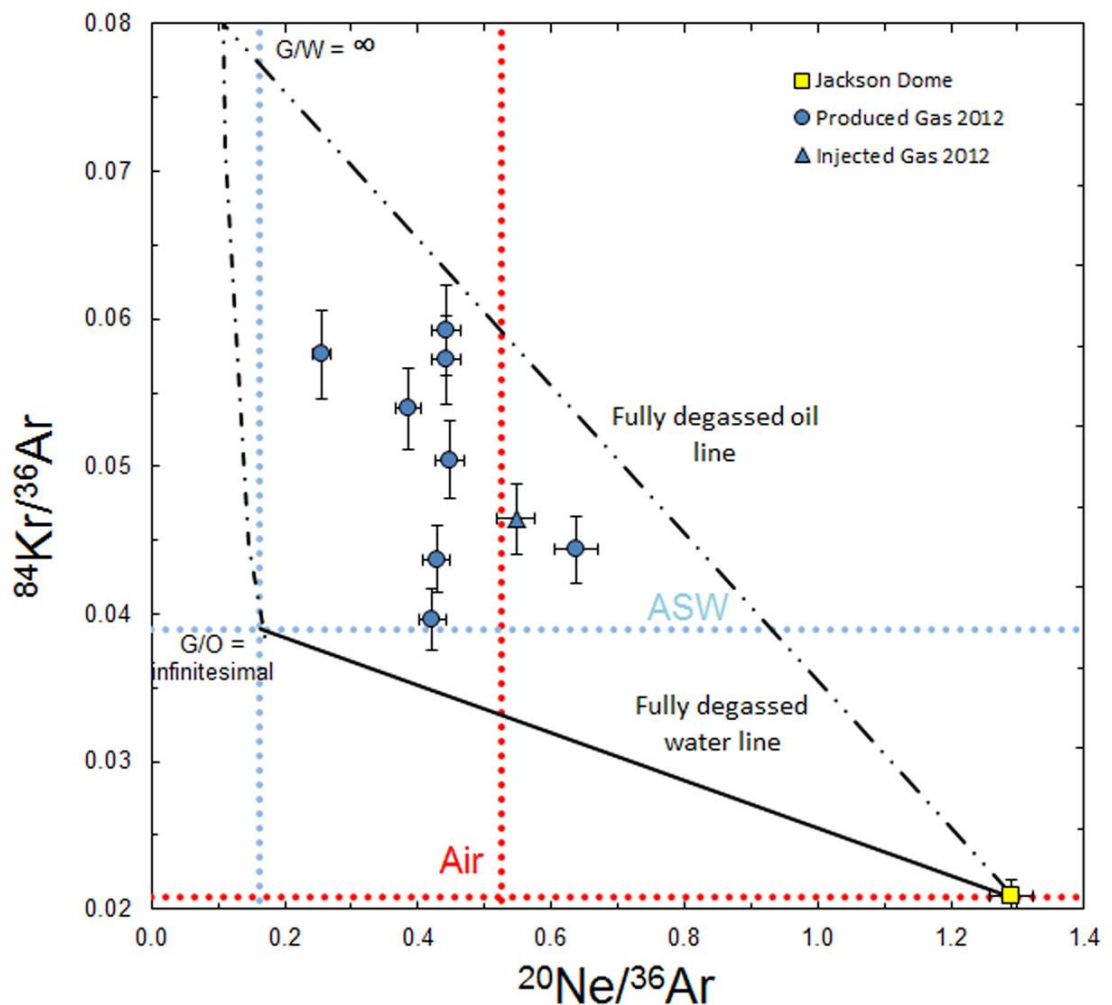


Figure 6.7. The plot of $^{84}\text{Kr}/^{36}\text{Ar}$ against $^{20}\text{Ne}/^{36}\text{Ar}$ for well gases from 2012. Data from 2012 (blue circle) are explained by partial gas stripping from oil. The evolution of the noble gas composition caused by increasing degassing is represented by the fractionation curve (dash-dotted line) The area defined by the fractionation line and the two mixing lines (Jackson Dome–ASW = continuous line, fully degassed oil–Jackson Dome = double dotted dashed line) defines an envelope, in which partial degassing is observed. Most of the data are within that, indicating partial oil degassing. One datum overlaps with the fully degassed oil line, which is the latest sample that has been exposed to CO₂ flooding. Uncertainties are 1σ .

Table 6.3. Degree of oil degassing from well gases from Cranfield.

Well	Degree of oil degassing (%)
28-2	58
45F-4	60
27-5	56
28F-2	32
29-1	16
29-6	58
32F-10	87
70-2	78

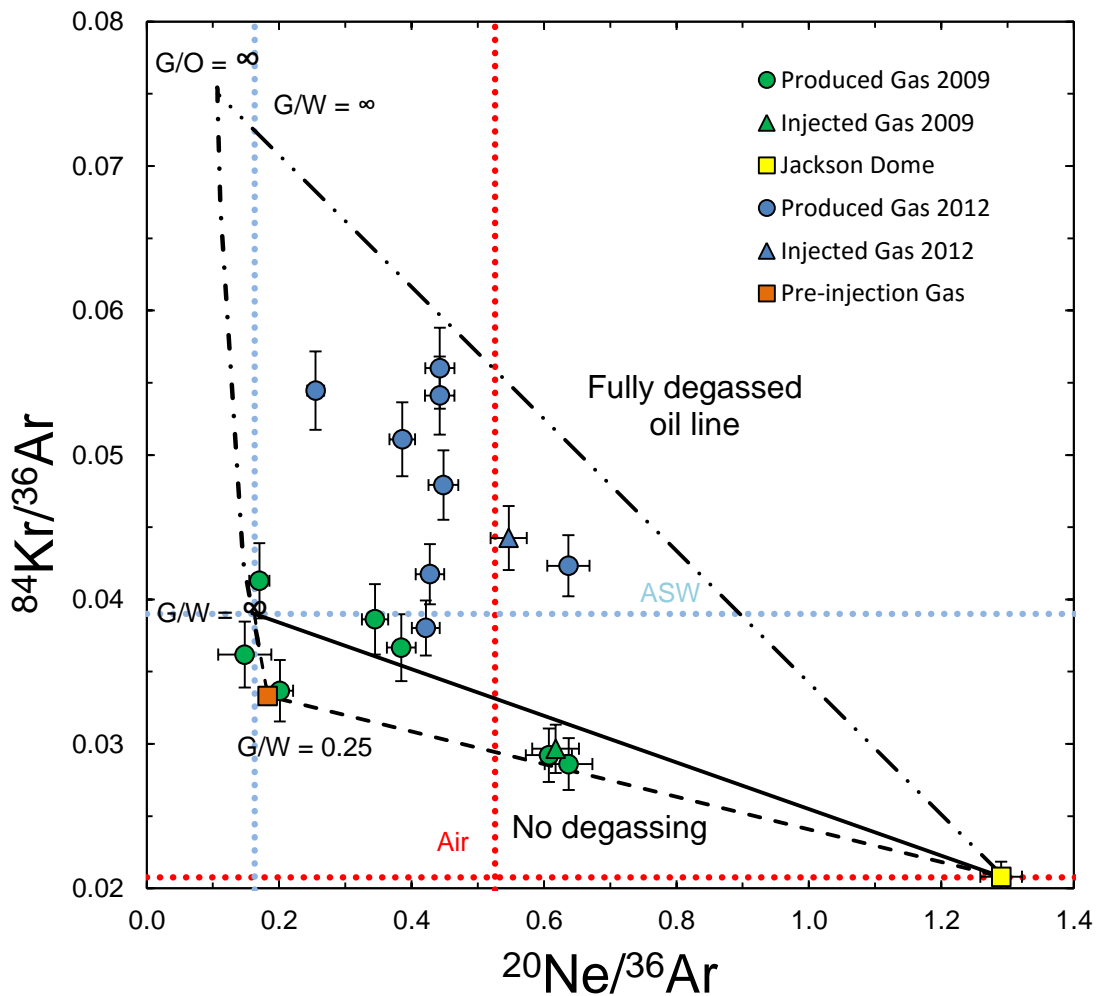


Figure 6.8. Combined diagram of $^{84}\text{Kr}/^{36}\text{Ar}$ against $^{20}\text{Ne}/^{36}\text{Ar}$ from 2009 and 2012. Line code is as per Figure 6.5 & 6.7.

6.5.3 $^{132}\text{Xe}/^{36}\text{Ar}$

The $^{132}\text{Xe}/^{36}\text{Ar}$ data of the 2012 well gases are plotted against $^{20}\text{Ne}/^{36}\text{Ar}$ ratios in Figure 6.9. The batch fractionation line does not start from ASW value due to the composition of the remaining water phase, explained earlier. The location of the majority of data on Figure 6.9 is similar to the location of the Xe-Ar-Ne data from 2009 well data in Figure 6.6. However four samples (injected gas, 27-5, 70-2 and 32F-10) show more than 100% oil degassing. The explanation for this is the presence of excess Xe in the 2009 production well samples (see section 6.4.3).

Excess Xe has been described in sedimentary basins as trapped in (or adsorbed on) organic-rich material (Zhou et al., 2005). If such an excess Xe is present in Cranfield it will have been transferred into the water phase by phase equilibrium resulting in high concentrations of ^{132}Xe in the water phase. Water degassing is the key mechanism to explain the 2009 data. This results in most of the Xe being transferred into the gas phase, giving high $^{132}\text{Xe}/^{36}\text{Ar}$ (Figure 6.6). In the 2012 well gases (Figure 6.9) the sum of the degassed Xe is seen in the gas phase that had been degassed from the water (2009) and from the oil (2012). Data from both 2009 and 2012 sampling campaigns are summarized in Figure 6.10. The similarity of the 2009 and 2012 $^{132}\text{Xe}/^{36}\text{Ar}$ data reflects the small contribution of Xe from the oil phase. This in turn reflects the difficulty of degassing Xe from the oil phase due its high solubility in oil. Consequently the dominant source of Xe in the gas phase in 2012 is still what had been degassed from the water in 2009.

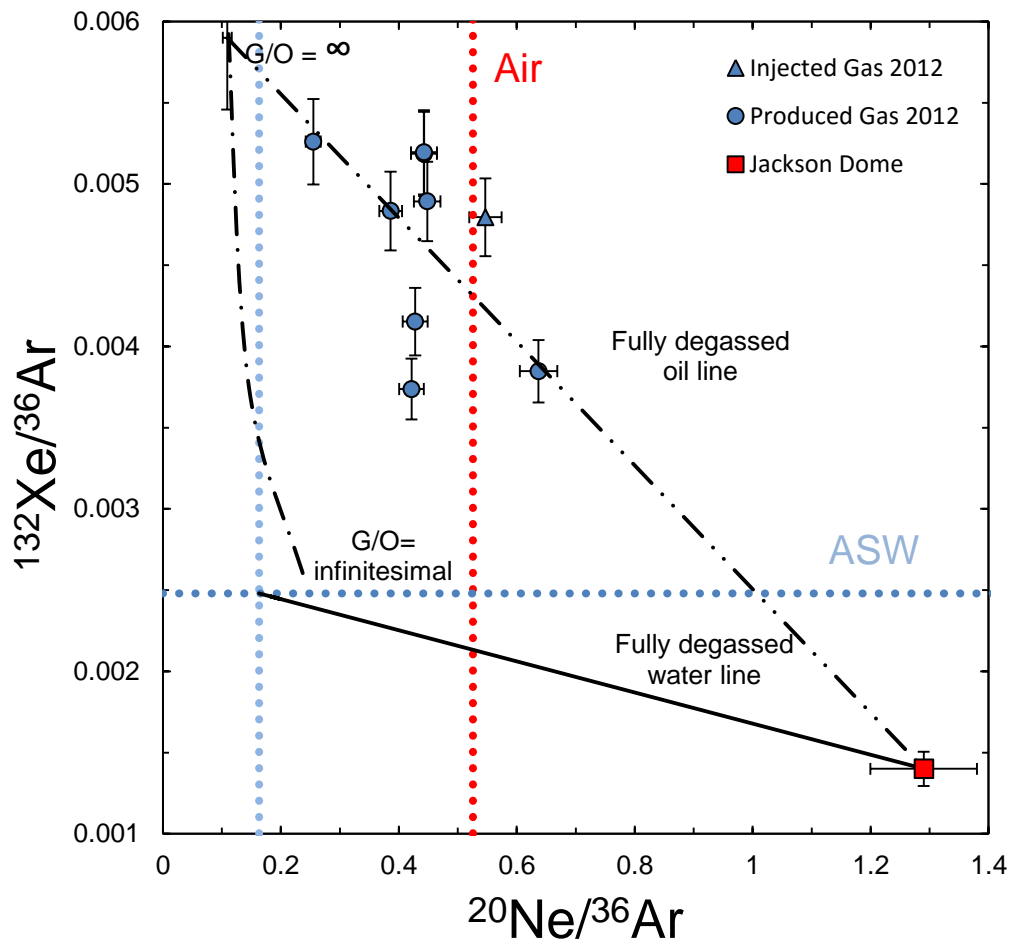


Figure 6.9. The plot of $^{132}\text{Xe}/^{36}\text{Ar}$ against $^{20}\text{Ne}/^{36}\text{Ar}$ for well gases from 2012. Although the data may show almost full degassing of oil, data are rather explained by presence of Xe, degassed from the water (see Figure 6.8) and inefficient degassing of Xe from the oil due to its high solubility. Fractionation line starting point is not ASW and see text in section 6.5.1. The meaning of the different lines are as per Figure 6.7. Uncertainties are 1σ .

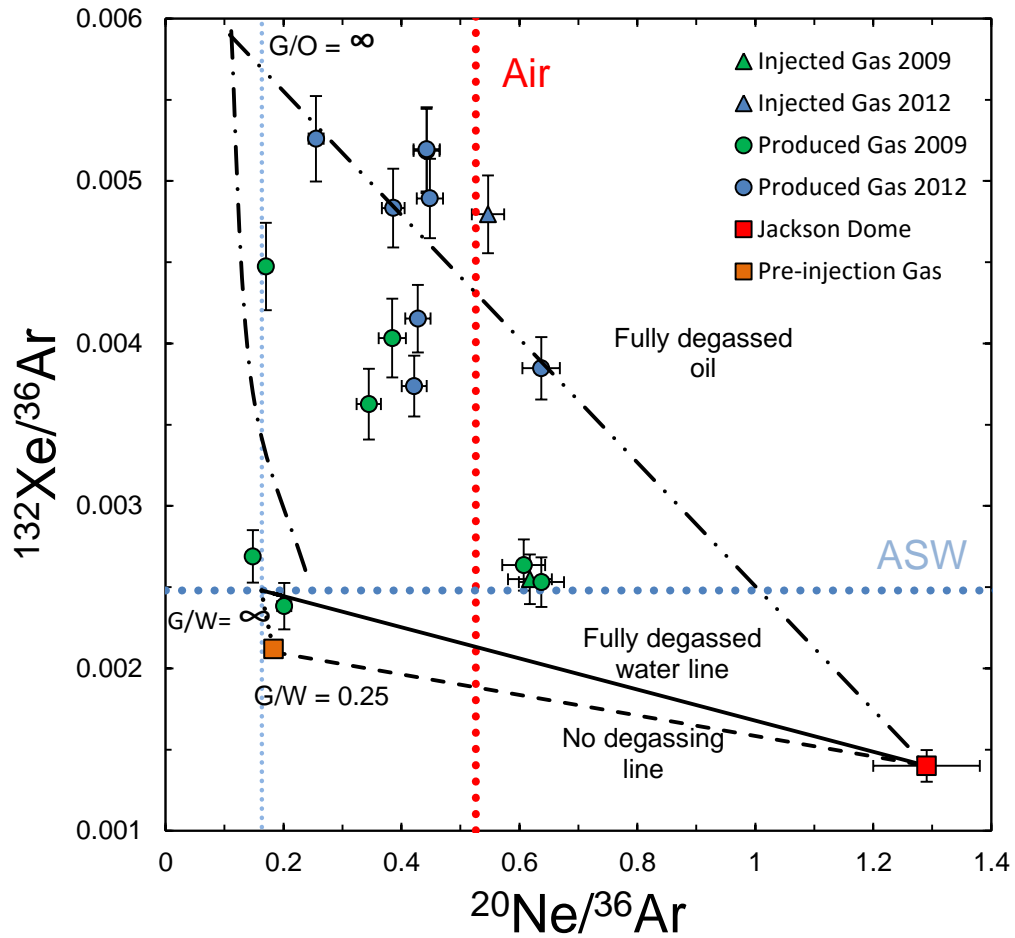


Figure 6.10. Combined diagram of $^{132}\text{Xe}/^{36}\text{Ar}$ against $^{20}\text{Ne}/^{36}\text{Ar}$ from 2009 and 2012. Lines are as per Figure 6.8.

6.6 Future development

Temporal changes in noble gas data appear to have the potential to estimate the relative efficiency of individual production wells. The interpretation of the changes in the heavy noble gases and $^3\text{He}/^4\text{He}$ seems to be consistent with the temporal changes in the gas/oil ratio observed by the field operator, which is in turn connected to the well displacement efficiency. Noble gas data are available for five wells that were sampled in both 2009 and 2012.

Well 28-2: The $^3\text{He}/^4\text{He}$ value (2.75 (3) and 2.77 (6) R_A in 2009 and 2012) is unchanged over time. This means that the injected gas had already equilibrated with the reservoir fluids by December 2009. The $^{20}\text{Ne}/^{36}\text{Ar}$ and $^{84}\text{Kr}/^{36}\text{Ar}$ data from 2012 are consistent with oil degassing, indicating that oil is the major source of non-radiogenic noble gases and not the injected CO_2 . This suggests constantly high oil production. This is supported by the steady gas/water and gas/oil ratios in 2009 and 2012: ~2,500 and ~1,300 and 32 and 21, respectively. The amounts of produced water and oil are largely unchanged, which means that the well acts as an efficient producer.

Well 27-5 shows a change in $^3\text{He}/^4\text{He}$ from 1.71 (4) in 2009 to 2.85 (5) R_A in 2012, indicating that water degassing appears to have been recently completed in 2009. Following this the CO_2 promotes degassing (mobilizing) oil. This is reflected by the increase in the $^{84}\text{Kr}/^{36}\text{Ar}$ (from 0.041 to 0.047). However by 2012 the Kr/Ar composition reflects more strongly the injected gas composition, indicating that the oil displacement is more difficult than in case of well 28-2. This is supported by the increase in the gas/water (from 230 to 1,500) and gas/oil ratios (from 540 to 4,200). This well must have become an effective producer between the two sampling campaigns.

Well 28F-2 exhibits a similar, but more pronounced change between the two sampling campaigns, compared to well 27-5. There is a significant change in the $^3\text{He}/^4\text{He}$ (from 0.21 (2) R_A to 3.22 (5) R_A) which means that the water, the sink of CO_2 in 2009 (see 5.3) must have been fully saturated with respect to CO_2 by 2012 and was then mobilizing oil. The gas/water ratios increased two orders of magnitude (from 70 to 2,700) and the gas/oil from zero to 3,700.

Well 29-6: It has been shown that the CO_2 -water contact is not effective therefore the same can be expected for the CO_2 -oil system. Due to the low degree of contact between CO_2 and water and oil and the high amount of injected gas present, the $^3\text{He}/^4\text{He}$ is unchanged (4.18 R_A in both years). The low (and unchanged) efficiency to degas water

would predict the need of an extremely high amount of gas to start degassing oil. Actually this well shows the highest gas/oil ratio (50,000) of the five wells. In terms of the gas needed for mobilizing oil the well is ineffective.

Well 29-1: There is a modest change in $^3\text{He}/^4\text{He}$ (2.85 (6) to 3.23 (8)). Although the water was fully degassed by December 2009, and consequently the CO_2 must have started the oil degassing (mobilizing) the air derived noble gases still define 16% of oil degassing only by March 2012. The amount of injected gas in the area of the well (see 5.4) is high but the amount of produced gas is the lowest among the five wells discussed here. This indicates that the majority of the injected gas is not reaching this well and not helping to extract oil. The gas/oil ratio increased from 1,000 to 8,000 from 2009 to 2012, due to both the increase in the amount of gas and the decrease in the amount of oil.

6.7 Conclusions

There is no strong indication of a contribution of injected Kr and Xe at the DAS site in to the main reservoir. Consequently, the heavy noble gas dataset can be used to trace processes occurring to the fluids (injected gas, water and oil) in the Cranfield main reservoir.

Gas stripping, induced by CO_2 injection into water has been described by Gilfillan et al. (2008). This model was developed for natural gas fields where CO_2 injection occurred on long time scales and complete degassing was achieved.

I propose that partial gas stripping has occurred for the gas-water-oil system at Cranfield. This can fully explain the data obtained from an industrial CO_2 injection field, where the CO_2 has been injected for ~3 years. This short period of time allows the degassing process to be looked at with high resolution. It has been found that water degassing happened in the early stage of injection (2009), when the oil degassing was unimportant. By the later

stage of injection (2012) the degassing of oil reached sufficient level and governs the observed data.

The water degassing has shown significant heterogeneity throughout the reservoir. Some wells show a relatively free flow path, where little formation water is contacted. Those, where CO₂ loss has been identified previously show active and ongoing contact, while others show complete degassing of the water.

Degassing of oil may be a regional event. CO₂ mixes with the oil (miscible flooding), decreasing its viscosity. It is mobilised from the pore space during which process noble gases are being degassed but it takes much longer until the 'mobilised' oil gets produced. By 2012 the interaction between injected CO₂ and oil (so the cumulative produced oil) has become significant meaning that the majority of noble gases from the oil phase are transferred to the gas phase. Significantly, the results from 2012 show that there has not been sufficient contact of the supercritical CO₂ with oil to fully degas it.

The Xe/Ar ratios imply that there is significant excess xenon in the gas phase that must have been present in the water phase prior to injection.

The temporal investigation of non-radiogenic noble gases obtained from individual samples, along with ³He/⁴He could be used to constrain the oil displacement efficiency for each well and data are consistent with production data. The requirement of the amount of gas needed and therefore the G/O ratio can be estimated for a certain well.

Chapter 7

Conclusion and future work

7.1 Summary

Enhanced oil recovery by CO₂ injection into depleted hydrocarbon reservoirs is an analogue for the large CO₂ sequestration projects that will be required to ameliorate atmospheric CO₂ (Whittaker and Perkins, 2013). Consequently EOR fields provide an opportunity for research into the process of carbon sequestration (e.g. Boot-Handford et al., 2014). In order to deploy CCS safely, methods need to be developed for tracing and verifying the secure underground storage of CO₂ (Scott et al., 2013). The work presented here is the first to systematically use the naturally occurring noble gases in injected CO₂ to trace its movement and history of interaction with reservoir fluids.

The He, Ne and Ar isotopic compositions of production well gases from the Cranfield EOR field define a two-component mixture between the injected gas and the in-place reservoir gas, with minimal effect from contaminating atmosphere-derived gases. Each component has a distinct Ne isotope composition. Consequently plotting the He and Ar isotope composition against the ²⁰Ne/²²Ne allows the composition of the reservoir gas to be defined.

³He/⁴He and ⁴⁰Ar*/⁴He data from the production wells plot on theoretical mixing lines with CO₂ concentrations. Generally they are more sensitive to changes in CO₂ concentration over the whole range of CO₂ concentration than δ¹³C_{CO2} due to the difference in shape of mixing curves. Production well gas samples with the lowest CO₂ content sampled during the 2009 sampling campaign sit above the mixing lines. The most plausible explanation is that a considerable amount of CO₂ has been lost from the gas phase.

The amount of CO₂ lost from each well can be estimated by the ³He/⁴He-CO₂ relationship, although values determined using the ⁴⁰Ar*/⁴He and CO₂/³He ratio overlap. The proportion

of gas loss ranges from 22 to 97%. The lost CO₂ scaled to the whole field represents only the 0.09% (~10 kt) of the total injected CO₂ (~1.4 Mt). The fractionated CO₂/³He, ⁴⁰Ar*/⁴He and δ¹³C_{CO2} of the low CO₂ samples are consistent with dissolution of CO₂ into the groundwater.

The majority of production wells did not reveal any CO₂ loss, consistent with trapping of free CO₂ in pore space in the reservoir rock (stratigraphic trapping) as the main sequestration mechanism. This was noted previously (Lu et al., 2013) and also expected within the timescale of CO₂ injection (Bachu et al., 2007). Further evidence for the different trapping mechanism observed spatially and temporary are supported by the differences in the average CO₂ flux under production wells.

The non-radiogenic noble gases isotopes (²⁰Ne, ³⁶Ar, ⁸⁴Kr, ¹³²Xe) are ultimately atmospheric in origin, having entered the reservoir in groundwater. This generated a unique composition in the reservoir in the gas, water and the oil phase by phase equilibrium. The elemental ratios in the gases sampled in 2009 imply an origin from water degassing by CO₂ flooding. However the degree of water degassing was not uniform throughout the reservoir. Some wells show high rates of gas flow with little contact with formation waters while others showed active and ongoing contact, as well as complete degassing of water.

By 2012 the interaction between the oil and the injected CO₂ has become significant. The heavy noble gases from the oil phase are present in the free gas indicating that the oil is degassing. Results from 2012 show that there has not been sufficient contact of the CO₂ with oil to fully degas it. The elemental ratios can be described by partial gas stripping, similar to that of Gilfillan et al. (2008) developed for natural gas fields. The non-radiogenic noble gases, combined with ³He/⁴He appear to reflect the changes in the oil displacement efficiency spatially as well as with time. The data are consistent with the changes in the measured gas/oil ratios. The degree of oil degassing, determined by the fractionation of the

non-radiogenic noble gases, can be used to estimate the requirement of the amount of gas needed. The $^3\text{He}/^4\text{He}$ reflects when a major change in the efficiency on the oil production happened in the well, which is in turn, can be used to quantify how economic the well is. These findings suggest that noble gases have potential not only in CO_2 – reservoir fluid interaction modelling but reservoir engineering.

7.2 Future work

Previous studies of noble gases in CO_2 injection have largely been based on the injection of single elements (e.g. Giese et al., 2009). However this is costly even on the scale of small, short-term injection tests (e.g. over a few weeks, Lu et al., 2012a), and would be prohibitively expensive when scaled up to CCS projects that are necessary to impact the global CO_2 inventory (see 1.4.2).

Although this work has successfully demonstrated that the noble gas isotopes that naturally exist as minor components in injected CO_2 can be used to trace the fate of the injected gas, it remains to be shown that they are applicable in future large scale CCS projects.

In this study the noble gas isotopic composition of the injected and the reservoir gas were significantly different. This may not be the case in commercial CCS. Specifically the injected gas has a composition with a strong mantle signature in the He and Ne isotope composition. In all likelihood commercial CCS projects will source CO_2 from power stations where the initial noble gas isotopic composition will derive from coal or gas, and therefore will be strongly radiogenic. In this case He, Ne and (likely) Ar isotopes will be similar to the natural gases and groundwaters that exist in the reservoir. This not only means a possible lower resolution in the noble gas – CO_2 system but also a greater need to precisely determine the isotopic composition (and it's variability) of the fluids in the reservoir prior to injection.

This study has also succeeded because the concentration of the noble gases in the injected gases has been in the range where analysis has been possible with conventional analytical protocols. There are several methods of capture and purification of anthropogenic CO₂ prior to injection (Yang et al., 2008). It is likely that these techniques will remove the noble gases. There is no published work in this field, and it is clearly a topic that would benefit from further research. If it proves to be the case it might be used to modify the purification technique to leave the noble gases in the mixture.

Atmosphere derived noble gases have shown the ability to track CO₂-fluid interaction history in the reservoir. This could be exploited in future CCS trials. The quantification of the CO₂-fluid interaction is essential to better understand the timescale where solubility and mineral trapping operates in a certain field. Dissolution and mineralization are the mechanisms by which CO₂ is ultimately aimed to be stored. Consequently research into the heavy noble gases in CCS trials would provide a better constraint on long term and safe CO₂ storage.

Appendix I

Raw data

Table I.1. The mass 44/15, measured on the QMS from calibration gases with different CO₂ contents. Uncertainties are 1 σ . Data are plotted on Figure 2.4.

Gas	Gas amount cm ³ (STP) x 10 ⁻⁵	Mass 44/15	d(mass 44/15)
Pure CH ₄	2.100	0.0049	1.75E-05
Pure CH ₄	3.790	0.0037	1.66E-05
Pure CO ₂	2.200	444.6699	1.86E+00
Pure CO ₂	3.628	821.8366	1.22E+00
96% CO ₂	3.753	16.2478	1.65E-02
96% CO ₂	2.100	13.1368	6.66E-02
30% CO ₂	3.940	0.6344	6.57E-04
30% CO ₂	2.080	0.4968	9.52E-04
80% CO ₂	3.980	3.3050	1.43E-03
80% CO ₂	2.080	3.3446	2.89E-03
70% CO ₂	2.765	1.7710	2.11E-03
70% CO ₂	3.815	1.7759	1.65E-03
70% CO ₂	2.050	1.5590	1.50E-03
70% CO ₂	2.440	1.6780	1.79E-03
70% CO ₂	3.050	1.6020	2.20E-03
70% CO ₂	3.501	1.7416	1.87E-03

Table I.2. Selected calibration data of mass 44/15 over time from the QMS. Data are plotted on Figure 2.5.

Date of run	Mass 44/15	d(mass 44/15)
10/04/2014	1.690	0.0159
11/04/2014	1.654	0.0164
12/04/2014	1.684	0.0170
13/04/2014	1.710	0.0165
14/04/2014	1.700	0.0175
15/04/2014	1.687	0.0182
16/04/2014	1.671	0.0198
12/07/2014	1.677	0.0145
13/07/2014	1.710	0.0194
14/07/2014	1.648	0.0200
15/07/2014	1.689	0.0174
16/07/2014	1.698	0.0165
17/07/2014	1.678	0.0160
18/07/2014	1.698	0.0178
19/07/2014	1.699	0.0189

Table I.3. The measured ^{84}Kr of selected samples on both QMS and noble gas mass spectrometer. Data are plotted on Figure 2.6. Volumes are in cm^3 (STP).

^{84}Kr (A)/ V_{gas} in QMS (10^{12})	$V^{84}\text{Kr}$ /aliquot from noble gas reservoir (x 10^{-10})
64.70	138.33
99.83	388.36
26.43	130.86
32.30	190.47
24.34	126.05
22303.24	3739.39
25431.68	3739.39
27841.63	3402.95
25700.64	3402.95
28389.13	3402.95
2.73	11.17
10.57	40.47
8.78	40.47
9.30	42.19
2.27	7.57
1.40	8.61
5.24	29.48
2.79	36.62
2.71	58.55
2.95	147.17
3.03	21.80
4.35	17.35
7.12	34.96
8.75	61.56
1.45	9.10
1.54	7.47
3.52	23.48
1.42	7.68
2.40	20.54
4.87	45.50

Table I.4. Selected $\delta^{13}\text{C}_{\text{CO}_2}$ calibration data over time from the IRMS. The CO_2 originates from the bottle that contains 70% CO_2 – 30% CH_4 gas mixture and is permanently attached to the UHV system. The real $\delta^{13}\text{C}_{\text{CO}_2}$ of that gas is unknown and irrelevant for this thesis. Uncertainties are 1σ . Data are plotted on Figure 2.7.

Date of run	$\delta^{13}\text{C}_{\text{CO}_2}$ ‰ (PDB)	Uncertainty
10/04/2014	-33.284	0.017
11/04/2014	-33.477	0.055
12/04/2014	-33.733	0.016
13/04/2014	-33.529	0.025
14/04/2014	-33.757	0.011
15/04/2014	-33.635	0.024
16/04/2014	-33.800	0.032
17/04/2014	-33.339	0.022
18/04/2014	-33.518	0.009
19/04/2014	-33.257	0.011
20/04/2014	-33.478	0.009
21/04/2014	-33.955	0.013
22/04/2014	-33.576	0.018
23/04/2014	-33.764	0.012
12/07/2014	-33.503	0.015
13/07/2014	-33.436	0.044
14/07/2014	-33.352	0.045
15/07/2014	-33.365	0.046
16/07/2014	-33.380	0.038
17/07/2014	-33.394	0.047
18/07/2014	-33.317	0.022
19/07/2014	-33.503	0.007
20/07/2014	-33.199	0.010
21/07/2014	-33.390	0.007
22/07/2014	-33.255	0.020
23/07/2014	-33.349	0.019
24/07/2014	-33.758	0.039

Table I.5. Selected He calibration data from the noble gas mass spectrometer. Data are plotted on Figure 2.8., uncertainties are 1σ .

Date of run	$^3\text{He}/^4\text{He}$ Cps/V	$d(^3\text{He}/^4\text{He})$ Cps/V
23/04/2014	1897	38
24/04/2014	1806	10
25/04/2014	1883	20
26/04/2014	1949	19
27/04/2014	1907	15
28/04/2014	1804	14
10/05/2014	1856	20
11/05/2014	1806	44
12/05/2014	1910	54
13/05/2014	1967	34
14/05/2014	1930	32
15/05/2014	1908	40
16/05/2014	1947	62
17/05/2014	1982	45
01/07/2014	1902	35
02/07/2014	1968	28
03/07/2014	1825	14
04/07/2014	1812	27
05/07/2014	1827	20
06/07/2014	1909	16
07/07/2014	1874	41
08/07/2014	1898	38
09/07/2014	1876	21
10/07/2014	1946	17
11/07/2014	1973	18
12/07/2014	1966	21
13/07/2014	1858	24
14/07/2014	1783	31
15/07/2014	1830	36
16/07/2014	1832	34
17/07/2014	1821	17
18/07/2014	1813	20

Table I.6. Selected Ne calibration data from the noble gas mass spectrometer. Data are plotted on Figure 2.9. and show mass fractionation in comparison to air. Uncertainties are 1σ .

ID	$^{20}\text{Ne}/^{22}\text{Ne}$	$d(^{20}\text{Ne}/^{22}\text{Ne})$	$^{21}\text{Ne}/^{22}\text{Ne}$	$d(^{21}\text{Ne}/^{22}\text{Ne})$
1	9.907	0.01967	0.0288	0.00018
2	9.946	0.01872	0.0288	0.00025
3	9.959	0.02036	0.0288	0.00019
4	9.886	0.03579	0.0283	0.00028
5	10.003	0.01727	0.0281	0.00014
6	10.023	0.01900	0.0285	0.00020
7	9.954	0.01892	0.0284	0.00016
8	9.996	0.01702	0.0286	0.00028
9	9.991	0.01881	0.0286	0.00018
10	9.998	0.02615	0.0283	0.00011
11	9.939	0.02745	0.0280	0.00024
12	10.014	0.02873	0.0286	0.00021
13	9.918	0.01991	0.0286	0.00025
14	9.953	0.01260	0.0283	0.00016
15	9.974	0.01256	0.0287	0.00027
16	9.980	0.01683	0.0289	0.00014
17	10.052	0.01447	0.0288	0.00008
18	9.929	0.01922	0.0283	0.00017
19	9.983	0.03252	0.0288	0.00020
20	9.826	0.02339	0.0290	0.00030
21	9.983	0.02685	0.0287	0.00009
22	9.795	0.01253	0.0283	0.00017

Table I.7. Selected Ar calibration data from the noble gas mass spectrometer. Data are plotted on Figure 2.10. and show mass fractionation in comparison to air. Uncertainties are 1σ .

ID	$^{40}\text{Ar}/^{36}\text{Ar}$	$d(^{40}\text{Ar}/^{36}\text{Ar})$	$^{38}\text{Ar}/^{36}\text{Ar}$	$d(^{38}\text{Ar}/^{36}\text{Ar})$
1	293.3	0.6	0.19	0.001
2	293.7	0.4	0.19	0.002
3	293.9	0.3	0.19	0.002
4	293.8	0.5	0.19	0.002
5	292.6	0.5	0.2	0.002
6	291.4	0.4	0.2	0.003
7	295.5	0.4	0.19	0.001
8	292.8	0.3	0.19	0.003
9	293.1	0.3	0.19	0.002
10	289.3	0.7	0.19	0.004
11	294.0	0.3	0.18	0.003
12	293.0	0.4	0.19	0.002
13	299.0	1	0.19	0.003
14	294.2	0.7	0.19	0.003
15	294.5	0.8	0.19	0.002
16	294.3	0.7	0.19	0.002
17	303.0	1	0.23	0.002
18	298.2	0.8	0.19	0.001
19	293.0	0.6	0.19	0.003
20	294.0	0.5	0.19	0.002
21	296.6	0.3	0.19	0.003
22	295.6	1.9	0.19	0.002
23	296.4	0.39	0.19	0.003
24	297.8	1.28	0.19	0.002
25	301.9	0.64	0.19	0.004
26	295.8	0.68	0.19	0.002
27	294.9	0.63	0.19	0.002

Table I.8. Selected Kr and Xe calibration data from the noble gas mass spectrometer. Data are plotted on Figure 2.11. Uncertainties are 1σ .

Date of run	$^{84}\text{Kr}/^{132}\text{Xe}$	$d(^{84}\text{Kr}/^{132}\text{Xe})$
15/10/2014	23.027	0.182
16/10/2014	22.984	0.143
17/10/2014	21.791	0.205
18/10/2014	24.615	0.162
19/10/2014	23.392	0.138
20/10/2014	23.667	0.240
21/10/2014	24.678	0.190
22/10/2014	22.831	0.240
05/12/2014	22.558	0.240
06/12/2014	22.676	0.880
07/12/2014	22.984	0.143
08/12/2014	22.273	0.260
09/12/2014	23.570	0.239
10/12/2014	22.841	0.205
11/12/2014	23.027	0.182
12/12/2014	22.984	0.143
13/12/2014	23.125	0.146
02/02/2015	24.164	0.199
03/02/2015	23.450	0.268
04/02/2015	22.984	0.143
05/02/2015	23.125	0.146
06/02/2015	22.121	0.075
07/02/2015	22.387	0.281
08/02/2015	23.667	0.240
09/02/2015	24.678	0.190
10/02/2015	22.831	0.240
11/02/2015	22.558	0.240

Table I.9. The obtained $^{40}\text{Ar}/\text{aliquot}$ from the air calibration bottle from two different standards. Results overlap within 2σ uncertainty. Data are plotted on Figure 2.12.

Standard	Obtained $^{40}\text{Ar}/\text{aliquot}$	Uncertainty
CREU-1	4.56E-07	3.24E-08
GA1550	4.78E-07	2.18E-08

Table I.10. Recorded production well data on the Cranfield field at the time of sampling.

Well ID	Year of sampling	Pressure MPa	Oil/Water (O/W)	Gas/Oil (G/O)	Gas/Water (G/W)
27-3	2009	6.65	0.163	4773.4	779.0
27-3	2012	7.34	0.797	6219.3	4956.0
29F-1	2009	2.17	0.100	327.6	32.8
29F-1	2012	3.06	0.235	2274.1	535.2
29-5	2009	1.89	0	NA	26.3
29-5	2012	7.55	0.140	12497.9	1749.7
28-2	2009	9.06	0.609	4086.2	2487.2
28-2	2012	7.20	0.374	3414.7	1277.8
28F-2	2009	1.31	0	NA	68.6
28F-2	2012	8.03	0.724	3741.9	2709.1
29-6	2009	6.65	0.040	14622.4	577.6
29-6	2012	6.86	0.042	49902.6	2107.0
29-9	2009	6.31	0.042	6544.3	275.7
29-9	2012	2.17	0.005	74037.1	383.9
29-1	2009	2.01	0.102	1067.6	109.1
29-1	2012	2.65	0.092	7965.9	731.0
27-5	2009	6.65	0.413	544.8	224.9
27-5	2012	7.41	0.356	4282.4	1523.2
44-2	2009	0.79	0	NA	62.9
45F-4	2012	7.41	0.023	42402.7	982.0
32F-10	2012	Unknown	Unknown	Unknown	Unknown
70-2	2012	Unknown	Unknown	Unknown	Unknown

Table I.11. Fractionation of $\text{CO}_2/{}^3\text{He}$ and ${}^{40}\text{Ar}^*/{}^4\text{He}$ during gas dissolution in the Cranfield reservoir. Data are plotted on Figure 5.2.

Gas/Water (G/W)	$\text{CO}_2/{}^3\text{He}$ ($\times 10^9$)	28F-2	29F-1	44-2	29-5
		${}^{40}\text{Ar}^*/{}^4\text{He}$	${}^{40}\text{Ar}^*/{}^4\text{He}$	${}^{40}\text{Ar}^*/{}^4\text{He}$	${}^{40}\text{Ar}^*/{}^4\text{He}$
100	2.526	0.142	0.190	0.260	0.360
50	2.522	0.142	0.190	0.260	0.360
10	2.485	0.142	0.189	0.260	0.359
1	2.179	0.141	0.189	0.259	0.359
0.1	1.070	0.137	0.184	0.252	0.348
0.01	0.252	0.116	0.155	0.213	0.294
0.001	0.130	0.097	0.131	0.179	0.248
0.0001	0.118	0.094	0.126	0.173	0.239

Table I.12. Fractionation of $\text{CO}_2/{}^3\text{He}$ and $\delta^{13}\text{C}_{\text{CO}_2}$ in Cranfield during CO_2 precipitation and dissolution. $\delta^{13}\text{C}_{\text{CO}_2}$ is relative to PDB.

Dissolved CO_2 %	Precipitation as calcite			Dissolution into water		
	$\text{CO}_2/{}^3\text{He}$ ($\times 10^9$)	$\delta^{13}\text{C}_{\text{CO}_2}$	$\text{CO}_2/{}^3\text{He}$ ($\times 10^9$)	$\delta^{13}\text{C}_{\text{CO}_2}$	$\delta^{13}\text{C}_{\text{CO}_2}$	$\delta^{13}\text{C}_{\text{CO}_2}$
				pH = 6	pH = 7	pH = 8
1	2.50	-2.98	2.50	-2.96	-2.97	-2.97
10	2.28	-3.18	2.28	-2.98	-3.08	-3.11
20	2.02	-3.43	2.04	-3.01	-3.22	-3.28
30	1.77	-3.72	1.79	-3.04	-3.38	-3.47
40	1.52	-4.05	1.54	-3.08	-3.56	-3.70
50	1.27	-4.44	1.29	-3.12	-3.77	-3.96
60	1.01	-4.91	1.04	-3.17	-4.03	-4.28
70	0.76	-5.52	0.78	-3.24	-4.36	-4.69
80	0.51	-6.38	0.53	-3.33	-4.84	-5.28
90	0.25	-7.86	0.26	-3.50	-5.64	-6.28
99	0.25	-12.76	0.27	-4.03	-8.33	-9.59

Table I.13. The isotopic composition of the injected tracer into the DAS site in 2009 and in 2010. The composition of atmospheric air is after Berglund and Wieser, (2011). The injected gas in composition in both cases is identical to air. 1σ uncertainties are in parenthesis. The measurements have been carried out by the University of Rochester after Poreda and Farley (1992).

	Atmospheric air	Injected gas (03/12/2009)	Injected gas (15/04/2010)
${}^{124}\text{Xe}/{}^{132}\text{Xe}$	0.0035 (0)	0.0031 (1)	0.0032 (1)
${}^{126}\text{Xe}/{}^{132}\text{Xe}$	0.0033 (0)	0.0028 (1)	0.0024 (1)
${}^{128}\text{Xe}/{}^{132}\text{Xe}$	0.0710 (0)	0.071 (1)	0.071 (1)
${}^{129}\text{Xe}/{}^{132}\text{Xe}$	0.9811 (3)	0.987 (11)	0.981 (9)
${}^{130}\text{Xe}/{}^{132}\text{Xe}$	0.1513 (1)	0.151 (2)	0.151 (2)
${}^{131}\text{Xe}/{}^{132}\text{Xe}$	0.7891 (1)	0.789 (9)	0.788 (8)
${}^{134}\text{Xe}/{}^{132}\text{Xe}$	0.3878 (1)	0.387 (5)	0.388 (6)
${}^{136}\text{Xe}/{}^{132}\text{Xe}$	0.3292 (2)	0.328 (4)	0.330 (4)
${}^{80}\text{Kr}/{}^{84}\text{Kr}$	0.040 (0)	0.041 (1)	0.040 (1)
${}^{82}\text{Kr}/{}^{84}\text{Kr}$	0.203 (1)	0.204 (2)	0.204 (1)
${}^{83}\text{Kr}/{}^{84}\text{Kr}$	0.202 (0)	0.202 (2)	0.202 (2)
${}^{86}\text{Kr}/{}^{84}\text{Kr}$	0.304 (1)	0.301 (4)	0.302 (3)

Table I.14. The fractionation of ASW-like noble gases with decreasing G/W ratio in the Cranfield reservoir. The Cranfield pre-injection end-member is defined at G/W = 0.25.

Gas/Water (G/W)	$^{20}\text{Ne}/^{36}\text{Ar}$	$^{84}\text{Kr}/^{36}\text{Ar}$	$^{132}\text{Xe}/^{36}\text{Ar}$
Infinite (ASW)	0.163	0.039	0.00248
1000	0.1630	0.0390	0.002480
500	0.1630	0.0390	0.002480
100	0.1631	0.0390	0.002478
10	0.1637	0.0388	0.002464
1	0.1691	0.0369	0.002346
0.25	0.1829	0.0333	0.002118
0.1	0.1990	0.0304	0.001931

Table I.15. The fractionation of ASW-like noble gases during water-oil contact in the Cranfield field. The pre-injection oil/water ratio in Cranfield is 0.001 (see text).

Oil/Water (O/W)	water equilibrated oil (WEO)			water after oil equilibrium (WAOE)		
	$^{20}\text{Ne}/^{36}\text{Ar}$	$^{84}\text{Kr}/^{36}\text{Ar}$	$^{132}\text{Xe}/^{36}\text{Ar}$	$^{20}\text{Ne}/^{36}\text{Ar}$	$^{84}\text{Kr}/^{36}\text{Ar}$	$^{132}\text{Xe}/^{36}\text{Ar}$
Infinite	0.163	0.039	0.00248	0	0	0
0.99	0.1542	0.0411	0.00266	0.0002	0.0001	0.00007
0.9	0.1534	0.0414	0.00268	0.0237	0.0057	0.00057
0.8	0.1525	0.0416	0.00270	0.0451	0.0108	0.00100
0.7	0.1513	0.0420	0.00273	0.0646	0.0154	0.00133
0.6	0.1498	0.0424	0.00277	0.0823	0.0197	0.00160
0.5	0.1478	0.0431	0.00282	0.0986	0.0236	0.00181
0.4	0.1452	0.0439	0.00290	0.1135	0.0272	0.00199
0.3	0.1416	0.0453	0.00303	0.1273	0.0305	0.00214
0.2	0.1360	0.0477	0.00325	0.1401	0.0335	0.00227
0.1	0.1264	0.0531	0.00378	0.1520	0.0364	0.00238
0.05	0.1186	0.0594	0.00447	0.1576	0.0377	0.00243
0.02	0.1121	0.0669	0.00540	0.1609	0.0385	0.00246
0.01	0.1094	0.0708	0.00594	0.1619	0.0387	0.00247
0.005	0.1080	0.0732	0.00630	0.1625	0.0389	0.00248
0.002	0.1071	0.0749	0.00655	0.1628	0.0389	0.00248
0.001	0.1068	0.0754	0.00664	0.1629	0.0390	0.00248

Table I.16. The fractionation of noble gases during the degassing of the oil phase in the Cranfield field. Fractionation is calculated from the oil composition is that of after the oil-water equilibrium at O/W = 0.001.

Gas/Oil (G/O)	$^{20}\text{Ne}/^{36}\text{Ar}$	$^{84}\text{Kr}/^{36}\text{Ar}$	$^{132}\text{Xe}/^{36}\text{Ar}$
100	0.1068	0.0754	0.00663
50	0.1068	0.0754	0.00663
10	0.1069	0.0753	0.00663
1	0.1073	0.0744	0.00655
0.1	0.1116	0.0671	0.00590
0.01	0.1459	0.0426	0.00375

Appendix II

Publications of this work

In peer reviewed scientific journals

Györe, D., Stuart, F.M., Gilfillan, S., Waldron, S., 2015. Tracing injected CO₂ in the Cranfield enhanced oil recovery field (MS, USA) using He, Ne and Ar isotopes
International Journal of Greenhouse Gas Control, 42, p 554-561.

In international conferences

Györe, D., Stuart, F.M., Waldron, S., Gilfillan, S., 2015. Noble gas isotopes in injected CO₂ as a tracer in the Cranfield enhanced oil recovery field (MS, USA). 25th
Goldschmidt Conference, Prague, Aug 16-21, poster presentation.

Gilfillan, S., Haszedline, S., Stuart, F., Györe, D., Kilgallon, R., Wilkinson, M., 2014. The application of noble gases and carbon stable isotopes in tracing the fate, migration and storage of CO₂. *GHGT 12 Conference, University of Texas at Austin, 5-9 October, 2014; Energy Procedia 63, 4123.*

Gilfillan, S., Györe, D., Stuart, F. Talk entitled 'Tracing the migration and fate of CO₂ in the Cranfield CO₂-EOR field using noble gases' 14th April 2014 - *Geological Society of London Meeting on 'Geological Carbon Storage: Meeting the Global Challenge', at Burlington House, London.*

Gilfillan, S., Györe, D., Stuart, F. Talk entitled 'Tracing the migration and fate of CO₂ in the Cranfield CO₂-EOR field using noble gases', 28th Feb 2014 - *CRIUS workshop on 'Geochemical processes during CO₂ storage' in Keyworth, Nottingham.*

Györe, D. Stuart, F.M., Waldron, S., Gilfillan, S., Talk entitled 'Noble gases as natural tracers of carbon sequestration in injection fields' *10th Applied Isotope Geochemistry Conference, Budapest, September 22-27, 2013; Central European Geology, Acta Geologica Hungarica 56 (2-3), 147.*

Györe, D., Stuart, F., Gilfillan, S., Waldron, S. Talk entitled 'Stable and noble gas isotopes as tracers of subsurface processes acting on CO₂ injected' *12th Annual Conference on Carbon Capture, Utilization and Sequestration, May 13, 2013 Pittsburgh, PA, USA.*

References

- Aeschbach-Hertig, W., Peeters, F., Beyerle, U., Kipfer, R., 1999. Interpretation of dissolved atmospheric noble gases in natural waters. *Water Resour. Res.* 35, 2779-2792.
- Ajo-Franklin, J.B., Peterson, J., Doetsch, J., Daley, T.M., 2013. High-resolution characterization of a CO₂ plume using crosswell seismic tomography: Cranfield, MS, USA. *Int. J. Greenh. Gas Con.* 18, 497-509.
- Andersen, K.K., Azuma, N., Barnola, J.-M., Bigler, M., Biscaye, P., Caillon, N., Chappellaz, J., Clausen, H.B., Dahl-Jensen, D., Fischer, H., Flückiger, J., Fritzsche, D., Fujii, Y., Goto-Azuma, K., Grønvold, K., Gundestrup, N.S., Hansson, M., Huber, C., Hvidberg, C.S., Johnsen, C.J., Jonsell, U., Jouzel, J., Kipfstuhl, S., Landais, A., Leuenberger, M., Lorrain, R., Masson-Delmotte, V., Miller, H., Motoyama, H., Narita, H., Popp, T., Rasmussen, S.O., Raynaud, D., Rothlisberger, R., Ruth, U., Samyn, D., Schwander, J., Shoji, H., Siggard-Andersen, M.-L., Steffensen, J.P., Stocker, T., Sveinbjörnsdóttir, A.E., Svensson, A., Takata, M., Tison, J.-L., Thorsteinsson, T., Watanabe, O., Wilhelms, F., White, J.W.C., 2004. High-resolution record of Northern Hemisphere climate extending into the last interglacial period. *Nature* 431, 147-151.
- Andrews, J.N., 1985. The isotopic composition of radiogenic helium and its use to study groundwater movement in confined aquifers. *Chem. Geol.* 49, 339-351.
- Arts, R., Eiken, O., Chadwick, A., Zweigel, P., van der Meer, L., Zinszner, B., 2004. Monitoring of CO₂ injected at Sleipner using time-lapse seismic data. *Energy* 29, 1383-1392.
- Atkins, P.W., 1979. *Physical Chemistry*, Oxford University Press, Oxford, UK.
- Bachu, S., Bonijoly, D., Bradshaw, J., Burruss, R., Holloway, S., Christensen, N.P., Mathiassen, O.M., 2007. CO₂ storage capacity estimation: Methodology and gaps. *Int. J. Greenh. Gas Con.* 1, 430-443.
- Baines, S.J., Worden, R.H., 2004. The long-term fate of CO₂ in the subsurface: natural analogues for CO₂ storage. Geological Society, London, Special Publications 233, 59-85.
- Baksi, A.K., 1997. The timing of late Cretaceous alkalic igneous activity in the northern Gulf of Mexico Basin, southeastern USA. *J. Geol.* 105, 629-644.
- Ballentine, C.J., 1997. Resolving the mantle He/Ne and crustal ²¹Ne/²²Ne in well gases. *Earth. Planet. Sci. Lett.* 152, 233-249.

- Ballentine, C.J., Burgess, R., Marty, B., 2002. Tracing Fluid Origin, Transport and Interaction in the Crust, in: Porcelli, D., Ballentine, C.J., Wieler, R. (Eds.), *Reviews in Mineralogy & Geochemistry Volume 47, Noble Gases in Geochemistry and Cosmochemistry*, pp. 539-614.
- Ballentine, C.J., Burnard, P.G., 2002. Production, Release and Transport of Noble Gases in the Continental Crust, in: Porcelli, D., Ballentine, C.J., Wieler, R. (Eds.), *Reviews in Mineralogy & Geochemistry Volume 47, Noble Gases in Geochemistry and Cosmochemistry*, pp. 481-538.
- Ballentine, C.J., Marty, B., Sherwood Lollar, B., Cassidy, M., 2005. Neon isotopes constrain convection and volatile origin in the Earth's mantle. *Nature* 433, 33-38.
- Ballentine, C.J., O'Nions, R.K., 1991. The nature of mantle neon contributions to Vienna Basin hydrocarbon reservoirs. *Earth. Planet. Sci. Lett.* 113, 553-567.
- Ballentine, C.J., O'Nions, R.K., 1994. The use of natural He, Ne and Ar isotopes to study hydrocarbon-related fluid provenance, migration and mass balance in sedimentary basins. Geological Society, London, *Special Publications* 78, 347-361.
- Ballentine, C.J., O'Nions, R.K., Coleman, M.L., 1996. A Magnus opus: Helium, neon and argon isotopes in a North Sea oilfield. *Geochim. Cosmochim. Acta* 60, 831-849.
- Ballentine, C.J., O'Nions, R.K., Oxburgh, E.R., Horvath, F., Deak, J., 1991. Rare gas constraints on hydrocarbon accumulation, crustal degassing and groundwater flow in the Pannonian Basin. *Earth. Planet. Sci. Lett.* 105, 229-246.
- Basford, J.R., Dragon, C.J., Pepin, R.O., Coscio Jr, M.R., Murthy, V.R., 1973. Krypton and Xenon in lunar fines, *Proceedings of the 4th Lunar Science Conference 2:*, pp. 1915-1955.
- Battani, A., Sarda, P., Prinzhofer, A., 2000. Basin scale natural gas source, migration and trapping traced by noble gases and major elements: the Pakistan Indus basin. *Earth. Planet. Sci. Lett.* 181, 229-249.
- Bauch, D., Carstens, J., Wefer, G., Theide, J., 2000. The imprint of anthropogenic CO₂ in the Arctic Ocean: evidence from planktic delta C-13 from watercolumn and sediment surfaces. *DSR* 47, 1791-1808.
- Beaubien, S.E., Jones, D.G., Gal, F., Barkwith, A.K.A.P., Braibant, G., Baubron, J.C., Ciotoli, G., Graziani, S., Lister, T.R., Lombardi, S., Michel, K., Quattrocchi, F., Strutt, M.H., 2013. Monitoring of near-surface gas geochemistry at the Weyburn, Canada, CO₂-EOR site, 2001–2011. *Int. J. Greenh. Gas Con.* 16, S236-S262.
- Berglund, M., Wieser, M.E., 2011. Isotopic composition of the elements 2009 (IUPAC Technical Report, *Pure Appl. Chem*, 83 (2), 397-410.

- Bezard, R., Davidson, J.P., Turner, S., Macpherson, C.G., Lindsay, J.M., Boyce, A.J., 2014. Assimilation of sediments embedded in the oceanic arc crust: myth or reality? *Earth. Planet. Sci. Lett.* 395, 51-60.
- Blard, P.H., Balco, G., Burnard, P.G., Farley, K.A., Fenton, C.R., Friedrich, R., Jull, A.J.T., Niedermann, S., Pik, R., Schaefer, J.M., Scott, E.M., Shuster, D.L., Stuart, F.M., Stute, M., Tibari, B., Winckler, G., Zimmermann, L., 2015. An inter-laboratory comparison of cosmogenic ^3He and radiogenic ^4He in the CRONUS-P pyroxene standard. *Quat. Geochronol* 26, 11-19.
- Boot-Handford, M.E., Abanades, J.C., Anthony, E.J., Blunt, M.J., Brandani, S., Mac Dowell, N., Fernández, J.R., Ferrari, M.-C., Gross, R., Hallett, J.P., Haszeldine, R.S., Heptonstall, P., Lyngfelt, A., Makuch, Z., Mangano, E., Porter, R.T.J., Pourkashanian, M., Rochelle, G.T., Shah, N., Yao, J.G., Fennell, P.S., 2014. Carbon capture and storage update. *Energy & Environmental Sciences* 7, 130-189.
- Boreham, C., Underschultz, J., Stalker, L., Kirste, D., Freifeld, B., Jenkins, C., Ennis-King, J., 2011. Monitoring of CO₂ storage in a depleted natural gas reservoir: Gas geochemistry from the CO2CRC Otway Project, Australia. *Int. J. Greenh. Gas Con.* 5, 1039-1054.
- Bosch, A., Mazor, E., 1988. Natural gas association with water and oil as depicted by atmospheric noble gases: case studies from the southeastern Mediterranean Coastal Plain. *Earth. Planet. Sci. Lett.* 87, 338-346.
- Brewer, P.G., Friederich, G., Peltzer, E.T., Orr Jr, F.M., 1999. Direct Experiments on the Ocean Disposal of Fossil Fuel CO₂. *Science* 284, 943-945.
- Brohan, P., Kennedy, J.J., Harris, I., Tett, S.F.B., Jones, P.D., 2006. Uncertainty estimates in regional and global observed temperature changes: A new data set from 1850. *J. Geophys. Res.* 111.
- Carter, R.W., Spikes, K.T., 2013. Sensitivity analysis of Tuscaloosa sandstones to CO₂ saturation, Cranfield field, Cranfield, MS. *Int. J. Greenh. Gas Con.* 18, 485-496.
- Choi, J.-W., Nicot, J.-P., Hosseini, S.A., Clift, S.J., Hovorka, S.D., 2013. CO₂ recycling accounting and EOR operation scheduling to assist in storage capacity assessment at a U.S. gulf coast depleted reservoir. *Int. J. Greenh. Gas Con.* 18, 474-484.
- Clayton, J.L., Spencer, C.W., Koncz, I., Szalay, A., 1990. Origin and migration of hydrocarbon gases and carbon dioxide, Békés Basin, southeastern Hungary. *Org. Geochem.* 15, 233-247.
- CO2CRC, 2015. CO2CRC, <http://www.co2crc.com.au/> accessed in July 2015.

- Codilean, A.T., Bishop, P., Stuart, F.M., Hoey, T.B., Fabel, D., Freeman, S.P.H.T., 2008. Single-grain cosmogenic ^{21}Ne concentrations in fluvial sediments reveal spatially variable erosion rates. *Geo* 36, 159.
- Coleman, D.L., 2009. Transport infrastructure rationale for carbon dioxide capture & storage in the European Union to 2050. *Energy Procedia* 1, 1673-1681.
- Cornides, I., Takaoka, N., Nagao, K., Matsuo, S., 1986. Contribution of mantle-derived gases to subsurface gases in a tectonically quiescent area, the Carpathian Basin, Hungary revealed by noble gas measurements. *Geochem. J.* 20, 119-125.
- Cozzi, L., 2011. World Energy Outlook 2011, http://energycoalition.eu/sites/default/files/Cozzi%20WEO-2012%20Colation%20for%20energy%20savings%20general%20assembly_26%20April.pdf.
- Craig, H., 1957. Isotopic standards for carbon and oxygen and correction factors for mass-spectrometric analysis of carbon dioxide. *Geochim. Cosmochim. Acta* 12, 133-149.
- Crameik, T.D., Plassey, J.A., 1972. Carbon dioxide injection project Sacroc Unit, Scurry County, Texas, American Petroleum Institute Annual Meeting, Houston, Texas.
- Crovetto, R., Fernandez-Prini, R., Japas, M.L., (1982). Solubility of inert gases and methane in H_2O and in D_2O in the temperature range of 300 to 600 K. *J. Chem. Phys.* 76:1077-1086.
- Dean, J.A., 1998. Lange's handbook of chemistry, 15th ed.
- Deines, P., Langmuir, D., Harmon, R.S., 1974. Stable carbon isotope ratios and the existence of a gas phase in the evolution of carbonate ground waters. *Geochim. Cosmochim. Acta* 38, 1147-1164.
- Doleschall, S., Szittár, A., Udvardi, G., 1992. Review of the 30 years experience of the CO_2 imported oil recovery projects in Hungary, pp. 305-317.
- Dubacq, B., Bickle, M.J., Wigley, M., Kampman, N., Ballentine, C.J., Sherwood Lollar, B., 2012. Noble gas and carbon isotopic evidence for CO_2 -driven silicate dissolution in a recent natural CO_2 field. *Earth. Planet. Sci. Lett.* 341-344, 10-19.
- Dudley, J.H., 1993. Oil in the deep south. University Press of Mississippi.
- Dymond, J.H., Smith, E.B., (1980). The virial coefficients of gases and mixtures. Clarendon Press, Oxford, UK.
- Eberhardt, P., Eugster, O., Marti, K., 1965. A redetermination of the isotopic composition of atmospheric neon. *Z Naturforsch* 20a:, 623-624.

- Eiken, O., Ringrose, P., Hermanrud, C., Nazarian, B., Torp, T.A., Høier, L., 2011. Lessons learned from 14 years of CCS operations: Sleipner, In Salah and Snøhvit. *Energy Procedia* 4, 5541-5548.
- Elliot, T., Ballentine, C.J., O'Nions, R.K., Ricchiuto, T., 1993. Carbon, helium, neon and argon isotopes in the Po Basin (northern Italy) natural gas field. *Chem. Geol.* 106, 429-440.
- Emberley, S., Hutcheon, I., Shevalier, M., Durocher, K., Mayer, B., Gunter, W.D., Perkins, E.H., 2005. Monitoring of fluid–rock interaction and CO₂ storage through produced fluid sampling at the Weyburn CO₂-injection enhanced oil recovery site, Saskatchewan, Canada. *Appl. Geochem.* 20, 1131-1157.
- Ennis-King, J., Paterson, L., 2007. Coupling of geochemical reactions and convective mixing in the long-term geological storage of carbon dioxide. *Int. J. Greenh. Gas Con.* 1, 86-93.
- EPA, 2015. United States Environmental Protection Agency, <http://www.epa.gov/climate/climatechange/science/indicators/ghg/index.html> accessed in July, 2015.
- Feenstra, C.F.J., Mikunda, T., Brunsting, S., 2010. What happened in Barendrecht?, Case Study on the Planned Onshore Carbon dioxide Storage in Barendrecht. Energy Research Centre of Netherlands, The Netherlands.
- Flude, S., Gilfillan, S., Johnson, G., Györe, D., Stuart, F., Haszeldine, S., 2015. Fingerprinting capture CO₂ using natural tracers for CCS monitoring and verification. Poster presentation, Scottish Carbon Capture and Storage Conference, 17, October, 2015, Edinburgh, Scotland, UK.
- Fritz, P., Fontes, J.C., 1980. *Handbook of Environmental Isotope Geochemistry*. Elsevier.
- Gale, J., 2004. Why do we need to consider geological storage of CO₂. Geological Society, London, Special Publications 233, 7-15.
- Giese, R., Henniges, J., Lüth, S., Morozova, D., Schmidt-Hattenberger, C., Würdemann, H., Zimmer, M., Cosma, C., Juhlin, C., 2009. Monitoring at the CO₂ SINK site: A concept integrating geophysics, geochemistry and microbiology. *Energy Procedia* 1, 2251-2259.
- Gilfillan, S., Haszeldine, R.S., 2011. Report on noble gas, carbon stable isotope and HCO₃ measurements from the Kerr Quarter and surrounding area, Goodwater, Saskatchewan. The Kerr Investigation: Final Report, <http://www.geos.ed.ac.uk/homes/sgilfil1/Kerrreport.pdf>.

- Gilfillan, S., Haszeldine, S., Sherk, G., Poreda, R., 2013. Natural tracers quash fears over CO₂ storage leaks at Weyburn, Carbon Capture & Storage, Geological Society and AAPG joint meeting, 14-15 January, London, UK.
- Gilfillan, S.M., Haszeldine, S., Poreda, R.J., Hovorka, S., 2011. Natural and artificial noble gases as tracers of injected CO₂ migration within a deep reservoir, talk; 21st Goldschmidt Conference.
- Gilfillan, S.M.V., Ballentine, C.J., Holland, G., Blagburn, D., Sherwood Lollar, B., Scott, S., Schoell, M., Cassidy, M., 2008. The noble gas geochemistry of natural CO₂ gas reservoirs from the Colorado Plateau and Rocky Mountain provinces, USA. *Geochim. Cosmochim. Acta* 72, 1174-1198.
- Gilfillan, S.M.V., Sherwood Lollar, B., Holland, G., Blagburn, D., Stevens, S., Schoell, M., Cassidy, M., Ding, Z., Zhou, Z., Lacrampe-Couloume, G., Ballentine, C.J., 2009. Solubility trapping in formation water as dominant CO₂ sink in natural gas fields. *Nature* 458, 614-618.
- Global CCS Institute, 2015. Global CCS Institute, <http://www.globalccsinstitute.com/> accessed in July, 2015.
- Goldberg, D.S., Takahashi, T., Slagle, A.L., 2008. Carbon dioxide sequestration in deep-sea basalt. *Proc Natl Acad Sci U S A* 105, 9920-9925.
- Griesshaber, E., O'Nions, R.K., Oxburgh, E.R., 1992. Helium and carbon isotope systematics in crustal fluids from Eifel, the Rhine Graben and Black Forest, F.R.G. *Chem. Geol.* 99, 213-235.
- Haszeldine, R.S., Quinn, Q., England, G., Wilkinson, M., Shipton, Z.K., Evans, J.P., Heath, J., Crossey, L., Ballentine, C.J., Graham, C.M., 2005. Natural Geochemical Analogues for Carbon Dioxide Storage in Deep Geological Porous Reservoirs, a United Kingdom Perspective. *Oil Gas Sci. Technol.- Rev. IFP* 60, 33-49.
- Heath, G.A., O'Donoghue, P., Arent, D.J., Bazilian, M., 2014. Harmonization of initial estimates of shale gas life cycle greenhouse gas emissions for electric power generation. *Proc Natl Acad Sci U S A* 111, E3167-3176.
- Hennecke, E.W., Manuel, O.K., 1975. Noble gases in CO₂ well gas, Harding County, New Mexico. *Earth. Planet. Sci. Lett.* 27, 346-355.
- Herzog, H.J., 2011. Scaling up carbon dioxide capture and storage: From megatons to gigatons. *Energ. Econ.* 33, 597-604.
- Holland, G., Ballentine, C.J., 2006. Seawater subduction controls the heavy noble gas composition of the mantle. *Nature* 441, 186-191.

- Hooker, P.J., O'Nions, R.K., Oxburgh, E.R., 1985. Helium isotopes in North Sea gas fields and the Rhine rift. *Nature* 318, 273-275.
- Hosseini, S.A., Lashgari, H., Choi, J.W., Nicot, J.-P., Lu, J., Hovorka, S.D., 2013. Static and dynamic reservoir modeling for geological CO₂ sequestration at Cranfield, Mississippi, U.S.A. *Int. J. Greenh. Gas Con.* 18, 449-462.
- House, K.Z., Schrag, D.P., Harvey, C.F., Lackner, K.S., 2006. Permanent carbon dioxide storage in deep-sea sediments. *Proc Natl Acad Sci U S A* 103, 12291-12295.
- Hovorka, S.D., 2013. Three-Million-Metric-Ton-Monitored Injection at the Secarb Cranfield Project—Project Update. *Energy Procedia* 37, 6412-6423.
- Hovorka, S.D., Meckel, T.A., Treviño, R.H., 2013. Monitoring a large-volume injection at Cranfield, Mississippi—Project design and recommendations. *Int. J. Greenh. Gas Con.* 18, 345-360.
- Hovorka, S.D., Meckel, T.A., Trevino, R.H., Lu, J., Nicot, J.-P., Choi, J.-W., Freeman, D., Cook, P., Daley, T.M., Ajo-Franklin, J.B., Freifeild, B.M., Doughty, C., Carrigan, C.R., Brecque, D.L., Kharaka, Y.K., Thordsen, J.J., Phelps, T.J., Yang, C., Romanak, K.D., Zhang, T., Holt, R.M., Lindler, J.S., Butsch, R.J., 2011. Monitoring a large volume CO₂ injection: Year two results from SECARB project at Denbury's Cranfield, Mississippi, USA. *Energy Procedia* 4, 3478-3485.
- IEA, 2014a. International Energy Agency, CO₂ emissions from fuel combustion, highlights, <https://www.iea.org/publications/freepublications/publication/CO2EmissionsFromFuelCombustionHighlights2014.pdf>.
- IEA, 2014b. International Energy Agency, Renewable Energy, Medium-Term Market Report, executive summary, <https://www.iea.org/Textbase/npsum/MTrenew2014sum.pdf>.
- IEA, 2015. International Energy Agency, <http://www.iea.org/> accessed in July, 2015.
- IPCC, 2001. Climate Change 2001. The scientific basis. Summary for policy makers and technical summary of the Working Group I Report. Cambridge University Press, Cambridge.
- IPCC, 2005. IPCC special report on carbon dioxide capture and storage, Metz, B., Davidson, O., de Coninck, H.C., Loos, M., Meyer, L.A. (Eds.), Prepared by Working Group III of the Intergovernmental Panel on Climate Change. Cambridge University Press, Cambridge, United Kingdom/New York, NY, USA, p. 442.

- IPCC, 2007. *Climate Change 2007: Synthesis Report, Contribution of Working Groups I, II and III to the Fourth Assessment: Report of the Intergovernmental Panel on Climate Change (IPCC)*, Geneva, Switzerland.
- IPCC, 2014. *IPCC, 2014: Climate Change 2014: Synthesis Report. Contribution of Working Groups I, II and III to the Fifth Assessment Report of the Intergovernmental Panel on Climate Change [Core Writing Team, R.K. Pachauri and L.A. Meyer (eds.)]*. IPCC, Geneva, Switzerland, 151 pp.
- Javoy, M., Pineau, F., Delorme, H., 1986. Carbon and nitrogen isotopes in the mantle. *Chem. Geol.* 57, 41-62.
- Jeandel, E., Battani, A., Sarda, P., 2010. Lessons learned from natural and industrial analogues for storage of carbon dioxide. *Int. J. Greenh. Gas Con.* 4, 890-909.
- Jenden, P.D., Hilton, D.R., Kaplan, I.R., Craig, H., 1993. Abiogenic hydrocarbons and mantle helium in oil and gas fields, in: Howell, D.G. (Ed.), *The Future of Energy Gases - USGS Professional Paper, 1570*, pp. 31-56.
- Jenden, P.D., Kaplan, I.R., Poreda, R.J., Craig, H., 1988. Origin of nitrogen-rich natural gases in the California Great Valley: Evidence from helium, carbon and nitrogen isotope ratios *Geochim. Cosmochim. Acta* 52, 851-861.
- Johnson, G., Mayer, B., Shevalier, M., Nightingale, M., Hutcheon, I., 2011. Tracing the movement of CO₂ injected into a mature oilfield using carbon isotope abundance ratios: The example of the Pembina Cardium CO₂ Monitoring project. *Int. J. Greenh. Gas Con.* 5, 933-941.
- Johnson, G., Raistrick, M., Mayer, B., Shevalier, M., Taylor, S., Nightingale, M., Hutcheon, I., 2009. The use of stable isotope measurements for monitoring and verification of CO₂ storage. *Energy Procedia* 1, 2315-2322.
- Jouzel, J., Genthon, C., Lorius, C., Petit, J., Barkov, N., 1987. Vostok ice core-A continuous isotope temperature record over the last climatic cycle (160,000 years). *Nature* 329, 403-408.
- Jouzel, J., Masson-Delmotte, V., Cattani, O., Dreyfus, G., Falourd, S., Hoffmann, G., Minster, B., Nouet, J., Barnola, M., Chappellaz, J., Fisher, H., Gallet, J.C., Johnsen, S., Leuenberger, M., Loulergue, L., Luethi, D., Oerter, H., Parrenin, F., Raisbeck, G., Raynaud, D., Schilt, A., Schwander, J., Selmo, E., Souchez, R., Spahni, R., Stauffer, B., Steffensen, J.P., Stenni, B., Stocker, T.F., Tison, J.L., Werner, M., Wolff, E.W., 2007. Orbital and millennial antarctic climate variability over the past 800,000 years. *Science* 317, 793-796.

- Kennedy, B.M., Lynch, M.A., Reynolds, J.H., Smith, S.P., 1985. Intensive sampling of noble gases in fluids at Yellowstone: I. Early overview of the data, regional patterns. *Geochim. Cosmochim. Acta* 49, 1251-1261.
- Kennedy, B.M., Reynolds, J.H., Smith, S.P., 1988. Noble gas geochemistry in thermal springs. *Geochim. Cosmochim. Acta* 52, 1919-1928.
- Kennedy, B.M., Hiyagon, H., Reynolds, J.H., 1990. Crustal neon: a striking uniformity. *Earth Planet. Sci. Lett.* 98, 277-286.
- Kennedy, B.M., Torgersen, T., van Soest, M.C., 2002. Multiple atmospheric noble gas components in hydrocarbon reservoirs: A study of the Northwest Shelf, Delaware Basin, SE New Mexico. *Geochim. Cosmochim. Acta* 66, 2807-2822.
- Kharaka, Y.K., Cole, D.R., Thordsen, J.J., Kakouros, E., Nance, H.S., 2006. Gas–water–rock interactions in sedimentary basins: CO₂ sequestration in the Frio Formation, Texas, USA. *J. Geochem. Explor.* 89, 183-186.
- Kharaka, Y.K., Specht, D.J., 1988. The solubility of noble gases in crude oil at 25-100°C. *Appl. Geochem.* 3, 137-144.
- Kipfer, R., Aeschbach-Hertig, W., Peeters, F., Stute, M., 2002. Noble gases in lakes and ground waters, in: Porcelli, D., Ballentine, C.J., Wieler, R. (Eds.), *Reviews in Mineralogy & Geochemistry Volume 47, Noble Gases in Geochemistry and Cosmochemistry*, pp. 615-700.
- Knauss, K.G., Johnson, J.W., Steefel, C.I., 2005. Evaluation of the impact of CO₂, co-contaminant gas, aqueous fluid and reservoir rock interactions on the geologic sequestration of CO₂. *Chem. Geol.* 217, 339-350.
- Kotarba, M.J., Nagao, K., Karnkowski, P.H., 2014. Origin of gaseous hydrocarbons, noble gases, carbon dioxide and nitrogen in Carboniferous and Permian strata of the distal part of the Polish Basin: Geological and isotopic approach. *Chem. Geol.* 383, 164-179.
- Kusakabe, M., 2005. A closed pentane trap for separation of SO₂ from CO₂ for precise $\delta^{18}\text{O}$ and $\delta^{34}\text{S}$ measurements. *Geochem. J.* 39.
- Langmuir, C.H., Vocke Jr, R.D., Hanson, G.N., Hart, S.R., 1978. A general mixing equation with applications to Icelandic basalts. *Earth. Planet. Sci. Lett.* 37, 380-392.
- Levenson, L.L., 1974. Sublimation rates and vapour pressures of H₂O, CO₂, N₂O and Xe. *J. Chem. Eng. Data* 19, 107-110.
- Lewis, C.A., Shinn, J.H., 2001. Global Warming-An Oil and Gas Company Perspective: Prospects for geologic sequestration? *Environ.Geosci.* 8, 177-186.

- Lu, J., Cook, P.J., Hosseini, S.A., Yang, C., Romanak, K.D., Zhang, T., Freifeld, B.M., Smyth, R.C., Zeng, H., Hovorka, S.D., 2012a. Complex fluid flow revealed by monitoring CO₂ injection in a fluvial formation. *Journal of Geophysical Research: Solid Earth* 117, n/a-n/a.
- Lu, J., Kharaka, Y.K., Thordsen, J.J., Horita, J., Karamalidis, A., Griffith, C., Hakala, J.A., Ambats, G., Cole, D.R., Phelps, T.J., Manning, M.A., Cook, P.J., Hovorka, S.D., 2012b. CO₂-rock-brine interactions in Lower Tuscaloosa Formation at Cranfield CO₂ sequestration site, Mississippi, U.S.A. *Chem. Geol.* 291, 269-277.
- Lu, J., Kordi, M., Hovorka, S.D., Meckel, T.A., Christopher, C.A., 2013. Reservoir characterization and complications for trapping mechanisms at Cranfield CO₂ injection site. *Int. J. Greenh. Gas Con.* 18, 361-374.
- Lüthi, D., Le Floch, M., Bereiter, B., Blunier, T., Barnola, J.M., Siegenthaler, U., Raynaud, D., Jouzel, J., Fischer, H., Kawamura, K., Stocker, T.F., 2008. High-resolution carbon dioxide concentration record 650,000-800,000 years before present. *Nature* 453, 379-382.
- Mackenzie, F.T., Lerman, A., Ver, L.M.B., 2001. Recent, past and future of the global carbon cycle, in: Gerhard, L.C., Harrison, W.E., Hanson, B.M. (Eds.), *Studies in Geology*. American Association of Petroleum Geologists, Tulsa, OK, pp. 51-82.
- Magyari, D., Udvardi, G., 1991. Operation know-how obtained by production units of Nagylengyel CO₂ gas cap recovery. *Oil Gas J.* 22 July, 98-102.
- Mamyrin, B.A., Anufrijev, G.S., Kamenskii, I.L., Tolstikhin, I.N., 1970. Determination of the isotopic composition of atmospheric helium. *Geochem. Int.* 7, 498-505.
- Mark, D.F., Stuart, F.M., de Podesta, M., 2011. New high-precision measurements of the isotopic composition of atmospheric argon. *Geochim. Cosmochim. Acta* 75, 7494-7501.
- Marland, G., Schlamadinger, B., 1999. The Kyoto Protocol could make a difference for he optimal forest-based CO₂ mitigation strategy: some results from GORCAM. *Environmental Science & Policy* 2, 111-124.
- Martel, D.J., Deák, J., Dövényi, P., Horváth, F., O'Nions, R.K., Oxburgh, E.R., Stegena, L., Stute, M., 1989. Leakage of He from the Pannonian Basin. *Nature* 342, 908-912.
- Marty, B., Gunnlaugsson, E., Jambon, A., Oskarsson, N., Ozima, M., Pineau, F., Torssander, P., 1991. Gas geochemistry of geothermal fluids, the Hengill area, southwest rift zone of Iceland. *Chem. Geol.* 91, 207-225.

- Marty, B., Jambon, A., 1987. C / ^3He in volatile fluxes from the solid Earth: implications for carbon geodynamics. *Earth. Planet. Sci. Lett.* 83, 16-26.
- Marty, B., Jambon, A., Sano, Y., 1989. Helium isotopes and CO_2 in volcanic gases of Japan. *Chem. Geol.* 76, 25-40.
- Matsuda, J., Matsumoto, T., Sumino, H., Nagao, K., Yamamoto, J., Miura, Y., Kaneoka, I., Takahata, N., Sano, Y., 2002. The $^3\text{He}/^4\text{He}$ ratio of the new internal He Standard of Japan (HESJ). *Geochem. J.* 36, 191-195.
- Matter, J.M., Broecker, W.S., Stute, M., Gislason, S.R., Oelkers, E.H., Stefánsson, A., Wolff-Boenisch, D., Gunnlaugsson, E., Axelsson, G., Björnsson, G. (2009). Permanent Carbon Dioxide Storage into Basalt: The CarbFix Pilot Project, Iceland, *Energy Procedia*, 1, 3641-3646.
- Matthews, A., Fouillac, C., Hill, R., O'Nions, R.K., Oxburgh, E.R., 1987. Mantle-derived volatiles in continental crust: the Massif Central of France. *Earth. Planet. Sci. Lett.* 85, 117-128.
- Mayer, B., Humez, P., Becker, V., Dalkhaa, C., Rock, L., Myrntinen, A., Barth, J.A.C., 2015. Assessing the usefulness of the isotopic composition of CO_2 for leakage monitoring at CO_2 storage sites: A review. *Int. J. Greenh. Gas Con.* 37, 46-60.
- McDougall, I., Wellman, P., 2011. Calibration of GA1550 biotite standard for K/Ar and $^{40}\text{Ar}/^{39}\text{Ar}$ dating. *Chem. Geol.* 280, 19-25.
- McGrail, B.P., Schaef, H.T., Ho, A.M., Chien, Y.-J., Dooley, J.J., Davidson, C.L. (2006). Potential for carbon dioxide sequestration in flood basalts. *J. Geophys. Res.* 111, B12201.
- Moniz, E.J., Tinker, S.W., 2010. Role of enhanced oil recovery in accelerating the deployment of carbon capture and sequestration, MIT Energy initiative and Bureau of Economic Geology at UT Austin Symposium.
- Mook, W.G., Bommerson, J.C., Staverman, W.H., 1974. Carbon isotope fractionation between dissolved bicarbonate and gaseous carbon dioxide. *Earth. Planet. Sci. Lett.* 22, 169-176.
- MSOGB, 2015. Mississippi Oil and Gas Board Online Database, <http://gis.ogb.state.ms.us/MSOGBOnline/> accessed in July, 2015.
- Myrntinen, A., Becker, V., van Geldern, R., Würdemann, H., Morozova, D., Zimmer, M., Taubald, H., Blum, P., Barth, J.A.C., 2010. Carbon and oxygen isotope indications for CO_2 behaviour after injection: First results from the Ketzin site (Germany). *Int. J. Greenh. Gas Con.* 4, 1000-1006.

- Nagao, K., Takaoka, N., Matsubayashi, O., 1981. Rare gas isotopic compositions in natural gases of Japan. *Earth. Planet. Sci. Lett.* 53, 175-188.
- NaturalGas, 2015. NaturalGas, <http://naturalgas.org/naturalgas/storage/> accessed in July, 2015.
- Nicot, J.-P., Oldenburg, C.M., Houseworth, J.E., Choi, J.-W., 2013. Analysis of potential leakage pathways at the Cranfield, MS, U.S.A., CO₂ sequestration site. *Int. J. Greenh. Gas Con.* 18, 388-400.
- Nimz, G.J., Hudson, G.B., 2005. The use of noble gas isotopes for monitoring leakage of geologically stored CO₂, in: Thomas, D.C., Benson, S.M. (Eds.), *Carbon Dioxide Capture for Storage in Deep Geologic Formations*, Elsevier, pp. 1113-1128.
- Ozima, M., Podosek, F.A., 2001. *Noble Gas Geochemistry* (2nd Ed.), Cambridge University Press, Cambridge, 367.
- Paustian, K., Andr n, O., Janzen, H.H., Lal, R., Smith, P., Tian, G., Tiessen, H., Van Noordwijk, M., Woomer, P.L., 1997. Agricultural soil as a sink to mitigate CO₂ emission. *Soil Use Manage*, 13, 230-244.
- Pinti, D.L., Marty, B., 1995. Noble gases in crude oils from the Paris Basin, France: Implications for the origin of fluids and constraints on oil-water-gas interactions. *Geochim. Cosmochim. Acta* 59, 3389-3404.
- Poreda, R.J., Farley, K.A., 1992. Rare gases in Samoan Xenolites. *Earth. Planet. Sci. Lett.* 113, 129-144.
- Poreda, R.J., Jenden, P.D., Kaplan, I.R., Craig, H., 1986. Mantle helium in Sacramento basin natural gas wells. *Geochim. Cosmochim. Acta* 50, 2847-2853.
- Price, L., Blount, C., Gowan, D., Wenger, L., Bebout, D., Bachman, A., 1981. Methane solubility in brines with application to the geopressed resource, *Geothermal Energy*, Baton Rouge, La, pp. 205-214.
- Prinzhofer, A., 2013. Noble gas in oil and gas accumulations, in: Burnard, P. (Ed.), *The Noble Gases as Geochemical Tracers*, pp. 225-247.
- Raistrick, M., Mayer, B., Shevalier, M., Perez, R.J., Hutcheon, I., Perkins, E., Gunter, B., 2006. Using chemical and isotopic data to quantify ionic trapping of injected carbon dioxide in oil field brines. *Environ. Sci. Technol.* 40, 6744-6749.
- Rem nyi, I., Szitt r, A., Udvardi, G., 1995. CO₂ IOR in the Szank Field using CO₂ from sweetening plant, 8th European Symposium on Improved Oil Recovery, Gas Processes, 15 May.

- Renne, P.R., Cassata, W.S., Morgan, L.E., 2009. The isotopic composition of atmospheric argon and $^{40}\text{Ar}/^{39}\text{Ar}$ geochronology: Time for a change? *Quat. Geochronol* 4, 288-298.
- Risk, D., Lavoie, M., Nickerson, N., 2015. Using the Kerr investigations at Weyburn to screen geochemical tracers for near-surface detection and attribution of leakage at CCS/EOR sites. *Int. J. Greenh. Gas Con.* 35, 13-17.
- Robinson, B.W., Kusakabe, M., 1975. Quantitative Preparation of Sulfur Dioxide, for $^{34}\text{S}/^{32}\text{S}$ Analyses, from Sulfides by Combustion with Cuprous Oxide. *Anal. Chem.* 47, 1179-1181.
- Romanak, K., Sherk, G.W., Hovorka, S., Yang, C., 2013. Assessment of Alleged CO_2 Leakage at the Kerr Farm using a Simple Process-based Soil Gas Technique: Implications for Carbon Capture, Utilization, and Storage (CCUS) Monitoring. *Energy Procedia* 37, 4242-4248.
- Romanak, K.D., Bennett, P.C., Yang, C., Hovorka, S.D., 2012. Process-based approach to CO_2 leakage detection by vadose zone gas monitoring at geologic CO_2 storage sites. *Geophys. Res. Lett.* 39.
- Saadatpoor, E., Bryant, S.L., Sepehrnoori, K., 2009. New Trapping Mechanism in Carbon Sequestration. *TPM* 82, 3-17.
- Sathaye, K.J., Hesse, M.A., Cassidy, M., Stockli, D.F., 2014. Constraints on the magnitude and rate of CO_2 dissolution at Bravo Dome natural gas field. *PNAS* 111, 43, 15332-15337.
- SCCS, 2015. Scottish Carbon Capture and Storage, <http://www.sccs.org.uk/> accessed in July 2015.
- Scott, V., Gilfillan, S., Markusson, N., Chalmers, H., Haszeldine, R.S., 2013. Last chance for carbon capture and storage. *Nature Clim. Change* 3, 105-111.
- SECARB, 2015. SECARB, Southeast Regional Carbon Sequestration Partnership, http://www.secarbon.org/?page_id=8 accessed in July, 2015.
- Sherwood Lollar, B., Ballentine, C.J., O'Nions, R.K., 1997. The fate of mantle-derived carbon in a continental sedimentary basin: Integration of C/He relationships and stable isotope signatures. *Geochim. Cosmochim. Acta* 61, 2295-2307.
- Shi, J.-Q., Mazumder, S., Wolf, K.-H., Durucan, S., 2008. Competitive Methane Desorption by Supercritical CO_2 Injection in Coal. *TPM* 75, 35-54.
- Smith, S.P., (1985). Noble gas solubility in water at high temperatures, *EOS Trans. Am. Geophys. Union*, 66:397.

- Smith, S.P., Kennedy, B.M., 1983. The solubility of noble gases in water and in NaCl brine. *Geochim. Cosmochim. Acta* 47, 503-515.
- Stalker, L., Boreham, C., Underschultz, J., Freifeld, B., Perkins, E., Schacht, U., Sharma, S., 2015. Application of tracers to measure, monitor and verify breakthrough of sequestered CO₂ at the CO2CRC Otway Project, Victoria, Australia. *Chem. Geol.* 399, 2-19.
- Stancliffe, R.J., Adams, E.R., 1986. Lower Tuscaloosa fluvial channel styles at Liberty Field, Amite County, Mississippi. *Gulf Coast Association of Geological TRANSACTIONS* 36, 305-313.
- Stuart, F.M., Turner, G., 1992. The abundance and isotopic composition of the noble gases in ancient fluids. *Chem. Geol.* 101, 97-109.
- Studlick, J.R.J., Shew, R.D., Basye, G.L., Ray, J.R., 1987. Carbon dioxide source development, northeast Jackson Dome, Mississippi. *AAPG Bull* 71(5), 619.
- Studlick, J.R.J., Shew, R.D., Basye, G.L., Ray, J.R., 1990. A giant carbon dioxide accumulation in the Norphlet formation, Pisgah Anticline, Mississippi, in: Barwis/McPherson/Studlick (Ed.), *Sandstone Petroleum Reservoirs*, pp. 181-203.
- Stute, M., Sonntag, C., Deák, J., Schlosser, P., 1992. Helium in deep circulating groundwater in the Great Hungarian Plane: Flow dynamics and crustal and mantle helium fluxes. *Geochim. Cosmochim. Acta* 56, 2051-2067.
- Suehiro, Y., Nakajima, M., Yamada, K., Uematsu, M., 1996. Critical parameters of $\{x\text{CO}_2 + (1-x)\text{CHF}_3\}$ for $x = (1.0000, 0.7496, 0.5013, 0.2522)$. *J. Chem. Thermodyn.* 28, 1153-1164.
- Thibeau, S., Mucha, V., 2011. How we overestimated saline aquifer CO₂ storage capacities. *Oil Gas Sci. Technol.- Rev. IFP* 66, 81-92.
- Tollefson, J. 2013. Pilot projects bury carbon dioxide in basalt. *Nature*, 500, 18.
- Tomkinson, T., Lee, M.R., Mark, D.F., Smith, C.L., (2003). Sequestration of Martian CO₂ by mineral carbonation. *Nat. Commun.* 4, 2662.
- Tondeur, D., Teng, F., 2008. Carbon Capture and Storage for Greenhouse Effect Mitigation, in: Letcher, T.M. (Ed.), *Future Energy*, Chapter 18, pp. 305-331.
- Torgersen, T., Kennedy, B.M., Hiyagon, H., Chiou, K.Y., Reynolds, J.H., Clarke, W.B., 1989. Argon accumulation and the crustal degassing flux of ⁴⁰Ar in the Great Artesian Basin, Australia. *Earth. Planet. Sci. Lett.* 92, 43-56.
- Torp, T.A., Brown, K.R., 2005. CO₂ underground storage costs as experienced at Sleipner and Weyburn, in: Rubin, E.S., Keith, D.W., Gilboy, C.F. (Eds.), *Greenhouse Gas Control Technologies*, Volume I., pp. 531-538.

- Verdon, J.P., Stork, A.L., Bissell, R.C., Bond, C.E., Werner, M.J., 2015. Simulation of seismic events induced by CO₂ injection at In Salah, Algeria. *Earth. Planet. Sci. Lett.* 426, 118-129.
- Vermeesch, P., Balco, G., Blard, P.-H., Dunai, T.J., Kober, F., Niedermann, S., Shuster, D.L., Strasky, S., Stuart, F.M., Wieler, R., Zimmermann, L., 2015. Interlaboratory comparison of cosmogenic ²¹Ne in quartz. *Quat. Geochronol* 26, 20-28.
- Vogel, J.C., Grootes, P.M., Mook, W.G., 1970. Isotopic fractionation between gaseous and dissolved carbon dioxide. *ZPhyA* 230, 225-238.
- Warr, O., Rochelle, C.A., Masters, A., Ballentine, C.J., 2015. Determining noble gas partitioning within a CO₂-H₂O system at elevated temperatures and pressures. *Geochim. Cosmochim. Acta* 159, 112-125.
- Watson, J., Kern, F., Markusson, N., 2014. Resolving or managing uncertainties for carbon capture and storage: Lessons from historical analogues. *Technological Forecasting and Social Change* 81, 192-204.
- Welhan, J.A., Poreda, R.J., Rison, W., Craig, H., 1988. Helium isotopes in geothermal and volcanic gases of the western United States, II. Long Valley Caldera. *JVGR* 34, 201-209.
- White, S.P., Allis, R.G., Moore, J., Chidsey, T., Morgan, C., Gwynn, W., Adams, M., 2005. Simulation of reactive transport of injected CO₂ on the Colorado Plateau, Utah, USA. *Chem. Geol.* 217, 387-405.
- Whiticar, M.J., 1999. Carbon and hydrogen isotope systematics of bacterial formation and oxidation of methane. *Chem. Geol.* 161, 291-314.
- Whittaker, S., Perkins, E., 2013. Technical aspects of CO₂ enhanced oil recovery and associated carbon storage, Global CCS Institute.
- Widory, D., 2006. Combustibles, fuels and their combustion products: A view through carbon isotopes. *Combustion Theory and Modelling* 10, 831-841.
- Wilkinson, M., Gilfillan, S.M.V., Haszeldine, R.S., Ballentine, C.J., 2009. Plumbing the Depths: Testing Natural Tracers of Subsurface CO₂ Origin and Migration, Utah, in: Grobe, M., Pashin, J.C., Dodge, R.L. (Eds.), *Carbon dioxide sequestration in geological media—State of the science: AAPG Studies in Geology* 59, pp. 619-634.
- Wycherley, H., Fleet, A., Shaw, H., 1999. Some observations on the origins of large volumes of carbon dioxide accumulations in sedimentary basins. *Mar. Petrol. Geol.* 16, 489-494.
- Xu, S., Nakai, S.I., Wakita, H., Wang, X., 1995. Mantle-derived noble gases in natural gases from Songliao Basin, China. *Geochim. Cosmochim. Acta* 59, 4675-4683.

- Xu, T., Apps, J.A., Pruess, K., 2005. Mineral sequestration of carbon dioxide in a sandstone–shale system. *Chem. Geol.* 217, 295-318.
- Yang, H., Xu, Z., Fan, M., Gupta, R., Slimane, R.B., Bland, A.E., Wright, I., 2008. Progress in carbon dioxide separation and capture: A review. *JEnvS* 20, 14-27.
- Zartman, R.E., Wasserburg, G.J., Reynolds, J.H., 1961. Helium, Argon, and Carbon in some natural gases. *J. Geophys. Res.* 66, 277-306.
- Zero, 2015. ZERO CO₂, <http://www.zero.co2.no/> accessed in July, 2015.
- Zhang, D., Song, J., 2014. Mechanisms for Geological Carbon Sequestration. *Procedia IUTAM* 10, 319-327.
- Zhang, R., Ghosh, R., Sen, M.K., Srinivasan, S., 2013. Time-lapse surface seismic inversion with thin bed resolution for monitoring CO₂ sequestration: A case study from Cranfield, Mississippi. *Int. J. Greenh. Gas Con.* 18, 430-438.
- Zhang, R., Sen, M.K., Srinivasan, S., 2014. Time-lapse pre-stack seismic inversion with thin bed resolution for CO₂ sequestration from Cranfield, Mississippi. *Int. J. Greenh. Gas Con.* 20, 223-229.
- Zhou, Z., Ballentine, C.J., Kipfer, R., Schoell, M., Thibodeaux, S., 2005. Noble gas tracing of groundwater/coalbed methane interaction in the San Juan Basin, USA. *Geochim. Cosmochim. Acta* 69, 5413-5428.
- Zhou, Z., Ballentine, C.J., Schoell, M., Stevens, S.H., 2012. Identifying and quantifying natural CO₂ sequestration processes over geological timescales: The Jackson Dome CO₂ Deposit, USA. *Geochim. Cosmochim. Acta* 86, 257-275.